

# Propelling the hydrogen economy: from chemical storage and delivery to utilization in biomass conversion

Présentée le 20 janvier 2021

Faculté des sciences de base  
Laboratoire de chimie organométallique et médicinale  
Programme doctoral en chimie et génie chimique

pour l'obtention du grade de Docteur ès Sciences

par

**Lu CHEN**

Acceptée sur proposition du jury

Prof. K. Severin, président du jury  
Prof. G. Laurenczy, Prof. P. J. Dyson, directeurs de thèse  
Prof. Q. Xu, rapporteur  
Prof. H. Liu, rapporteuse  
Prof. K. Sivula, rapporteur

*Au milieu de l'hiver,  
j'ai découvert en moi un invincible été.*

*- Albert Camus*

---

## Abstract

Since H<sub>2</sub> is a non-polluting, inexhaustible, efficient, and sustainable energy carrier, it has been forecast to become one of the major carriers of energy in the future and is also essential in the production of feedstock chemicals derived from renewable carbon sources. Initially, a Ru(II) catalyst with *meta*-trisulfonated triphenylphosphine ligands was shown to be a versatile homogeneous catalyst for the reversible dehydrogenation/hydrogenation of N-heterocycles. N-heterocyclic liquid organic hydrogen carrier compounds are attractive H<sub>2</sub> storage and delivery compounds. Hydrogen is also essential in reductive fragmentation of lignin, an abundant biomass source that can be cleaved under reductive conditions to produce value-added renewable aromatic platform chemicals. In native lignin most of the units are linked by C-O bonds. Therefore, selective catalytic cleavage of the C-O bonds plays a pivotal role in maximizing the efficiency of the process while maintaining desirable functionality. A pseudo-homogeneous catalytic system consisting of *in situ* generated platinum nanoparticles dispersed in ionic liquids was used for upgrading high oxygen content bio-oil through hydrodeoxygenation. To improve further the stability of the catalyst, well-defined rhodium nanoparticles dispersed in sub-micrometer size carbon hollow spheres were prepared, which were able to hydrogenate lignin derived products under mild conditions. Confinement of active rhodium nanoparticles within a carbon shell, prevents the intact lignin polymer from entering and interacting with the catalyst. Thus, this catalysts was used to demonstrate that solvolysis leads to fractionation and fragmentation of lignin, with the internal catalysts hydrogenating any reactive fragments generated. An atomically dispersed catalyst, comprising single Pt atoms on Ni nanoparticles supported on carbon, were used in depolymerization of lignin and showed enhanced activity on selective C-O bonds cleavage.

---

## **Keywords**

Lignin, catalysis, ionic liquid, heterogeneous catalyst, homogeneous catalyst, sustainable chemistry, chemical hydrogen-storage/delivery, single atom alloy.

---

## Résumé

Comme l' $H_2$  est un vecteur énergétique non polluant, inépuisable, efficace et durable, il est prévu qu'il devienne l'un des principaux vecteurs d'énergie à l'avenir et est également essentiel dans la production de produits chimiques de base dérivés de sources de carbone renouvelables. Au départ, un catalyseur Ru(II) avec des ligands de triphénylphosphine méta-trisulfonée s'est révélé être un catalyseur homogène polyvalent pour la déshydrogénation/hydrogénation réversible des N-hétérocycles. Les N-hétérocycles liquides organiques porteurs d'hydrogène sont des composés de stockage et de livraison d' $H_2$  intéressants. L'hydrogène est également essentiel dans la fragmentation réductrice de la lignine, une source de biomasse abondante qui peut être clivée dans des conditions réductrices pour produire des plates-formes chimiques aromatiques renouvelables à valeur ajoutée. Dans la lignine native, la plupart des unités sont liées par des liaisons C-O. Par conséquent, le clivage catalytique sélectif des liaisons C-O joue un rôle essentiel dans l'optimisation de l'efficacité du processus tout en conservant les fonctionnalités souhaitées. Un système catalytique pseudo-homogène composé de nanoparticules de platine générées in situ et dispersées dans des liquides ioniques a été utilisé pour améliorer la biohuile à haute teneur en oxygène par hydrodésoxygénation. Pour améliorer encore la stabilité du catalyseur, des nanoparticules de rhodium bien définies, dispersées dans des sphères creuses en carbone de taille inférieure au micromètre, ont été préparées, capables d'hydrogéner des produits dérivés de la lignine dans des conditions douces. Le confinement des nanoparticules de rhodium actives dans une enveloppe de carbone empêche le polymère de lignine intact de pénétrer et d'interagir avec le catalyseur. Ainsi, ce catalyseur a été utilisé pour démontrer que la solvolysse entraîne le fractionnement et la fragmentation de la lignine, les catalyseurs internes hydrogénant tous les fragments réactifs générés. Un catalyseur atomique dispersé, comprenant des atomes de Pt uniques sur des nanoparticules de Ni supportées par du carbone, a été utilisé pour la dépolymérisation de la lignine et a montré une activité accrue sur le clivage sélectif des liaisons C-O.

---

## **Mots-clés**

Lignine, catalyse, liquide ionique, catalyseur hétérogène, catalyseur homogène, chimie durable, stockage et livraison d'hydrogène chimique, alliage à un seul atome.

---

## Contents

Abstract .....	II
Keywords .....	III
Résumé.....	IV
Mots-clés.....	VI
Chapter 1 Introduction .....	1
1.1 Energy challenges .....	1
1.2 Hydrogen nexus.....	1
1.3 Hydrogen storage and delivery .....	4
1.4 Using hydrogen in biomass conversion.....	5
1.5 References .....	19
Chapter 2 A viable hydrogen-storage/delivery system with N-heterocycles by a versatile ruthenium catalyst.....	29
2.1 Introduction .....	30
2.2 Results and discussion .....	31
2.3 Conclusions .....	36
2.4 Methods .....	36
2.4.1 Materials and methods.....	36
Dehydrogenation/Hydrogenation.....	36
2.4.2 Hydrogenation and dehydrogenation cycle .....	37
2.5 References .....	38
Chapter 3 An efficient Pt nanoparticle-ionic liquid system for the hydrodeoxygenation of bio-derived phenols under mild conditions .....	41
3.1 Introduction .....	43
3.2 Results and discussion .....	44

---

3.2.1	Characterizations of Pt NPs.....	44
3.2.2	Conversion of phenol.....	48
3.2.3	Influence of the IL anions.....	51
3.2.4	Evaluation of acids as co-catalysts .....	52
3.2.5	Reaction optimisation .....	53
3.2.6	Substrate scope .....	56
3.3	Conclusions .....	58
3.4	Methods .....	58
3.4.1	Materials and methods.....	58
3.4.2	Pt NPs characterisation.....	58
3.4.3	Catalyst Testing and Product Analysis .....	58
3.5	References .....	60
Chapter 4 Selective hydrogenation of lignin-derived model compounds and sawdust under mild conditions .....		65
4.1	Introduction .....	67
4.2	Results and discussion.....	68
4.2.1	Characterizations of Rh@HCS.....	68
4.2.2	Catalytic activity tests of Rh@HCS in lignin model compounds ..	70
4.2.3	Catalytic activity tests of Rh@HCS in lignin conversion .....	78
4.3	Conclusions .....	85
4.4	Methods .....	86
4.4.1	Synthesis of the catalysts.....	86
4.4.2	Catalyst Testing .....	86
4.4.3	Lignin product analysis .....	87
4.4.4	Analytical methods .....	87



---

4.5	References .....	89
Chapter 5 Embedding single platinum atoms into nickel nanoparticles to afford a highly selective catalyst for lignin conversion.....		
		95
5.1	Introduction .....	97
5.2	Results and discussion .....	98
5.3	Conclusions .....	106
5.4	Methods .....	106
5.4.1	Synthesis of Ni/C and Pt <sub>1</sub> Ni/C.....	106
5.4.2	Synthesis of Pt <sub>1</sub> /C .....	106
5.4.3	XAFS analysis .....	107
5.4.4	TEM, XPS, XRD measurements .....	107
5.4.5	Catalytic tests.....	107
5.5	References .....	108
Chapter 6	Conclusions and Outlook.....	113
Chapter 7	Acknowledgements .....	115
Curriculum Vitae	.....	117

---

## Frequently used abbreviations

CO <sub>2</sub>	carbon dioxide
DA	2,4-dihydroxybenzoic acid
DCDA	dicyandiamide
DFT	density functional theory
DPE	diphenyl ether
EtOH	ethanol
[Emim]NTf <sub>2</sub>	1-Ethyl-3-methylimidazolium bis(trifluoromethylsulfonyl)imide
fcc	face-centered cubic
HDO	hydrodeoxygenation
HMT	hexamethylenetetramine
IL	ionic liquid
LOHC	liquid organic hydrogen carrier
<i>m</i> TPPDS	<i>meta</i> -disulfonated triphenylphosphine
<i>m</i> TPPMS	<i>meta</i> -monosulfonated triphenylphosphine
<i>m</i> TPPTS	<i>meta</i> -trisulfonated triphenylphosphine
NP	nanoparticle
NO <sub>x</sub>	nitrogen oxides
NMR	nuclear magnetic resonance
MeOH	methanol
RCF	reductive catalytic fractionation
SAA	single-atom alloy
SAC	single-atom catalyst
SO <sub>x</sub>	sulfur oxides
SO	sodium oleate
TEM	transmission electron microscopy
TPD	temperature-programmed desorption
TPR	temperature-programmed reaction
XANES	X-ray absorption near-edge spectroscopy
XPS	X-ray photoemission spectroscopy
XRD	X-ray diffraction

# Chapter 1 Introduction

## 1.1 Energy challenges

Energy not only provides food, light, mobility and heat, and also supports society and economic development. By 2030, the world is estimated to consume two-thirds more energy than it did in 2005.<sup>1</sup> Although fossil fuels, including oil, coal, and gas, are the dominant sources of energy now, as finite resources, the earth-mined fossil fuels cannot supply the whole world with hugely increased demand for a long time. Moreover, the century-long strongly reliance on fossil fuels has caused a range of severe environmental problems, including global warming owing to the increased emission of (carbon dioxide) CO<sub>2</sub>, acid rain and smog owing to harmful emission of sulfur oxides (SO<sub>x</sub>), nitrogen oxides (NO<sub>x</sub>), and water pollution that caused by huge amount wastewater produced during oil and gas extraction process.

The growing demand for fuels and chemicals and the environmental problems caused by nonrenewable petroleum can be addressed simultaneously through the development of renewable resources and sustainable technologies.<sup>2-4</sup> Innovation and technology development will be essential for a global energy transition. Efficient utilization of solar energy, hydrogen, biomass, wind and other sustainable energy are good options for the replacement.

## 1.2 Hydrogen nexus

Hydrogen nexus is a concept developed for “hydrogen economy” where hydrogen as energy carrier may fulfil, at least in part of the central role currently occupied by carbon in the “carbon economy” (Figure 1.1). In the “carbon economy”, energy is originally obtained from the sun and is stored as chemical potential energy within chemical bonds in carbon-rich fossil fuel materials. Afterwards it is liberated by oxidation for consumption, with generating CO<sub>2</sub> as the by-product. Unfortunately, the CO<sub>2</sub> will consecutively trigger temperature increasing of the earth, and then cause global warming. Against this backdrop, there is a possibility of the so-called “hydrogen economy” to tackle the energy crisis and environmental problems. In the hydrogen

economy, energy can be obtained from renewable resources such as solar, wind, etc. and stored as chemical energy in hydrogen and hydrogen-rich materials. In contrast to the carbon economy, during the consumption of hydrogen energy, only water is produced hence avoiding the environmental problems associated with the emission of  $\text{CO}_2$ .<sup>5,6</sup> Hydrogen can also be applied as an attractive storage medium for electricity generated from intermittent renewable resources such as solar, wind, wave and tidal power. Therefore, it provides the solution to solve intermittency of supply problem with sustainable energy resources. As  $\text{H}_2$  is a non-polluting, inexhaustible, efficient, and sustainable energy carrier, it has been forecast to become one of the major carrier in the future.

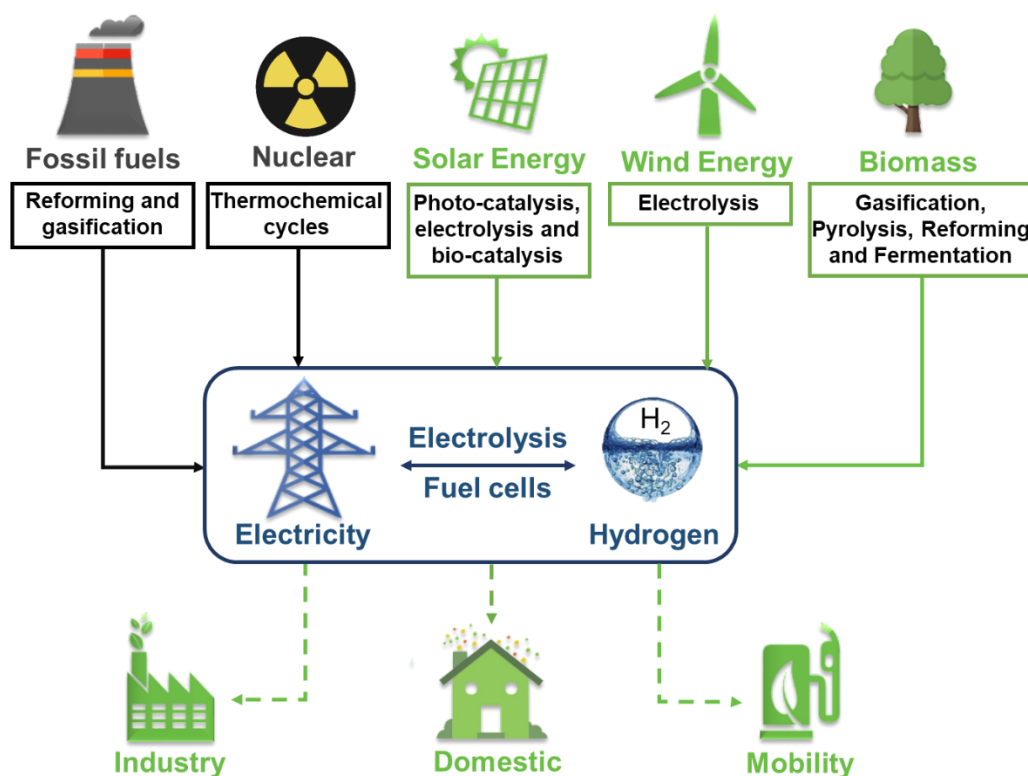


Figure 1.1 Hydrogen nexus: a possible model for a hydrogen energy economy.

For the  $\text{H}_2$  production, it consumes energy because hydrogen is invariably bounding up with other elements. Therefore, the efficient and sustainable generation of hydrogen is essential for an ultimately sustainable hydrogen economy. Various methods for the production of hydrogen have been developed including from carbon-based systems, renewable sources and nuclear power. At present, the most commonly applied in industrial process accounting for almost 50% of total hydrogen production is the steam

reforming of methane with CO<sub>2</sub> as a byproduct.<sup>7,8</sup> Even though this is an economic method, CO<sub>2</sub> emission is still a suspended problem. Nuclear energy can be applied to produce hydrogen by the electrolysis of water without CO<sub>2</sub> emission. Although it is possible to meet the high demand for hydrogen, the extraordinary safety risks related to the deadly radiation have forced many industrializations to discontinue the usage of nuclear power for energy production.<sup>9,10</sup>

Because of the enormous potential of solar and wind, it is possible that they can supply future hydrogen demand. The hydrogen production pathways from solar and wind energy include electrolysis<sup>11,12</sup>, photolysis<sup>13,14</sup>, and bio-catalysis. The intrinsic advantage of electrolysis of water is the process that does not depend on the source of the electricity. In addition, with these unstable and intermittent renewable sources of energy (e.g. wind, tidal, wave), it is challenging to integrate them into the power grid. Hydrogen is one of the most attractive potential energy store method in conjunction with intermittent energy sources. Besides, it is potentially carbon-free and might provide local sources of sustainable hydrogen. Despite the fact that the efficiency of commercial electrolysis of water for production of hydrogen is as high as 80–85%.<sup>9,10</sup> the cost of it is still 3 to 5 times higher than that produced from fossil fuels.<sup>15,16</sup> Using sunlight to split water directly by photocatalysis is more efficiently than with attendant of electricity.<sup>17</sup> The solar photocatalysis of water is probably one major and long-term solution to a CO<sub>2</sub>-free route for production of hydrogen.<sup>5</sup> To realize a low-cost and efficient direct production of hydrogen from solar energy, it requires novel catalysts, novel techniques or new enzymes. Since the inefficient initial catalysis step by the enzyme, efforts are under way to modify them by genetic engineering.<sup>18</sup>

Several thermochemical and biological routes have been developed for the production of H<sub>2</sub> from biomass, including fermentation<sup>19,20</sup>, gasification<sup>21–23</sup>, pyrolysis<sup>24,25</sup>, alcohol steam reforming<sup>26–28</sup> and sugar aqueous reforming<sup>23,29,30</sup>. The advantages of these routes are the application of readily available and renewable starting materials, i.e. biomass. The environment friendly, efficient routes produce little or no harmful emissions. Biomass can be efficiently converted into a number of liquid fuels, including methanol (MeOH), ethanol (EtOH), biodiesel, and pyrolysis oil, which could be transported and applied to generate hydrogen on site.<sup>31,32</sup> Despite these advantages, obstacles still exist for the commercialization of hydrogen production from lignocellulosic biomass. At least in certain developing countries with the food-limited and carbon-constrained conditions, it is better to treat biomass for food or as a chemical

feedstock rather than resources for H<sub>2</sub> production.

The economic feasibility of these hydrogen production methods are not only strongly dependent on the activity of the catalysts, but also related to certain regional factors, such as availability of renewable energy sources, efficiency of delivery approaches, supportive policies. Hydrogen can be produced both centrally in large scale and also locally in small scale in refueling stations.<sup>33</sup> In conclusion, hydrogen nexus provides the powerful link between sustainable energy sources and utilization.

### 1.3 Hydrogen storage and delivery

Environmental friendly products based on hydrogen with high energy density are foreseen to be main energy carriers in the future.<sup>17</sup> A major concern is to develop safe and suitable techniques to store and deliver hydrogen by using of the existing energy infrastructure. Traditional hydrogen-storage methods, such as high-pressure gas containers and cryogenic liquid/gas containers, have cost and safety issues.<sup>34</sup> Consequently, materials suitable for hydrogen-storage, such as formic acid<sup>35,36</sup>, metal hydrides<sup>37</sup> and carbon nanostructures<sup>38</sup>, have been developed. However, most of these hydrogen-storage methods still have challenges related to safety issues, with disadvantages in low storage density and relatively high costs.<sup>39-42</sup>

Using Liquid Organic Hydrogen Carrier (LOHC) compounds is an attractive alternative technique, to provide energy for mobile applications due to the similar energy storage densities and manageability compared to fossil fuels.<sup>43</sup> The LOHC system consists of a hydrogen-lean organic compound and a hydrogen-rich organic compound. Hydrogen is stored and released through reversible hydrogenation and dehydrogenation between LOHCs.

LOHCs as the energy carriers have many advantages. LOHCs are liquid at room temperature so that they can be easily stored in large quantities under ambient conditions. Handling and operation of LOHC systems is also more convenient than those with high pressures with the storage and delivery (hydrogenation and dehydrogenation of LOHCs) being able to be performed at relatively mild conditions. More importantly, the LOHC system can be easily integrated into an existing energy infrastructure for fuels, since LOHCs have the similar properties with petroleum.

A world leader in specialty chemicals, Clariant, established commercial scale units

using LOHCs to improve safety, scalability and convenience in hydrogen storage and transportation. It is confirmed that Clariant will continue to further broaden the applicability and efficiency.

To date, benzene and cyclohexane, toluene and methyl-cyclohexane, naphthalene and decalin, N-ethyl-carbazole and perhydro-N-ethylcarbazole and dibenzyltoluene and perhydrodibenzyltoluene have been used as LOHCs.<sup>43</sup> Compared to cycloalkanes, N-heterocycles have lower enthalpy changes  $\Delta H^0$  in dehydrogenation and hydrogenation reactions, thus N-heterocycles are excellent candidates as LOHCs.<sup>44,45</sup> Till now, for the catalytic dehydrogenation of N-heterocycles, heterogeneous catalysts were mostly investigated.<sup>46,47</sup> However, these heterogeneous systems need harsh reaction conditions and show poor functional-group tolerance. In addition, rational tuning and designing of heterogeneous catalysts are difficult due to the lack of understanding in the mechanism. On the other hand, homogeneous catalysts were rarely studied in the hydrogenation and dehydrogenation of N-heterocycles.<sup>46,47</sup> With both hydrogenation and dehydrogenation applying the same catalyst, an additional step of catalyst separation can be avoided. Therefore, homogeneous catalysts are as good as heterogeneous catalysts in the perspective of products separation.

## **1.4 Using hydrogen in biomass conversion**

The vast majority of industrially produced fuels and chemicals depend on fossil fuels now. As the depletion of fossil fuels, one of the foremost challenges in the future is the exploration of sustainable alternatives for fossil resources. Lignocellulose may contribute to the substitution of fossil fuels, since it is renewable, sustainable and inedible. Lignocellulose biomass (Figure 1.2), mainly composed of cellulose, hemicellulose, and lignin, is one of the few ideal resources that fulfills these essential criteria. Lignocellulose with large quantities is widely available from the forestry and agricultural worldwide as primary sources. Lignocellulosic wastes are also produced by food and paper industry, such as maize straws, sugarcane bagasse and paper waste, on a daily basis.<sup>48–50</sup> To economically realize the biomass industrialization, all three major constituents of lignocelluloses (cellulose, hemicellulose, and lignin) should be valorized to bio-chemicals or bio-fuels.<sup>51,52</sup>

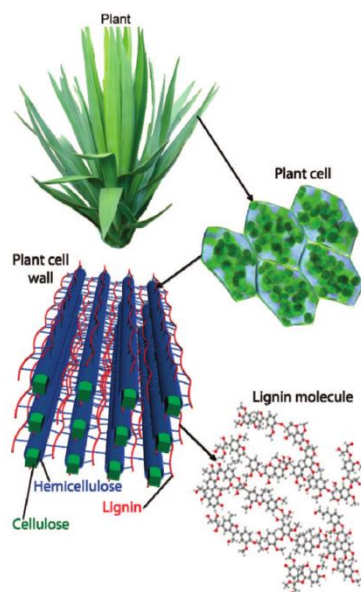


Figure 1.2 Schematic representation of the location and structure of lignin in lignocellulosic material<sup>53</sup>

While great progress has already been made in the catalytic conversion of cellulose, lignin valorization remains one of the foremost challenges of new biorefinery strategies.<sup>54–58</sup> Because of the unique natural amorphous polymer structure of lignin, it is robust and complicated. However, as the largest renewable source of aromatic building blocks, lignin still has huge potential for the production of bulk or functionalized aromatic compounds such as phenols (Figure 1.3).<sup>2,3,59,60</sup> Hence, the conversion of renewable biomass to high value-added platform chemicals currently attracts considerable attention. Therefore, the economic viability is still one of the most essential problem in industrialization of the lignocellulose biomass conversion. Typically, there are four monolignols in lignin: 4-n-propanolsyringol, 4-n-propanolguaiacol, 4-n-propylsyringol and 4-n-propylguaiacol.<sup>53</sup> These monomers can be applied in resins production. They can also be used as building blocks for aromatics chemicals production.<sup>61</sup> From lignin to chemicals, it is a promising and economical perspective technique in lignin conversion. Therefore, the cleavage of the C-O bonds between units within the lignin structure without the hydrogenation of the benzene ring is essential import as it represents an attractive route for the production of monolignols.



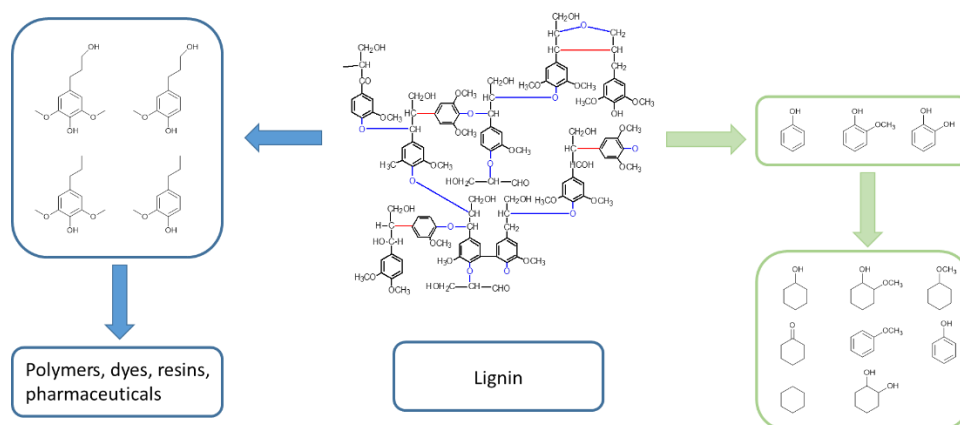


Figure 1.3 Valuable products potentially obtained from lignin<sup>3</sup>

Catalysts play a central role in the reductive catalytic depolymerization process. For the reductive catalytic depolymerization of lignin with focus on the C-O bonds cleavage, almost all the catalysts are metal based. In principal, these catalysts can be divided into three categories: noble metal catalysts, non-noble metal catalysts and alloy catalysts.

#### 1.4.1 Noble metal catalysts in lignin reductive depolymerization

Noble metal catalysts show high activity in reductive catalytic lignin conversion, transforming native lignin to low molecular weight products. The lignin-derived aromatic monomers are dissolved in most of the organic solvents and can be easily separated from the solids containing cellulose and the heterogeneous catalyst. Table 1.1 summarized the lignin conversion with noble metal catalysts.

The dominant linkage in lignin is the  $\beta$ -O-4 linkage, consisting of approximately 50% of spruce linkages and 60% of birch linkages.<sup>62,63</sup> Hydrogenolysis or solvolysis are the most common methods to breakdown the C-O bonds.<sup>64,65</sup> The products distribution of monolignols are strongly depend on the solvent and catalyst,<sup>66</sup> since hydrogenolysis of C-O bonds, both cleavage of the C-OH bonds and C-O-CH<sub>3</sub>, are metal dependent.<sup>53,67,68</sup>

Since the hydrogenolysis of C-O bonds is dependent on the metal catalyst used, the catalyst plays a vital role. It has been reported that the activities of Ru/C, Pd/C, Rh/C, and Pt/C in lignin depolymerization differ significantly in H<sub>2</sub>O under the same conditions (Table 1.1, Entries 1-4).<sup>65</sup> Instead of pure H<sub>2</sub>O, the mixture of dioxane and

H<sub>2</sub>O as the solvent led to higher monomers yields. Performing lignin depolymerization in the mixture of dioxane and H<sub>2</sub>O with Pt/C, the monomers yields increased from 33.6% to 41.7 wt% (Table 1.1, Entries 5).<sup>69</sup> By employing the mixture of dioxane and H<sub>2</sub>O with addition of H<sub>3</sub>PO<sub>4</sub>, the yields of the monomers with Pt/C and Rh/C as the catalyst increased from 33.6% to 46.5 wt% and 19.7% to 45.2%, respectively (Table 1.1, Entry 6, 7).<sup>69</sup> To examine the role of metal, Ru/C and Pd/C were compared under same reaction conditions (Table 1.1, Entries 8, 9). Changing the catalyst from Ru/C to Pd/C, a drastic increase in the OH-content of the lignin-derived products can be observed.<sup>70</sup> The lignin monomers products distribution are different, albeit the lignin monomers yields were similar for both catalysts. With Pd/C catalyst, preferentially 4-propanol-derivatives with higher OH-content were produced rather than 4-propylphenolics (Table 1. Entry 8, 9).<sup>70</sup> With Pd/C catalyst, preferentially 4-propanol-derivatives with higher OH-content were produced rather than 4-propylphenolics, albeit the lignin monomers yields were similar.

When the same metal catalyst is applied, the monomers distribution after the lignin depolymerization is governed by several factors including the lignin sources, the pretreatment of the lignocellulose, the employed solvent, the reaction conditions and the additives. The solvent effects were demonstrated by using bio-derived solvents with Pd/C as the catalyst in depolymerization of birch wood. Under the identical reaction conditions, it has been proposed that the degree of depolymerization decreased with the increasing solvent polarity (Table 1.1, Entries 10-16).<sup>71</sup> Lignin product yield and depolymerization degree are generally enhanced by raising the reaction temperature and the increase in the polarity of the reaction solvent.<sup>71</sup> Methanol (MeOH) and ethylene glycol were identified as the best performing bio-derivable solvents.<sup>71</sup> When MeOH is used as solvent, the MeOH itself can also participate in the depolymerization of lignin, contributing to the overall C-O bonds cleavage through solvolysis. Compare to MeOH, H<sub>2</sub>O, dioxane and 2-propanol, show less activity in the formation of monolignols (Table 1. Entries 17-21).<sup>72-74</sup> For MeOH/water and EtOH/water blends, 30 vol% water concentrations results in high lignin monomers yield and most of the carbohydrates are preserved in the solid pulp (Table 1.1, Entries 22, 23).<sup>75</sup>

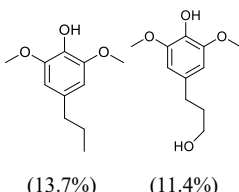
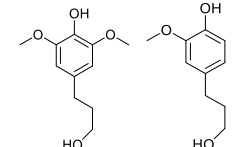
Depolymerization of lignin at mild temperature and pressure generally require the addition of acid or alkaline additives. With the addition of small quantities of H<sub>3</sub>PO<sub>4</sub>, both depolymerization of lignin and alcoholysis of hemicellulose in poplar sawdust are promoted resulting liquid products, with a cellulose-rich pulp as the solid product

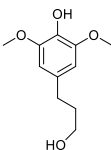
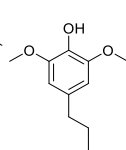
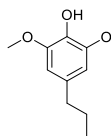
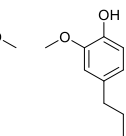
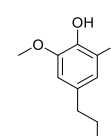
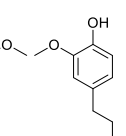
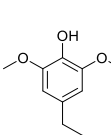
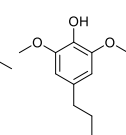
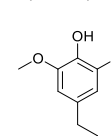
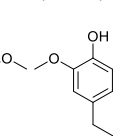
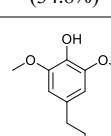
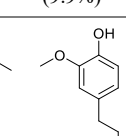
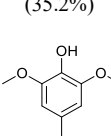
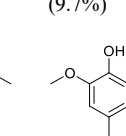
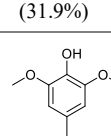
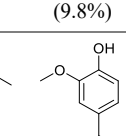
(Table 1.1, Entry 24).<sup>76</sup> In contrast, addition of small quantities of NaOH, leads to severe repolymerization, resulting in low yields of monomer. When water-tolerant metal aluminum triflate ( $\text{Al}(\text{OTf})_3$ ) is applied as a co-catalyst, the yields of lignin monomers were higher than that without  $\text{Al}(\text{OTf})_3$  (Table 1.1, Entry 25, 26).<sup>77,78</sup> Using these additives were not only the resulting environment problem in dealing with the wasters, but also the excessive conversion of hemicellulose or cellulose resulting in additional problems in products separation.

In the pretreatment of the lignocellulose, using of acid or high temperatures during lignin extraction can lead to repolymerization, namely C-O bonds are cleaved, and stable carbon-carbon (C-C) bonds are formed. The direct depolymerization of native lignin can prevent severe and irreversible condensation during the pretreatment. However, mass transfer limitations might decrease the depolymerization rate. Other than addition of acid or alkaline additives, it has been demonstrated that formaldehyde (FA) and formaldehyde can stabilize lignin during extraction. As a result, three to seven times higher yield of monomers can be obtained compared to those using the analogous method in the absence of FA (Table 1.1, Entry 27).<sup>79,80</sup>

The effect of the support of the catalyst was studied through the comparison of a wide range of supported Ru catalysts ( $\text{Ru}/\text{Nb}_2\text{O}_5$ ,  $\text{Ru}/\text{ZrO}_2$ ,  $\text{Ru}/\text{Al}_2\text{O}_3$ ,  $\text{Ru}/\text{TiO}_2$ ,  $\text{Ru}/\text{H-ZSM-5}$  and  $\text{Ru}/\text{C}$ ) (Table 1.1, Entry 29-34).<sup>81</sup> The synergism between the Ru nanoparticles and the acidity of  $\text{Nb}_2\text{O}_5$  plays a key role in lignin depolymerization. The acidity of support favour to cleavage of C-O ether bonds through hydropyrolysis.

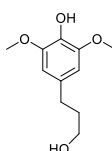
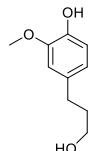
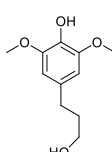
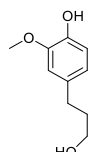
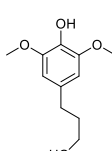
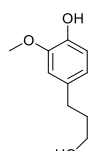
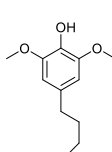
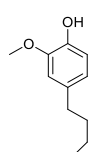
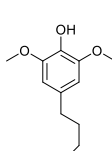
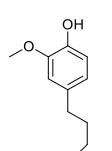
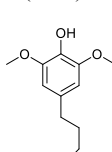
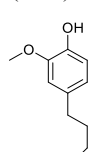
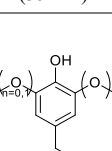
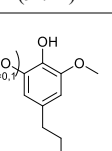
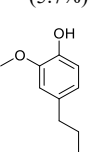
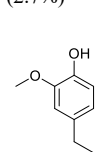
Table 1.1 Summary of lignin reductive depolymerization with noble metal catalysts

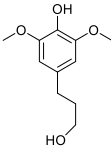
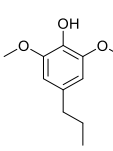
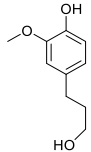
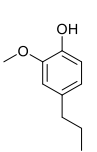
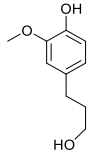
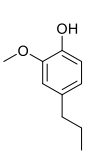
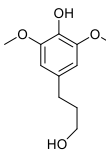
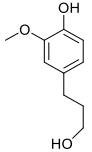
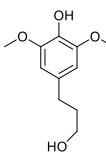
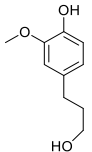
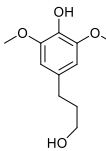
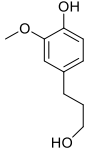
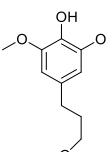
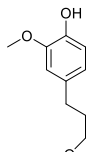
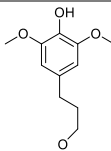
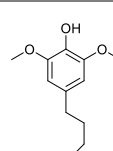
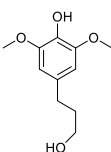
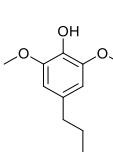
No.	Feedstock	Catalyst	Solvent	T/°C	$P_{\text{H}_2}/$ bar	Monomers yield/%	Yield of main monomers	Ref.
1	Birch	Pt/C	$\text{H}_2\text{O}$	200	40	33.6	 (13.7%) (11.4%)	69
2	Birch	Pd/C	$\text{H}_2\text{O}$	200	40	25.5		

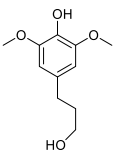
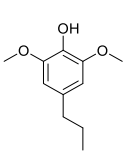
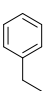
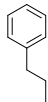
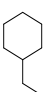
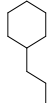
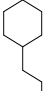
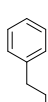
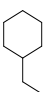
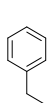
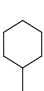
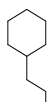
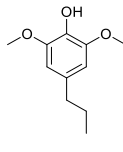
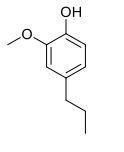
3	Birch	Ru/C	H <sub>2</sub> O	200	40	4.6	(15.7%)	(5.3%)
								
4	Birch	Rh/C	H <sub>2</sub> O	200	40	19.7	(2.4%)	(1.1%)
								
5	Birch	Pt/C	Dioxane/H <sub>2</sub> O (1:1)	200	40	41.7	(15.7%)	(5.3%)
								
6	Birch	Pt/C	Dioxane/H <sub>2</sub> O(1:1)+H <sub>3</sub> P O <sub>4</sub>	200	40	46.5	(21.8%)	(9.1%)
								
7	Birch	Rh/C	Dioxane/H <sub>2</sub> O(1:1)+H <sub>3</sub> P O <sub>4</sub>	200	40	45.2	(21.1%)	(14.5%)
								
8	Birch	Pd/C	MeOH	250	30	49.3	(34.8%)	(9.9%)
								
9	Birch	Ru/C	MeOH	250	30	49.7	(35.2%)	(9.7%)
								
10	Birch	Pd/C	H <sub>2</sub> O	200	30	43.8	(31.9%)	(9.8%)
								

70

71

11	Birch	Pd/C	MeOH	200	30	28.1			(19.3%)	(5.7%)
12	Birch	Pd/C	Ethylene glycol	200	30	26.9			(18.6%)	(5.2%)
13	Birch	Pd/C	EtOH	200	30	17.4			(11.8%)	(4.1%)
14	Birch	Pd/C	2-Propanol	200	30	12.2			(8.5%)	(3.0%)
15	Birch	Pd/C	1-Butanol	200	30	10.8			(7.4%)	(2.8%)
16	Birch	Pd/C	MeOH	250	30	49.0			(35.2%)	(9.7%)
17	Acetonesolv lignin	Pd/C	Dioxane	200	1	15			(5.7%)	(2.7%)
18	Pine	Pd/C	Dioxane/H <sub>2</sub> O(1:1)	195	34.5	22.4			(20.8%)	(1.6%)

19	Birch	Pd/C	MeOH+H <sub>2</sub> O+H <sub>3</sub> PO <sub>4</sub>	180	30	37.0	 (18.2%)	 (10.6%)	73
20	enzymatic mild acidolysis lignin	Pd/C	Dioxane/H <sub>2</sub> O(1:1)	195	34	21	 (18.2%)	 (10.6%)	74
21	Wood	Pd/C	Dioxane/H <sub>2</sub> O(1:1)	195	34	22	 (18.2%)	 (10.6%)	
22	Poplar	Pd/C	MeOH/ H <sub>2</sub> O(7:3)	200	20	43.5	 (21.5%)	 (14.0%)	75
23	Poplar	Pd/C	EtOH/ H <sub>2</sub> O(1:1)	200	20	43.3	 (21.5%)	 (14.2%)	
24	Poplar	Pd/C	MeOH+H <sub>3</sub> PO <sub>4</sub>	200	20	42	 (21%)	 (14%)	76
25	Birch	Pd/C+Al(O Tf) <sub>3</sub>	MeOH	180	30	55.0	 (33.6%)	 (8.4%)	77
26	Oak	Pd/C+Al(O Tf) <sub>3</sub>	MeOH	180	30	46.0	 (11.5%)	 (9.9%)	78
27	Formaldehy de pretreated polar lignin	Ru/C	THF	250	40		 (18.2%)	 (10.6%)	79

							(18.6%)	(16.5%)	
28	Aspen	Rh/C	Dioxane/H <sub>2</sub> O(1:1)	195	34	50.1			82
							(25.6%)	(12.9%)	
29	Birch lignin	Ru/Nb <sub>2</sub> O <sub>5</sub>	H <sub>2</sub> O	250	7	35.5			
							(9.1%)	(8.5%)	
30	Birch lignin	Ru/C	H <sub>2</sub> O	250	7	33			
							(14.4%)	(11.7%)	
31	Birch lignin	Ru/HZSM-5	H <sub>2</sub> O	250	7	16.2			81
							(1.7%)	(0.7%)	
32	Birch lignin	Ru/TiO <sub>2</sub>	H <sub>2</sub> O	250	7	14.6			
							(1.5%)	(1.1%)	
33	Birch lignin	Ru/Al <sub>2</sub> O <sub>3</sub>	H <sub>2</sub> O	250	7	20.7			
							(4.4%)	(3.6%)	
34	Birch lignin	-	H <sub>2</sub> O	250	7	1.4	-	-	
35	Birch lignin	Ru/C	H <sub>2</sub> O	250	30	51.5			83
							(30.5%)	(10.4%)	

### 1.4.2 Non-noble metal catalysts in lignin reductive depolymerization

The activity of the noble metal in hydrogenation is generally high, but the cost and recyclability are still big issue. One technique to solve this problem is development of non-noble metal catalysts with low cost. Nickel (Ni) is one of the non-noble metal that good at the hydrogen activation with low activation energy.<sup>84,85</sup> Some Ni-based catalyst

are ferromagnetic catalysts, can be easily separated from the carbohydrate pulp after reaction which is convenient for catalyst recycling. Therefore, nickel as a non-precious metal has been widely applied as a hydrogenation catalyst for lignin (Table 1.2, Entries 1-8).<sup>86-94</sup> Raney Ni as pure metal form shows good activity with a monomer yield 27.3% in the mixture of dioxane and H<sub>2</sub>O with NaOH as a co-catalyst (Table 1.2, Entries 1).<sup>88</sup> To improve the activity of Raney Ni, Raney Ni and a zeolite H-USY (H-USY/Raney Ni) catalytic system was developed. It is believed that the zeolite acted as the Brønsted and/or Lewis acid for improved acidic solvolysis and dehydration (Table 1.2, Entries 2,3).<sup>86</sup>

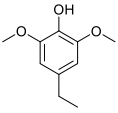
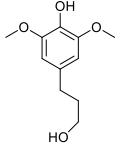
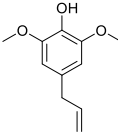
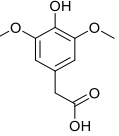
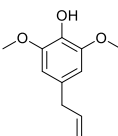
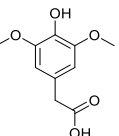
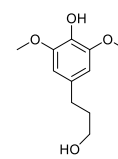
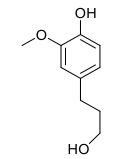
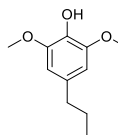
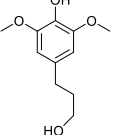
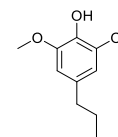
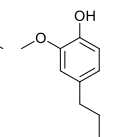
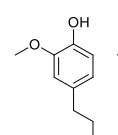
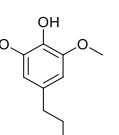
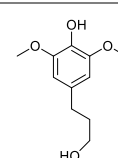
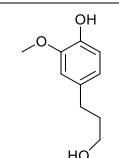
Nickel nanoparticles supported on carbon (Ni/C) has been studied as catalyst for lignocelluloses depolymerization in different solvents. Similar to the process using noble metal catalysts, MeOH is the most effective solvent in lignocelluloses depolymerization. Using a Ni/C catalyst in a MeOH-H<sub>2</sub>O co-solvent, catalytic fractionation of beech sawdust has also been reported. The total monomer yield increased from 39.3 wt % to 51.4 wt % when 40 vol % water was added to pure MeOH (Table 1.2, Entries 8).<sup>92</sup> Other solvents such as hydrofurfuryl alcohol (THFA) and 1,4-dioxane have been also investigated as solvent for lignin depolymerization and the yield of the lignin monomers is generally lower than that obtained in MeOH, albeit the quality of the formed cellulose is good (Table 1.2, Entries 1-8).<sup>87</sup> Different biomass sources with different structure, such as birch, bamboo, corn stover, produced different yield and monomers distribution (Table 1.2, Entries 4-8). The Ni/C not only be applied in the batch reactor, but also flowthrough reactor to continuously extract and depolymerize lignin into monomeric phenols (Table 1.2, Entries 9).<sup>95</sup>

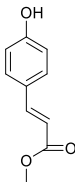
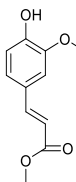
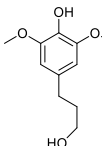
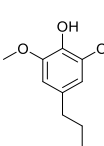
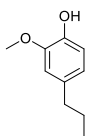
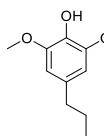
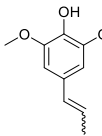
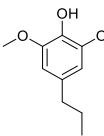
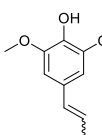
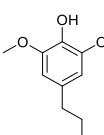
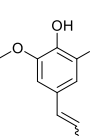
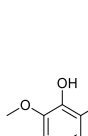
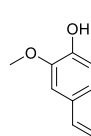
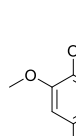
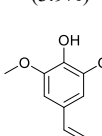
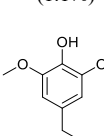
Other non-noble metal based catalyst such as Cu or Mo oxides have been also applied in the reductive lignin conversion.<sup>96,97</sup> Molybdenum oxide supported on carbon nanotubes (CNT) (MoOx/CNT) as the catalyst displayed good activity in reductive depolymerization of isolated lignin from hardwood (birch, eucalyptus and poplar), softwood (Pinus), and herbaceous crop (Miscanthus) (Table 1.2, Entries 12-16).<sup>97</sup> Cu-PMO, a porous metal oxide catalyst (PMO), can nearly completely convert lignin in the presence of H<sub>2</sub> in MeOH under mild conditions (Table 1.2, Entries 17, 18).<sup>96</sup>

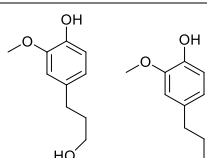
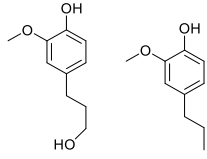
Table 1.2 Summary of lignin reductive depolymerization with non-noble metal catalysts

No.	Feedstock	Catalyst	Solvent	T/°C	P <sub>H<sub>2</sub></sub> /bar	Monomers yield/%	Yield of main monomers	Ref.
-----	-----------	----------	---------	------	---------------------------------	---------------------	------------------------	------



1	Maple	Raney Ni	Dioxane/ H <sub>2</sub> O+Na OH	225	213	27.3	 (15.4%)	 (6.2%)	88
2	Bamboo lignin	H-USY/ Raney Ni	MeOH/ H <sub>2</sub> O(7:3)	270	10	26.1	 (9.8%)	 (8.7%)	86
3	Bamboo lignin	Raney Ni	MeOH/ H <sub>2</sub> O(7:3)	270	10	12.9	 (3.6%)	 (3.7%)	
4	Beech THFA lignin	Ni/C	THFA/ Dioxane	220	20	14.7	 (9.3%)	 (2.7%)	87
5	Birch	Ni/C	MeOH	200	Ar	54	 (36.2%)	 (11.9%)	89
6	Birch	Ni/C	MeOH	200	N <sub>2</sub>	32	 (18%)	 (10%)	90
7	Miscanthus	Ni/C	MeOH	225	60	68	 (21%)	 (19%)	91
8	Beech	Ni/C	MeOH/ H <sub>2</sub> O	200	60	51.4	 (28.9%)	 (9.8%)	92

9	Corn stover	Ni/C	MeOH	200	30	24.5	 (8.7%)	 (7.2%)	93
10	Birch	Ni/Al <sub>2</sub> O <sub>3</sub>	MeOH	250	30	36	 (21%)	 (5%)	94
11	Poplar	Ni/C	MeOH	190	60	17.3	 (12.1%)	 (5.1%)	95
12	Birch lignin	MoOx/CN T	MeOH	260	30	47	 (22.2%)	 (6.1%)	
13	Eucalyptus	MoOx/CN T	MeOH	260	30	40	 (10.7%)	 (3.4%)	
14	Poplar	MoOx/CN T	MeOH	260	30	28	 (4.5%)	 (5.3%)	97
15	Pinus	MoOx/CN T	MeOH	260	30	13	 (3.9%)	 (1.1%)	
16	Miscanthus	MoOx/CN T	MeOH	260	30	25	 (11.6%)	 (2.4%)	

17	Candlenut lignin	Cu-PMO	MeOH	180	40	49.3		96
18	Candlenut lignin	Cu-PMO	MeOH	140	40	63.7	 (43.3%)	96

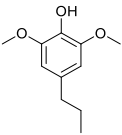
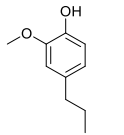
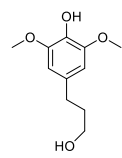
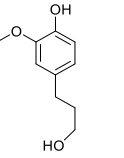
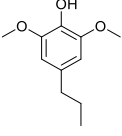
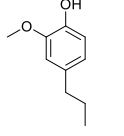
### 1.4.3 Alloy catalysts in lignin reductive depolymerization

To combine the low cost of earth abundant metals with the activity of noble metals, bimetallic alloys are popular. Usually, bimetallic alloys show significantly different catalytic activity and selectivity from monometallic analogues owing to synergistic effect.<sup>98,99</sup> Each component in the alloy catalysts is active in lignin hydrogenolysis, and the combination leads to overcoming the limitations of both noble metal and non-noble metal catalysts.

For the hydrogenolysis of lignin C-O bonds, bimetallic alloy which has the synergistic effect is superior over single-component catalysts.<sup>100</sup> An alloy Zn/Pd/C catalyst, which is more effective than Pd/C alone in hydrogenolysis of the  $\beta$ -O-4 lignin model compounds, resulted in 40 - 54% monomers yield from depolymerization of the native lignin (Table 1.3, Entry 1).<sup>101</sup>

As mentioned before, Ni is good at the hydrogen activation, therefore, bimetallic catalysts based on nickel have been prepared for lignin depolymerization. The synergistic effect were clearly demonstrated over Ni<sub>7</sub>Au<sub>3</sub> alloy catalyst (Table 1.3, Entry 2).<sup>102</sup> Other than single component catalyst, bimetallic Ni-M catalysts (M = precious metals) have been also studied for lignin depolymerization. Ni and Fe were combined as the non-precious bimetallic on activated carbon Ni-Fe/AC (activated carbon) catalysts obtained 39.5% monomers yield under the conditions of 200 °C, 2 MPa H<sub>2</sub> and 6 h (Table 1.3, Entry 3) Here the iron oxide provided acid sites which promoted the deoxygenation ability.<sup>103</sup>

Table 1.3 Summary of lignin reductive depolymerization with alloy catalysts

No.	Feedstock	Catalyst	Solvent	T/°C	P <sub>H<sub>2</sub></sub> /bar	Monomers yield/%	Yield of main monomers		Ref.
1	Poplar	Zn/Pd/C	MeOH	225	34.5	54			101
							(29.7%)	(24.3%)	
2	Birch lignin	Ni <sub>7</sub> Au <sub>3</sub>	H <sub>2</sub> O/ NaOH	160	10	10.9			102
							(6.05%)	(1.95%)	
3	Birch	NiFe/C	MeOH	200	20	39.5			103
							(23.70%)	(11.06%)	

A catalytic process takes place only on the surface of a catalyst. For traditional alloy catalysts in aggregated form, only active species on the catalyst surface can directly interact with substrates resulting in low atomic efficiency as the majority of the catalyst inside being unable to participate in the interaction with the substrates (practically wasted). Single-atom alloy (SAA), a highly dilute alloy formed by doping small amounts of an active element (as single atoms) in the surface of a host metal (as clusters/NPs), can offer synergistic effect of the alloy and ultimately utilize the active metal atoms. It has been proposed and developed single-atom alloys (SAAs) for facile hydrogen dissociation, spillover, and reaction on Pd-doped Cu surfaces.<sup>105</sup> Between the minority and the majority elements in SAAs, it has been proposed that there is the weak wave function which results in a free-atom-like electronic structure, i.e. the d band of those atoms becomes atomically narrow, on the minority element.<sup>101</sup> For transition metals, the d-band center is a good measure of the ability of the atoms forming bonds to an adsorbate.<sup>106</sup> This free-atom-like electronic structure changed the activity and selectivity of the catalyst through changing electronic structure of the single atoms, i.e. changing the adsorption-desorption behavior of substrate molecules. Thus SAA is a design approach for unprecedented catalytic properties.

Despite the substantial success that has been achieved in reductive reactions with SAAs so far,<sup>107–109</sup> application of SAAs in the conversion of native lignin has been elusive. Since density functional theory (DFT) calculations combined with microkinetic modeling has already provided theoretical guidance for the design of highly active and selective Ni-based bimetallic SAAs for hydrodeoxygenation (HDO) of phenol,<sup>110</sup> it is possible to design an alloyed catalyst with the minority atoms modifying the electronic structure of local active sites through the ligand effect by lifting d-band centers of three nearest neighboring Ni–M–Ni atoms which can smoothly remove –OH group. It is therefore optimistic to believe that SAAs’s application in lignin depolymerization will unfold in the near future.

We summarized progress has been made in lignin reductive depolymerization with noble metal catalysts, non-noble metal catalysts and alloy catalysts. Future efforts should be made in real lignin conversion with some SAAs that have high activity, good selectivity and good recyclability. A special effort will be made in the replacement of noble metals by non-noble metal in the SAAs. Based on the success already achieved, based on the promising results already achieved, it is reasonable to expect that SAAs will find practical application in chemical conversion of lignocellulosic biomass in the near future

## 1.5 References

- (1) J. P. Dorian; H. T. Franssen; D. R. Simbeck. Global Challenges in Energy. *Energy Policy* **2006**, 34 (15), 1984–1991.
- (2) Z. Sun; B. Fridrich; A. de Santi; S. Elangovan; K. Barta. Bright Side of Lignin Depolymerization: Toward New Platform Chemicals. *Chem. Rev.* **2018**, 118 (2), 614–678.
- (3) W. Schutyser; T. Renders; S. Van Den Bosch; S.-F. F. Koelewijn; G. T. Beckham; B. F. Sels. Chemicals from Lignin: An Interplay of Lignocellulose Fractionation, Depolymerisation, and Upgrading. *Chem. Soc. Rev.* **2018**, 47 (3), 852–908.
- (4) C. O. Tuck; E. Pérez; I. T. Horváth; R. A. Sheldon; M. Poliakoff. Valorization of Biomass: Deriving More Value from Waste. *Science*. American Association for the Advancement of Science August 10, 2012, pp 695–699.
- (5) S. Dunn. Hydrogen Futures: Toward a Sustainable Energy System. *Int. J.*

- Hydrogen Energy* **2002**, 27 (3), 235–264.
- (6) R. Masel. Hydrogen Quick and Clean. *Nature* **2006**, 442 (7102), 521–522.
  - (7) A. Iulianelli; S. Liguori; J. Wilcox; A. Basile. Advances on Methane Steam Reforming to Produce Hydrogen through Membrane Reactors Technology: A Review. *Catal. Rev. - Sci. Eng.* **2016**, 58 (1), 1–35.
  - (8) L. Kaiwen; Y. Bin; Z. Tao. Economic Analysis of Hydrogen Production from Steam Reforming Process: A Literature Review. *Energy Sources, Part B: Economics, Planning and Policy*. Taylor and Francis Inc. February 1, 2018, pp 109–115.
  - (9) M. Hayashi; L. Hughes. The Fukushima Nuclear Accident and Its Effect on Global Energy Security. *Energy Policy* **2013**, 59, 102–111.
  - (10) M. Hayashi; L. Hughes. The Policy Responses to the Fukushima Nuclear Accident and Their Effect on Japanese Energy Security. *Energy Policy* **2013**, 59, 86–101.
  - (11) J. Rossmeisl; Z. W. Qu; H. Zhu; G. J. Kroes; J. K. Nørskov. Electrolysis of Water on Oxide Surfaces. *J. Electroanal. Chem.* **2007**, 607 (1–2), 83–89.
  - (12) T. E. Mallouk. *Water Electrolysis: Divide and Conquer*; 2013; Vol. 5.
  - (13) K. Zhang; M. Ma; P. Li; D. H. Wang; J. H. Park. Water Splitting Progress in Tandem Devices: Moving Photolysis beyond Electrolysis. *Advanced Energy Materials*. Wiley-VCH Verlag August 10, 2016.
  - (14) Y. Lan; Y. Lu; Z. Ren. Mini Review on Photocatalysis of Titanium Dioxide Nanoparticles and Their Solar Applications. *Nano Energy*. September 2013, pp 1031–1045.
  - (15) G. Marbán; T. Valdés-Solís. Towards the Hydrogen Economy? *Int. J. Hydrogen Energy* **2007**, 32 (12), 1625–1637.
  - (16) S. S. Penner. Steps toward the Hydrogen Economy. *Energy* **2006**, 31 (1 SPEC. ISS.), 33–43.
  - (17) A. Sartbaeva; V. L. Kuznetsov; S. A. Wells; P. P. Edwards. Hydrogen Nexus in a Sustainable Energy Future. *Energy Environ. Sci.* **2008**, 1 (1), 79–85.
  - (18) T. Maeda; V. Sanchez-Torres; T. K. Wood. Protein Engineering of Hydrogenase 3 to Enhance Hydrogen Production. *Appl. Microbiol. Biotechnol.* **2008**, 79 (1), 77–86.
  - (19) P. E. P. Koskinen; A. H. Kaksonen; J. A. Puhakka. The Relationship between Instability of H<sub>2</sub> Production and Compositions of Bacterial Communities within a Dark Fermentation Fluidized-Bed Bioreactor. *Biotechnol. Bioeng.* **2007**, 97 (4), 742–758.

- 
- (20) D. N. Tekucheve; A. A. Tsygankov. Combined Biological Hydrogen-Producing Systems: A Review. *Appl. Biochem. Microbiol.* **2012**, 48 (4), 319–337.
- (21) D. Chen; L. He. Towards an Efficient Hydrogen Production from Biomass: A Review of Processes and Materials. *ChemCatChem*. March 7, 2011, pp 490–511.
- (22) N. Q. Ren; L. Zhao; C. Chen; W. Q. Guo; G. L. Cao. A Review on Bioconversion of Lignocellulosic Biomass to H<sub>2</sub>: Key Challenges and New Insights. *Bioresource Technology*. Elsevier Ltd September 1, 2016, pp 92–99.
- (23) J. L. Contreras; J. Salmones; J. A. Colín-Luna; L. Nuño; B. Quintana; I. Córdova; B. Zeifert; et al. Catalysts for H<sub>2</sub> Production Using the Ethanol Steam Reforming (a Review). *Int. J. Hydrogen Energy* **2014**, 39 (33), 18835–18853.
- (24) C. Li; K. Suzuki. Process Design and Simulation of H<sub>2</sub>-Rich Gases Production from Biomass Pyrolysis Process. *Bioresour. Technol.* **2010**, 101 (1 SUPPL.), S86–S90.
- (25) V. K. Skoulou; P. Manara; A. A. Zabaniotou. H<sub>2</sub> Enriched Fuels from Co-Pyrolysis of Crude Glycerol with Biomass. *J. Anal. Appl. Pyrolysis* **2012**, 97, 198–204.
- (26) P. D. Vaidya; A. E. Rodrigues. Glycerol Reforming for Hydrogen Production: A Review. *Chemical Engineering and Technology*. October 2009, pp 1463–1469.
- (27) L. He; J. M. S. Parra; E. A. Blekkan; D. Chen. Towards Efficient Hydrogen Production from Glycerol by Sorption Enhanced Steam Reforming. *Energy Environ. Sci.* **2010**, 3 (8), 1046–1056.
- (28) L. He; D. Chen. Hydrogen Production from Glucose and Sorbitol by Sorption-Enhanced Steam Reforming: Challenges and Promises. *ChemSusChem* **2012**, 5 (3), 587–595.
- (29) G. Wu; C. Zhang; S. Li; Z. Huang; S. Yan; S. Wang; X. Ma; et al. Sorption Enhanced Steam Reforming of Ethanol on Ni-CaO-Al<sub>2</sub>O<sub>3</sub> Multifunctional Catalysts Derived from Hydrotalcite-like Compounds. *Energy Environ. Sci.* **2012**, 5 (10), 8942–8949.
- (30) A. Haryanto; S. Fernando; N. Murali; S. Adhikari. Current Status of Hydrogen Production Techniques by Steam Reforming of Ethanol: A Review. *Energy and Fuels*. September 2005, pp 2098–2106.
- (31) T. Kandaramath Hari; Z. Yaakob; N. N. Binitha. Aviation Biofuel from Renewable Resources: Routes, Opportunities and Challenges. **2014**.
- (32) A. W. Bhutto; K. Qureshi; R. Abro; K. Harijan; Z. Zhao; A. A. Bazmi; T. Abbas; et al. Progress in the Production of Biomass-to-Liquid Biofuels to Decarbonize the Transport Sector-Prospects and Challenges. *RSC Advances*. Royal Society of Chemistry March 29, 2016, pp 32140–32170.

- 
- (33) J. A. Turner. Sustainable Hydrogen Production. *Science* (80-. ). **2004**, 305 (5686), 972–974.
- (34) L. Schlapbach; A. Züttel. Hydrogen-Storage Materials for Mobile Applications. *Nature*. Nature Publishing Group November 15, 2001, pp 353–358.
- (35) K. Sordakis; C. Tang; L. K. Vogt; H. Junge; P. J. Dyson; M. Beller; G. Laurenczy. Homogeneous Catalysis for Sustainable Hydrogen Storage in Formic Acid and Alcohols. *Chemical Reviews*. American Chemical Society January 24, 2018, pp 372–433.
- (36) C. Fellay; P. J. Dyson; G. Laurenczy. A Viable Hydrogen-Storage System Based on Selective Formic Acid Decomposition with a Ruthenium Catalyst. *Angew. Chemie - Int. Ed.* **2008**, 47 (21), 3966–3968.
- (37) Y. Filinchuk; D. Chernyshov; A. Nevidomskyy; V. Dmitriev. High-Pressure Polymorphism as a Step towards Destabilization of LiBH<sub>4</sub>. *Angew. Chemie Int. Ed.* **2008**, 47 (3), 529–532.
- (38) M. Mohan; V. K. Sharma; E. A. Kumar; V. Gayathri. Hydrogen Storage in Carbon Materials—A Review. *Energy Storage* **2019**, 1 (2), e35.
- (39) M. Grasemann; G. Laurenczy. Formic Acid as a Hydrogen Source - Recent Developments and Future Trends. *Energy and Environmental Science*. Royal Society of Chemistry July 18, 2012, pp 8171–8181.
- (40) S. Moret; P. J. Dyson; G. Laurenczy. Direct Synthesis of Formic Acid from Carbon Dioxide by Hydrogenation in Acidic Media. *Nat. Commun.* **2014**, 5 (1), 1–7.
- (41) A. F. Dalebrook; W. Gan; M. Grasemann; S. Moret; G. Laurenczy. Hydrogen Storage: Beyond Conventional Methods. *Chem. Commun.* **2013**, 49 (78), 8735–8751.
- (42) J. M. Yan; X. B. Zhang; S. Han; H. Shioyama; Q. Xu. Iron-Nanoparticle-Catalyzed Hydrolytic Dehydrogenation of Ammonia Borane for Chemical Hydrogen Storage. *Angew. Chemie - Int. Ed.* **2008**, 47 (12), 2287–2289.
- (43) P. M. Modisha; C. N. M. Ouma; R. Garidzirai; P. Wasserscheid; D. Bessarabov. The Prospect of Hydrogen Storage Using Liquid Organic Hydrogen Carriers. *Energy and Fuels*. American Chemical Society April 18, 2019, pp 2778–2796.
- (44) P. Makowski; A. Thomas; P. Kuhn; F. Goettmann. Organic Materials for Hydrogen Storage Applications: From Physisorption on Organic Solids to Chemisorption in Organic Molecules. *Energy and Environmental Science*. 2009, pp 480–490.
- (45) D. Teichmann; W. Arlt; P. Wasserscheid; R. Freymann. A Future Energy Supply Based on Liquid Organic Hydrogen Carriers (LOHC). *Energy and*



- Environmental Science*. 2011, pp 2767–2773.
- (46) K. I. Fujita; Y. Tanaka; M. Kobayashi; R. Yamaguchi. Homogeneous Perdehydrogenation and Perhydrogenation of Fused Bicyclic N-Heterocycles Catalyzed by Iridium Complexes Bearing a Functional Bipyridonate Ligand. *J. Am. Chem. Soc.* **2014**, *136* (13), 4829–4832.
- (47) F. Sotoodeh; B. J. M. Huber; K. J. Smith. The Effect of the N Atom on the Dehydrogenation of Heterocycles Used for Hydrogen Storage. *Appl. Catal. A Gen.* **2012**, *419–420*, 67–72.
- (48) T. L. Bezerra; A. J. Ragauskas. A Review of Sugarcane Bagasse for Second-Generation Bioethanol and Biopower Production. *Biofuels, Bioprod. Biorefining* **2016**, *10* (5), 634–647.
- (49) Y. Sun; J. Cheng. Hydrolysis of Lignocellulosic Materials for Ethanol Production: A Review. *Bioresour. Technol.* **2002**, *83* (1), 1–11.
- (50) R. Chandra; H. Takeuchi; T. Hasegawa. Methane Production from Lignocellulosic Agricultural Crop Wastes: A Review in Context to Second Generation of Biofuel Production. *Renew. Sustain. Energy Rev.* **2012**, *16* (3), 1462–1476.
- (51) E. Shahbazali. Biorefinery: From Biomass to Chemicals and Fuels. *Green Process. Synth.* **2013**, *2* (1), 87–88.
- (52) C. G. Wilkerson; S. D. Mansfield; F. Lu; S. Withers; J.-Y. Park; S. D. Karlen; E. Gonzales-Vigil; et al. Monolignol Ferulate Transferase Introduces Chemically Labile Linkages into the Lignin Backbone. *Science (80-. )*. **2014**, *344* (6179), 90–93.
- (53) J. Zakzeski; P. C. A. Bruijninx; A. L. Jongerius; B. M. Weckhuysen. The Catalytic Valorization of Lignin for the Production of Renewable Chemicals. *Chem. Rev.* **2010**, *110*, 3552–3599.
- (54) F. M. Gírio; C. Fonseca; F. Carneiro; L. C. Duarte; S. Marques; R. Bogel-Lukasik. Hemicelluloses for Fuel Ethanol: A Review. *Bioresour. Technol.* **2010**, *101* (13), 4775–4800.
- (55) P. Mäki-Arvela; T. Salmi; B. Holmbom; S. Willför; D. Y. Murzin. Synthesis of Sugars by Hydrolysis of Hemicelluloses- A Review. *Chem. Rev.* **2011**, *111* (9), 5638–5666.
- (56) P. Azadi; O. R. Inderwildi; R. Farnood; D. A. King. Liquid Fuels, Hydrogen and Chemicals from Lignin: A Critical Review. *Renew. Sustain. Energy Rev.* **2013**, *21*, 506–523.
- (57) M. Yabushita; H. Kobayashi; A. Fukuoka. Catalytic Transformation of Cellulose into Platform Chemicals. *Appl. Catal. B Environ.* **2014**, *145*, 1–9.

- 
- (58) P. YANG; H. KOBAYASHI; A. FUKUOKA. Recent Developments in the Catalytic Conversion of Cellulose into Valuable Chemicals. *Chinese J. Catal.* **2011**, 32 (5), 716–722.
- (59) C. Amen-Chen; H. Pakdel; C. Roy. Production of Monomeric Phenols by Thermochemical Conversion of Biomass: A Review. *Bioresour. Technol.* **2001**, 79 (3), 277–299.
- (60) P. Azadi; O. R. Inderwildi; R. Farnood; D. A. King. Liquid Fuels, Hydrogen and Chemicals from Lignin: A Critical Review. *Renew. Sustain. Energy Rev.* **2013**, 21, 506–523.
- (61) S. Van den Bosch; W. Schutyser; S.-F. Koelewijn; T. Renders; C. M. Courtin; B. F. Sels. Tuning the Lignin Oil OH-Content with Ru and Pd Catalysts during Lignin Hydrogenolysis on Birch Wood. *Chem. Commun.* **2015**, 51 (67), 13158–13161.
- (62) Y. Mottiar; R. Vanholme; W. Boerjan; J. Ralph; S. D. Mansfield. Designer Lignins: Harnessing the Plasticity of Lignification. *Curr. Opin. Biotechnol.* **2016**, 37, 190–200.
- (63) M. V. Galkin; A. T. Smit; E. Subbotina; K. A. Artemenko; J. Bergquist; W. J. J. Huijgen; J. S. M. Samec. Hydrogen-Free Catalytic Fractionation of Woody Biomass. *ChemSusChem* **2016**, 9 (23), 3280–3287.
- (64) S. Van Den Bosch; T. Renders; S. Kennis; S. F. Koelewijn; G. Van Den Bossche; T. Vangeel; A. Deneyer; et al. Integrating Lignin Valorization and Bio-Ethanol Production: On the Role of Ni-Al<sub>2</sub>O<sub>3</sub> Catalyst Pellets during Lignin-First Fractionation. *Green Chem.* **2017**, 19 (14), 3313–3326.
- (65) P. Sudarsanam; R. Zhong; S. Van Den Bosch; S. M. Coman; V. I. Parvulescu; B. F. Sels. Functionalised Heterogeneous Catalysts for Sustainable Biomass Valorisation. *Chem. Soc. Rev.* **2018**, 47 (22), 8349–8402.
- (66) W. Schutyser; S. Van den Bosch; T. Renders; T. De Boe; S.-F. Koelewijn; A. Dewaele; T. Ennaert; et al. Influence of Bio-Based Solvents on the Catalytic Reductive Fractionation of Birch Wood. *Green Chem.* **2015**, 17 (11), 5035–5045.
- (67) M. A. Dasari; P. P. Kiatsimkul; W. R. Sutterlin; G. J. Suppes. Low-Pressure Hydrogenolysis of Glycerol to Propylene Glycol. *Appl. Catal. A Gen.* **2005**, 281 (1–2), 225–231.
- (68) A. Gutierrez; R. K. Kaila; M. L. Honkela; R. Slioor; A. O. I. Krause. Hydrodeoxygenation of Guaiacol on Noble Metal Catalysts. *Catalysis Today*. 2009, pp 239–246.
- (69) N. Yan; C. Zhao; P. J. Dyson; C. Wang; L. T. Liu; Y. Kou. Selective Degradation of Wood Lignin over Noble-Metal Catalysts in a Two-Step Process.

- ChemSusChem* **2008**, *1* (7), 626–629.
- (70) S. Van den Bosch; W. Schutyser; S.-F. Koelewijn; T. Renders; C. M. Courtin; B. F. Sels. Tuning the Lignin Oil OH-Content with Ru and Pd Catalysts during Lignin Hydrogenolysis on Birch Wood. *Chem. Commun.* **2015**, *51* (67), 13158–13161.
- (71) W. Schutyser; S. Van Den Bosch; T. Renders; T. De Boe; S. F. Koelewijn; A. Dewaele; T. Ennaert; et al. Influence of Bio-Based Solvents on the Catalytic Reductive Fractionation of Birch Wood. *Green Chem.* **2015**, *17* (11), 5035–5045.
- (72) F. Gao; J. D. Webb; H. Sorek; D. E. Wemmer; J. F. Hartwig. Fragmentation of Lignin Samples with Commercial Pd/C under Ambient Pressure of Hydrogen. *ACS Catal.* **2016**, *6* (11), 7385–7392.
- (73) S. Jonas Sävmarker. Lignin Depolymerization to Monophenolic Compounds in a Flow-through System. *Green Chem.* **2017**, *19*, 5767.
- (74) K. M. Torr; D. J. van de Pas; E. Cazeils; I. D. Suckling. Mild Hydrogenolysis of In-Situ and Isolated Pinus Radiata Lignins. *Bioresour. Technol.* **2011**, *102* (16), 7608–7611.
- (75) T. Renders; S. Van Den Bosch; T. Vangeel; T. Ennaert; S. F. Koelewijn; G. Van Den Bossche; C. M. Courtin; et al. Synergetic Effects of Alcohol/Water Mixing on the Catalytic Reductive Fractionation of Poplar Wood. *ACS Sustain. Chem. Eng.* **2016**, *4* (12), 6894–6904.
- (76) T. Renders; W. Schutyser; S. Van Den Bosch; S. F. Koelewijn; T. Vangeel; C. M. Courtin; B. F. Sels. Influence of Acidic (H<sub>3</sub>PO<sub>4</sub>) and Alkaline (NaOH) Additives on the Catalytic Reductive Fractionation of Lignocellulose. *ACS Catal.* **2016**, *6* (3), 2055–2066.
- (77) X. Huang; O. M. Morales Gonzalez; J. Zhu; T. I. Korányi; M. D. Boot; E. J. M. Hensen. Reductive Fractionation of Woody Biomass into Lignin Monomers and Cellulose by Tandem Metal Triflate and Pd/C Catalysis. *Green Chem.* **2017**, *19* (1), 175–187.
- (78) X. Huang; X. Ouyang; B. M. S. Hendriks; O. M. M. Gonzalez; J. Zhu; T. I. Korányi; M. D. Boot; et al. Selective Production of Mono-Aromatics from Lignocellulose over Pd/C Catalyst: The Influence of Acid Co-Catalysts. *Faraday Discuss.* **2017**, *202*, 141–156.
- (79) L. Shuai; M. T. Amiri; Y. M. Questell-Santiago; F. Héroguel; Y. Li; H. Kim; R. Meilan; et al. Formaldehyde Stabilization Facilitates Lignin Monomer Production during Biomass Depolymerization. *Science (80-. )*. **2016**, *354* (6310), 329–333.
- (80) L. Shuai; J. Luterbacher. Organic Solvent Effects in Biomass Conversion

- Reactions. *ChemSusChem*. Wiley-VCH Verlag January 21, 2016, pp 133–155.
- (81) Y. Shao; Q. Xia; L. Dong; X. Liu; X. Han; S. F. Parker; Y. Cheng; et al. Selective Production of Arenes via Direct Lignin Upgrading over a Niobium-Based Catalyst. *Nat. Commun.* **2017**, 8 (1), 1–9.
- (82) J. M. Pepper; P. Supathna. Lignin and Related Compounds. VI. A Study of Variables Affecting the Hydrogenolysis of Spruce Wood Lignin Using a Rhodium-on-Charcoal Catalyst. *Can. J. Chem.* **1978**, 56 (7), 899–902.
- (83) S. Van Den Bosch; W. Schutyser; R. Vanholme; T. Driessen; S. F. Koelewijn; T. Renders; B. De Meester; et al. Reductive Lignocellulose Fractionation into Soluble Lignin-Derived Phenolic Monomers and Dimers and Processable Carbohydrate Pulps. *Energy Environ. Sci.* **2015**, 8 (6), 1748–1763.
- (84) Y.-Y. Li; S.-L. Yu; W.-Y. Shen; J.-X. Gao. Iron-, Cobalt-, and Nickel-Catalyzed Asymmetric Transfer Hydrogenation and Asymmetric Hydrogenation of Ketones. *Acc. Chem. Res.* **2015**, 48 (9), 2587–2598.
- (85) M. Shevlin; M. R. Friedfeld; H. Sheng; N. A. Pierson; J. M. Hoyt; L.-C. Campeau; P. J. Chirik. Nickel-Catalyzed Asymmetric Alkene Hydrogenation of  $\alpha,\beta$ -Unsaturated Esters: High-Throughput Experimentation-Enabled Reaction Discovery, Optimization, and Mechanistic Elucidation. *J. Am. Chem. Soc.* **2016**, 138 (10), 3562–3569.
- (86) Y. Jiang; Z. Li; X. Tang; Y. Sun; X. Zeng; S. Liu; L. Lin. Depolymerization of Cellulolytic Enzyme Lignin for the Production of Monomeric Phenols over Raney Ni and Acidic Zeolite Catalysts. *Energy and Fuels* **2015**, 29 (3), 1662–1668.
- (87) X. Si; F. Lu; J. Chen; R. Lu; Q. Huang; H. Jiang; E. Taarning; et al. A Strategy for Generating High-Quality Cellulose and Lignin Simultaneously from Woody Biomass. *Green Chem.* **2017**, 19 (20), 4849–4857.
- (88) C. P. Brewer; L. M. Cooke; H. Hibbert. Studies on Lignin and Related Compounds. LXXXIV. The High Pressure Hydrogenation of Maple Wood: Hydrol Lignin. *J. Am. Chem. Soc.* **1948**, 70 (1), 57–59.
- (89) Q. Song; F. Wang; J. Cai; Y. Wang; J. Zhang; W. Yu; J. Xu. Lignin Depolymerization (LDP) in Alcohol over Nickel-Based Catalysts via a Fragmentation-Hydrogenolysis Process. *Energy Environ. Sci.* **2013**, 6 (3), 994–1007.
- (90) I. Klein; B. Saha; M. M. Abu-Omar. Lignin Depolymerization over Ni/C Catalyst in Methanol, a Continuation: Effect of Substrate and Catalyst Loading. *Catal. Sci. Technol.* **2015**, 5 (6), 3242–3245.
- (91) H. Luo; I. M. Klein; Y. Jiang; H. Zhu; B. Liu; H. I. Kenttämä; M. M. Abu-Omar.

- Total Utilization of Miscanthus Biomass, Lignin and Carbohydrates, Using Earth Abundant Nickel Catalyst. *ACS Sustain. Chem. Eng.* **2016**, 4 (4), 2316–2322.
- (92) J. Chen; F. Lu; X. Si; X. Nie; J. Chen; R. Lu; J. Xu. High Yield Production of Natural Phenolic Alcohols from Woody Biomass Using a Nickel-Based Catalyst. *ChemSusChem* **2016**, 9 (23), 3353–3360.
- (93) E. M. Anderson; R. Katahira; M. Reed; M. G. Resch; E. M. Karp; G. T. Beckham; Y. Románromán-Leshkov. Reductive Catalytic Fractionation of Corn Stover Lignin. **2016**.
- (94) S. Van Den Bosch; T. Renders; S. Kennis; S. F. Koelewijn; G. Van Den Bossche; T. Vangeel; A. Deneyer; et al. Integrating Lignin Valorization and Bio-Ethanol Production: On the Role of Ni-Al<sub>2</sub>O<sub>3</sub> Catalyst Pellets during Lignin-First Fractionation. *Green Chem.* **2017**, 19 (14), 3313–3326.
- (95) E. M. Anderson; M. L. Stone; R. Katahira; M. Reed; G. T. Beckham; Y. Román-Leshkov. Flowthrough Reductive Catalytic Fractionation of Biomass. *Joule* **2017**, 1 (3), 613–622.
- (96) K. Barta; G. R. Warner; E. S. Beach; P. T. Anastas. Depolymerization of Organosolv Lignin to Aromatic Compounds over Cu-Doped Porous Metal Oxides. *Green Chem.* **2014**, 16 (1), 191–196.
- (97) L. P. Xiao; S. Wang; H. Li; Z. Li; Z. J. Shi; L. Xiao; R. C. Sun; et al. Catalytic Hydrogenolysis of Lignins into Phenolic Compounds over Carbon Nanotube Supported Molybdenum Oxide. *ACS Catal.* **2017**, 7 (11), 7535–7542.
- (98) M. Sankar; N. Dimitratos; P. J. Miedziak; P. P. Wells; C. J. Kiely; G. J. Hutchings. Designing Bimetallic Catalysts for a Green and Sustainable Future. *Chem. Soc. Rev.* **2012**, 41 (24), 8099–8139.
- (99) Y. Wu; S. Cai; D. Wang; W. He; Y. Li. Syntheses of Water-Soluble Octahedral, Truncated Octahedral, and Cubic Pt-Ni Nanocrystals and Their Structure-Activity Study in Model Hydrogenation Reactions. *J. Am. Chem. Soc.* **2012**, 134 (21), 8975–8981.
- (100) J. Zhang; J. Teo; X. Chen; H. Asakura; T. Tanaka; K. Teramura; N. Yan. A Series of NiM (M = Ru, Rh, and Pd) Bimetallic Catalysts for Effective Lignin Hydrogenolysis in Water. *ACS Catal.* **2014**, 4 (5), 1574–1583.
- (101) T. Parsell; S. Yohe; J. Degenstein; T. Jarrell; I. Klein; E. Gencer; B. Hewetson; et al. A Synergistic Biorefinery Based on Catalytic Conversion of Lignin Prior to Cellulose Starting from Lignocellulosic Biomass. *Green Chem.* **2015**, 17 (3), 1492–1499.
- (102) H. Konnerth; J. Zhang; D. Ma; M. H. G. Precht; N. Yan. Base Promoted Hydrogenolysis of Lignin Model Compounds and Organosolv Lignin over Metal

- Catalysts in Water. *Chem. Eng. Sci.* **2015**, *123*, 155–163.
- (103) Y. Zhai; C. Li; G. Xu; Y. Ma; X. Liu; Y. Zhang. Depolymerization of Lignin: Via a Non-Precious Ni-Fe Alloy Catalyst Supported on Activated Carbon. *Green Chem.* **2017**, *19* (8), 1895–1903.
- (104) G. Kyriakou; M. B. Boucher; A. D. Jewell; E. A. Lewis; T. J. Lawton; A. E. Baber; H. L. Tierney; et al. Isolated Metal Atom Geometries as a Strategy for Selective Heterogeneous Hydrogenations. *Science* (80-. ). **2012**, *335* (6073), 1209–1212.
- (105) M. T. Greiner; T. E. Jones; S. Beeg; L. Zwiener; M. Scherzer; F. Girgsdies; S. Piccinin; et al. Free-Atom-like d States in Single-Atom Alloy Catalysts. *Nat. Chem.* **2018**, *10* (10), 1008–1015.
- (106) J. K. Nørskov; T. Bligaard; B. Hvolbæk; F. Abild-Pedersen; I. Chorkendorff; C. H. Christensen. The Nature of the Active Site in Heterogeneous Metal Catalysis. *Chemical Society Reviews*. Royal Society of Chemistry September 25, 2008, pp 2163–2171.
- (107) C. Yang; Z. Miao; F. Zhang; L. Li; Y. Liu; A. Wang; T. Zhang. Hydrogenolysis of Methyl Glycolate to Ethanol over a Pt-Cu/SiO<sub>2</sub> Single-Atom Alloy Catalyst: A Further Step from Cellulose to Ethanol. *Green Chem.* **2018**, *20* (9), 2142–2150.
- (108) X. Zhang; G. Cui; H. Feng; L. Chen; H. Wang; B. Wang; X. Zhang; et al. Platinum–Copper Single Atom Alloy Catalysts with High Performance towards Glycerol Hydrogenolysis. *Nat. Commun.* **2019**, *10* (1).
- (109) F. R. Lucci; M. T. Darby; M. F. G. Mattera; C. J. Ivimey; A. J. Therrien; A. Michaelides; M. Stamatakis; et al. Controlling Hydrogen Activation, Spillover, and Desorption with Pd-Au Single-Atom Alloys. *J. Phys. Chem. Lett.* **2016**, *7* (3), 480–485.
- (110) J. Zhou; W. An; Z. Wang; X. Jia. Hydrodeoxygenation of Phenol over Ni-Based Bimetallic Single-Atom Surface Alloys: Mechanism, Kinetics and Descriptor. *Catal. Sci. Technol.* **2019**, *9* (16), 4314–4326.

# **Chapter 2 A viable hydrogen-storage/delivery system with N-heterocycles by a versatile ruthenium catalyst**

## **Overview**

The chapter starts with an introduction to the situation of H<sub>2</sub> storage/delivery in order to provide some background information that allows a better understanding of the choice of the liquid organic hydrogen carriers (LOHCs) and catalytic system used in this work.

The results section commences with the hydrogenation and dehydrogenation of several pairs of N-heterocycles as the LOHCs. Optimization of the reaction conditions, including temperature and pressure, is presented. Lastly, to provide more information on the mechanism of the catalytic hydrogenation and dehydrogenation of N-heterocycles, multinuclear NMR studies have helped to identify key intermediates involved in the catalytic process. Based on these experimental observations, together with literature, a catalytic cycle is proposed.

## 2.1 Introduction

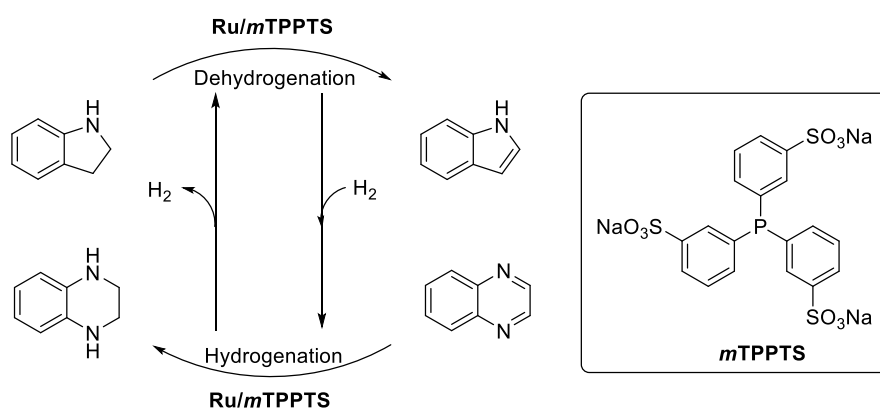
Hydrogen with high gravimetric energy density is foreseen to be a main environmental friendly energy carrier in the future.<sup>1</sup> A major problem is to find safe and suitable ways to store and deliver hydrogen with using of the existing energy infrastructure. Traditional hydrogen-storage methods, such as high-pressure gas containers and cryogenic liquid/gas containers, have weight and safety issues.<sup>2</sup> Consequently, researchers are developing chemicals and materials for hydrogen-storage, such as formic acid<sup>3,4</sup>, metal hydrides<sup>5</sup> and carbon nanostructures<sup>6</sup>. However, no entirely satisfactory options have been found so far. Using Liquid Organic Hydrogen Carrier (LOHC) compound is an promising attractive way to provide energy for mobile applications due to the similar energy storage volumetric densities and manageability as fossil fuels.<sup>7</sup> Compared with cycloalkanes, N-heterocycles have lower enthalpy changes  $\Delta H^0$  in dehydrogenation and hydrogenation reactions, thus N-heterocycles could be suitable candidates as LOHCs.<sup>8,9</sup>

Till now, the mostly used catalysts for the dehydrogenation of N-heterocycles are heterogeneous catalysts.<sup>10,11</sup> These heterogeneous systems usually require harsh reaction conditions and show poor functional-group tolerance. In addition, rational design and tuning of heterogeneous catalysts are difficult due to the lack of mechanistic information. On the other hand, homogeneous catalysts are rarely used in the hydrogenation and dehydrogenation of N-heterocycles.<sup>10,11</sup> If a catalyst can be applied for both hydrogenation and dehydrogenation, then there is no need for catalyst to separation. Therefore, homogeneous catalysts should be as good as heterogeneous catalysts with the respect to products separation. So far studies with iridium-based metal catalysts<sup>12-14</sup> and nickel-based catalysts have shown encouraging results in electrocatalytic hydrogen production,<sup>15</sup> albeit the reversibility and selectivity of the dehydrogenation and hydrogenation reactions are still insufficient. Among the most studied catalytic systems, homogeneous ruthenium phosphine catalysts are considered as highly active and robust catalytic systems in hydrogen production from formic acid.<sup>4,16,17</sup> However, they are not extended to the hydrogenation and dehydrogenation of N-heterocycles yet.

Encouraged by success in the dehydrogenation and hydrogenation activities shown by homogeneous phosphine ruthenium catalysts,<sup>18,19</sup> we planned to explore their potential



in catalytic dehydrogenation and hydrogenation of N-heterocycles. In the present work, we present herein an efficient, completely selective, and robust catalytic system for hydrogenation and dehydrogenation of a series of N-heterocycles using a homogeneous phosphine Ru(II) catalyst(Ru/*m*TPPTS) in which the Ru(II)-center are surrounded by meta-trisulfonated triphenylphosphine (*m*TPPTS) ligands. Due to the hydrophilic nature of the SO<sub>3</sub><sup>-</sup> group attached to the phosphine ligand, the resulting Ru(II) catalyst Ru/*m*TPPTS is highly soluble in aqueous solution, so that hydrogenation and dehydrogenation can be performed in a mixture of H<sub>2</sub>O and DMF solution. Hence, a “green” H<sub>2</sub> cycle could be achieved by hydrogenation and dehydrogenation of N-heterocycles (Scheme 2.1). By monitoring the reaction process and analyzing the reaction product using multi-nuclear nuclear magnetic resonance (NMR) spectroscopic analysis, a reaction mechanism has been proposed.



**Scheme 2.1** H<sub>2</sub> cycle proposed as a hydrogen-storage/delivery system.

## 2.2 Results and discussion

Initially we investigated the catalytic activity of Ru/*m*TPPTS for dehydrogenation of indoline (indoline –H<sub>2</sub>→ indole) and hydrogenation of indole (indole + H<sub>2</sub>→ indoline). To determine the optimum conditions for dehydrogenation of indoline using Ru/*m*TPPTS catalyst, a series catalytic reactions were performed at temperature between 80 and 140 °C using H<sub>2</sub>O/DMF binary solvent with different H<sub>2</sub>O to DMF ratios (Figure 2.1). It was found that the yield increase with the increase of the

temperature because the dehydrogenation reaction is endothermic. The dehydrogenation of indoline is faster when low ratio of H<sub>2</sub>O to DMF in the binary solvent is applied. The reason the slower reaction rate with higher H<sub>2</sub>O percentage is that the solubility of indoline in H<sub>2</sub>O is low.

Once the protocol for the Ru/*m*TPPTS-catalyzed hydrogenation and dehydrogenation of N-heterocycles was demonstrated, we became interested in carrying out the reverse of the dehydrogenation process with the same Ru/*m*TPPTS catalyst. For this purpose, a series of catalytic hydrogenation reactions of indole were carried out. At low pressure of 5 bar H<sub>2</sub> at 80 °C, hydrogenation of indole afforded less than 10% conversion. However, at high pressure of H<sub>2</sub> pressure 25 bar, almost quantitative (95%) hydrogenation of indole can be achieved (Figure 2.1). Under all of the pressures, the aromatic ring in the indoline remained intact after the reaction.

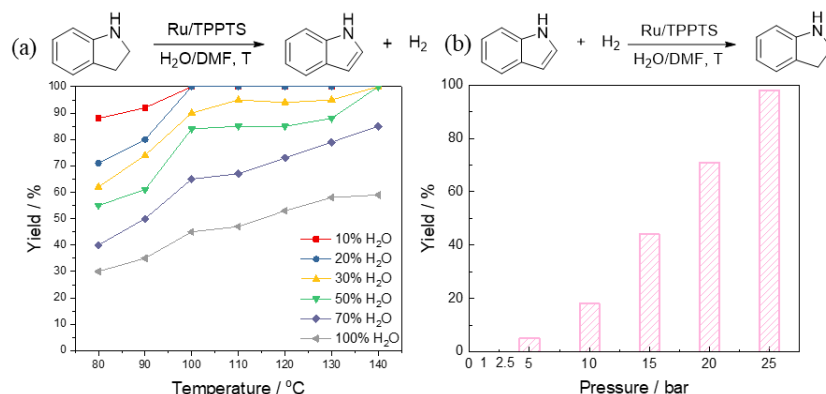


**Figure 2.1** (a) Dehydrogenation of indoline at different temperatures and different H<sub>2</sub>O concentration. Reaction conditions: Ru/*m*TPPTS 0.02 mmol, indoline 0.2 mmol, H<sub>2</sub>O/DMF 1.5 ml, 18 h; (b) Hydrogenation of indole at different H<sub>2</sub> pressures. Reaction conditions: Ru/*m*TPPTS 0.02 mmol, indoline 0.2 mmol, 20% H<sub>2</sub>O/DMF (20%v/v) 1.5 ml, 80 °C, 18 h. solid points: experiment data, line: curve for visualize tendency

Kinetic experiments of dehydrogenation of indoline and hydrogenation of indole were performed in high-pressure sapphire NMR tubes. The reaction progress was monitored by recording the *in-situ* <sup>1</sup>H NMR spectroscopy (Figure 2.2, 2.3). Without string, the reaction rate of hydrogenation and dehydrogenation in NMR tube should be slower than those performed in reactors. The intensity of the characteristic peaks at centered at 3.5

and 3.0 ppm representing the  $-\text{CH}_2\text{CH}_2$  in the indoline molecules decreases with time indicating the gradual dehydrogenation (Figure 2.2). As the opposite, the characteristic peaks at centered at 3.5 and 3.0 ppm increases with time representing the  $-\text{CH}_2\text{CH}_2$  indicating the gradual hydrogenation (Figure 2.3).

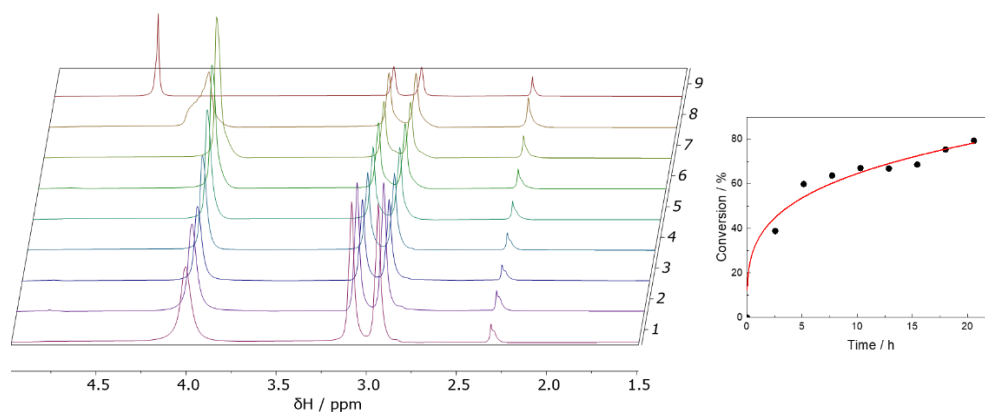


**Figure 2.2** Kinetic traces of dehydrogenation of indoline. Reaction conditions: Ru/*m*TPPTS 0.02 mmol, indoline 0.2 mmol,  $\text{H}_2\text{O}/\text{DMF-d}_6$  (20%v/v) 2.0 ml, 120 °C. solid points: experiment data, line: curve for visualize tendency

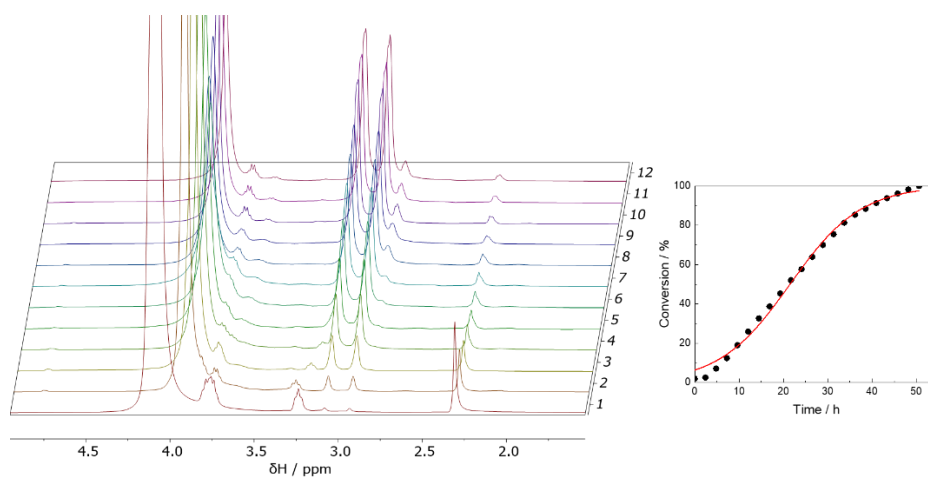


**Figure 2.3** Kinetic traces of hydrogenation of indole. Reaction conditions: Ru/*m*TPPTS 0.02 mmol, indoline 0.2 mmol, 20%  $\text{H}_2\text{O}/\text{DMF-d}_6$  (20%v/v) 2.0 ml, 70 °C, 15 bar. solid points: experiment data, line: curve for visualize tendency

We also investigated the influence of different phosphine ligands. Under the same conditions, Ru(II) with phosphine ligands, including meta-disulfonated

triphenylphosphine (*m*TPPDS), meta-monosulfonated triphenylphosphine (*m*TPPMS) and triphenylphosphine (PPh<sub>3</sub>) shows similar activity, and all the yields are more than 95% (Figure 2.4).

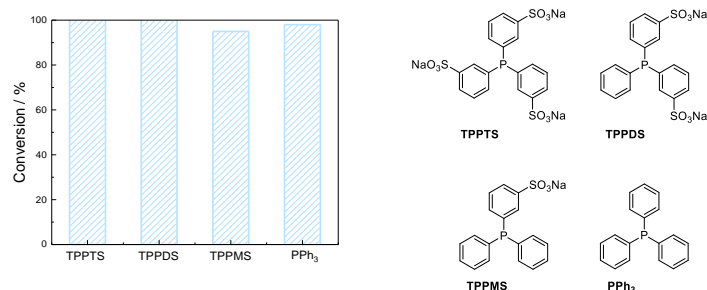


**Figure 2.4** Influence of the different phosphine ligands on the catalytic activity of the Ru(II) complexes in the dehydrogenation of indoline. Reaction conditions: Ru/*m*TPPTS 0.02 mmol, indoline 0.2 mmol, H<sub>2</sub>O/DMF (20%v/v) 1.5 ml, 18 h.

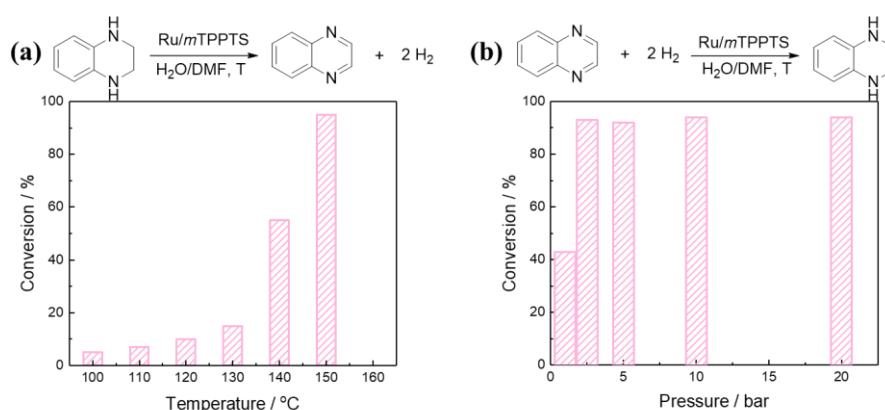


**Figure 2.5** (a) Dehydrogenation of 1,2,3,4-Tetrahydroquinoxaline at different temperatures and different H<sub>2</sub>O concentration. Reaction conditions: Ru/*m*TPPTS 0.02 mmol, 1,2,3,4-Tetrahydroquinoxaline 0.2 mmol, H<sub>2</sub>O/DMF (20%v/v) 1.5 ml, 18 h; (b) Hydrogenation of quinoxaline at different H<sub>2</sub> pressures. Reaction conditions: Ru/*m*TPPTS 0.02 mmol, quinoxaline 0.2 mmol, 20% H<sub>2</sub>O/DMF 1.5 ml, 80 °C, 18 h.

As following, we extend this catalytic system to more N-heterocycles couples. Catalytic dehydrogenation of 1,2,3,4-tetrahydroquinoxaline, containing two amine moieties in the same molecule, proceeded smoothly to yield the desired quinoxaline derivative as the sole product. With Ru/*m*TPPTS in 20%H<sub>2</sub>O/DMF, the yield for the dehydrogenation of 1,2,3,4-tetrahydroquinoxaline at 150 °C is 93%, and the yield for the hydrogenation of quinoxaline at 80 °C and 2.5 bar H<sub>2</sub> is 94%.

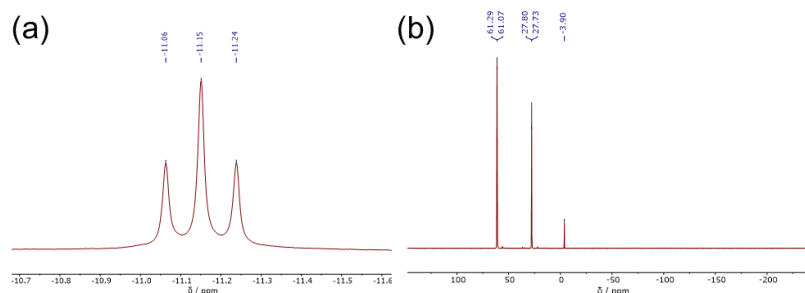
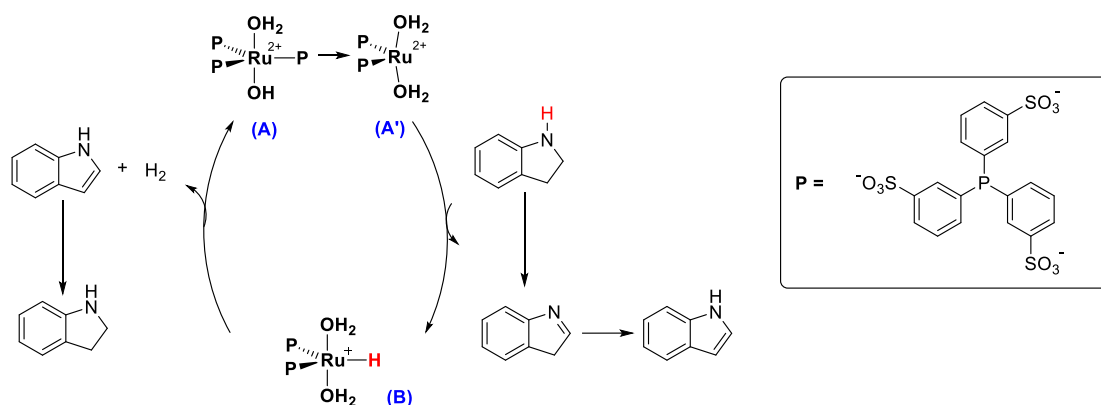


**Figure 2.6** (a)  $^1\text{H}$  (hydride region) and (b)  $^{31}\text{P}$  NMR spectrum after 2h, Ru/*m*TPPTS under 15 bar  $\text{H}_2$



**Scheme 2.2** Proposed catalytic pathway for the hydrogenation of indole and dehydrogenation of indoline

Inspired by the previous work of our group,<sup>4,17</sup> a possible catalytic pathway for the hydrogenation and dehydrogenation of N-heterocycles with Ru/*m*TPPTS is outlined in Scheme 2.2. By mixing  $\text{RuCl}_3$  with *m*TPPTS ligand in  $\text{H}_2\text{O}$ , a complex Ru/*m*TPPTS (A) is formed immediately. Upon the interaction of (A) with indoline, a dissociation of one *m*TPPTS ligand from the complex (A) occurred and an acceptorless dehydrogenation takes place yielding the dehydrogenated product indole and a ruthenium hydride B.<sup>20</sup> However, the presence of this Ru-hydride was clearly evidenced by *in-situ* NMR spectroscopy (Figure 2.4). The  $^1\text{H}$  NMR spectrum of this reaction mixture displays a triplet at  $\delta = -11.15$  ppm with a  $J(\text{HP})$  of 36 Hz, indicating a dissociation of one TPPTS ligand from the Ru/*m*TPPTS complex (A) and the formation of hydride (B) (Figure 2.5a). In the  $^{31}\text{P}$  NMR spectrum, a doublet peak at  $\delta = 61.07$  ppm with a  $J(\text{HP})$  of 36 Hz was observed along with a peak at  $-3.9$  ppm for the free

ligand TPPTS (the peak at 27.73 ppm represent the TPPTS oxide), a further evidence of the formation of the Ru-hydride intermediate (B). Both the  $^1\text{H}$  and  $^{31}\text{P}$  NMR shows the evidence that the Ru was surrounded by two equivalent TPPTS ligands. The large value of very large  $J(\text{HP})$  is typical for Ru(II)-hydride with phosphine ligands.<sup>21–23</sup>

Overall, the Ru(II) complex (A) can catalyze the dehydrogenation of N-heterocycles while the formed Ru-hydride (B) can catalyze the hydrogenation of N-heterocycles. To the best of our knowledge, this is the first example that a single Ru-based catalytic system capable of catalyzing both dehydrogenation and hydrogenation of N-heterocycles in one single system.

## 2.3 Conclusions

In summary, with Ru/*m*TPPTS as a versatile catalyst, achieved reversible dehydrogenation/hydrogenation of N-heterocycles herein provides an efficient method for hydrogen storage/delivery under mild conditions. Respective products from both dehydrogenation and hydrogenation reactions were formed with high conversions and yields. The catalyst is easily obtained in a simple method via mixing. Notably,  $\text{H}_2$  can easily be separated as the only gas phase. Without any gas phase by-product, the high purity  $\text{H}_2$  can be used directly in any types of fuel cells.

## 2.4 Methods

### 2.4.1 Materials and methods

All chemicals were purchased commercially from Aldrich, Fluka, Acros and Strem, and were used as received. NMR spectra were recorded on Bruker Avance DRX 400 MHz spectrometer.

#### Dehydrogenation/Hydrogenation

For dehydrogenation, a solution of 20% $\text{H}_2\text{O}/\text{DMF}$  (20%v/v, 1.5 mL) was placed in a Schlenk flask, containing  $\text{RuCl}_3 \cdot x\text{H}_2\text{O}$  (10.4 mg, 0.05 mmol), *m*TPPTS (85.3 mg, 0.15 mmol) and substrate (0.2 mmol). The solution was degassed and the reactor was purged with  $\text{N}_2$  for three times. Then it was placed into an oil bath, heated to 120 °C and the reactions were stirred for 18 h. After completion of the reaction, the flask was cooled

to room temperature, the mixture was extracted with diethyl ether (3x3 mL), and the combined extracts were analyzed by GS-MS.

For hydrogenation, a solution of 20% $\text{H}_2\text{O}/\text{DMF}$  (20%v/v, 1.5 mL) was added in a glass vial, containing  $\text{RuCl}_3 \cdot x\text{H}_2\text{O}$  (10.4 mg, 0.05 mmol), TPPTS (85.3 mg, 0.15 mmol) and substrate (0.2 mmol). The vial were fitted with cap and needle and then were placed into a 100 mL autoclave. The autoclave was purged three times with  $\text{H}_2$  and was then pressurized to 5 bar  $\text{H}_2$  pressure. Then it was placed into an aluminium block, heated to 80 °C and the reactions were stirred for 18 h. After completion of the reaction, the autoclave was cooled to room temperature, the mixture was extracted with diethyl ether (3x3 mL), and the combined extracts were analyzed by GS-MS.

The hydrogenation and dehydrogenation was also monitored by  $^1\text{H}$  NMR and  $^{31}\text{P}$  NMR spectroscopy, in which case the tube was heated directly in the spectrometer. The temperature was determined before and after measurement using an external temperature probe.  $^1\text{H}$  NMR and  $^{31}\text{P}$  NMR spectra were taken every 2 hours and conversions were calculated by integration of the substrates and products.

#### 2.4.2 Hydrogenation and dehydrogenation cycle

For hydrogenation and dehydrogenation cycles, we started with dehydrogenation of indoline following the above method. The solution of 20% $\text{H}_2\text{O}/\text{DMF}$  (2 g) was placed in a Schlenk flask, containing  $\text{RuCl}_3 \cdot x\text{H}_2\text{O}$  (20.8 mg, 0.1 mmol), *m*TPPTS (170.6 mg, 0.30 mmol) and indoline (59.6 mg, 0.5 mmol). The Schlenk flask was vacuumed and purged with  $\text{N}_2$  for three times. Then it was placed into an oil bath, heated to 120 °C and the reactions were stirred for 18 h. After completion of the reaction, the flask was cooled to room temperature, the mixture was transferred to a glass vial. The vial were fitted with cap and needle and then were placed into a 100 mL autoclave. The autoclave was purged three times with  $\text{H}_2$  and was then pressurized to 50 bar  $\text{H}_2$  pressure. Then it was placed into an aluminium block, heated to 80 °C and the reactions were stirred for 18 h. After completion of the reaction, the autoclave was cooled to room temperature, the mixture was extracted with diethyl ether (3x3 mL), followed by analysis of a sample by GC-MS.

## 2.5 References

1. Sartbaeva, A., Kuznetsov, V. L., Wells, S. A. & Edwards, P. P. Hydrogen nexus in a sustainable energy future. *Energy Environ. Sci.* **1**, 79–85 (2008).
2. Schlapbach, L. & Züttel, A. Hydrogen-storage materials for mobile applications. *Nature* **414**, 353–358 (2001).
3. Sordakis, K. *et al.* Homogeneous Catalysis for Sustainable Hydrogen Storage in Formic Acid and Alcohols. *Chemical Reviews* **118**, 372–433 (2018).
4. Fellay, C., Dyson, P. J. & Laurenczy, G. A viable hydrogen-storage system based on selective formic acid decomposition with a ruthenium catalyst. *Angew. Chemie - Int. Ed.* **47**, 3966–3968 (2008).
5. Filinchuk, Y., Chernyshov, D., Nevidomskyy, A. & Dmitriev, V. High-Pressure Polymorphism as a Step towards Destabilization of LiBH<sub>4</sub>. *Angew. Chemie Int. Ed.* **47**, 529–532 (2008).
6. Mohan, M., Sharma, V. K., Kumar, E. A. & Gayathri, V. Hydrogen storage in carbon materials—A review. *Energy Storage* **1**, e35 (2019).
7. Modisha, P. M., Ouma, C. N. M., Garidzirai, R., Wasserscheid, P. & Bessarabov, D. The Prospect of Hydrogen Storage Using Liquid Organic Hydrogen Carriers. *Energy and Fuels* **33**, 2778–2796 (2019).
8. Makowski, P., Thomas, A., Kuhn, P. & Goettmann, F. Organic materials for hydrogen storage applications: From physisorption on organic solids to chemisorption in organic molecules. *Energy and Environmental Science* **2**, 480–490 (2009).
9. Teichmann, D., Arlt, W., Wasserscheid, P. & Freymann, R. A future energy supply based on Liquid Organic Hydrogen Carriers (LOHC). *Energy and Environmental Science* **4**, 2767–2773 (2011).
10. Fujita, K. I., Tanaka, Y., Kobayashi, M. & Yamaguchi, R. Homogeneous perdehydrogenation and perhydrogenation of fused bicyclic N-heterocycles catalyzed by iridium complexes bearing a functional bipyridonate ligand. *J. Am. Chem. Soc.* **136**, 4829–4832 (2014).
11. Sotoodeh, F., Huber, B. J. M. & Smith, K. J. The effect of the N atom on the dehydrogenation of heterocycles used for hydrogen storage. *Appl. Catal. A Gen.* **419–420**, 67–72 (2012).
12. Wu, J., Talwar, D., Johnston, S., Yan, M. & Xiao, J. Acceptorless dehydrogenation of nitrogen heterocycles with a versatile iridium catalyst. *Angew. Chemie - Int. Ed.* **52**, 6983–6987 (2013).



13. Ryohei Yamaguchi, Chikako Ikeda, Yoshinori Takahashi & Ken-ichi Fujita. Homogeneous Catalytic System for Reversible Dehydrogenation-Hydrogenation Reactions of Nitrogen Heterocycles with Reversible Interconversion of Catalytic Species. *J. Am. Chem. Soc.* **131**, 8410–8412 (2009).
14. Chakraborty, S., Brennessel, W. W. & Jones, W. D. A Molecular Iron Catalyst for the Acceptorless Dehydrogenation and Hydrogenation of N-Heterocycles. *J. Am. Chem. Soc.* **136**, 8564–8567 (2014).
15. Luca, O. R., Huang, D. L., Takase, M. K. & Crabtree, R. H. Redox-active cyclopentadienyl Ni complexes with quinoid N-heterocyclic carbene ligands for the electrocatalytic hydrogen release from chemical fuels. *New J. Chem.* **37**, 3402–3405 (2013).
16. Guerriero, A. *et al.* Hydrogen production by selective dehydrogenation of HCOOH catalyzed by Ru-biaryl sulfonated phosphines in aqueous solution. *ACS Catal.* **4**, 3002–3012 (2014).
17. Thevenon, A., Frost-Pennington, E., Weijia, G., Dalebrook, A. F. & Laurenczy, G. Formic acid dehydrogenation catalysed by tris(TPPTS) ruthenium species: Mechanism of the initial ‘fast’ cycle. *ChemCatChem* **6**, 3146–3152 (2014).
18. Federsel, C., Jackstell, R., Boddien, A., Laurenczy, G. & Beller, M. Ruthenium-catalyzed hydrogenation of bicarbonate in water. *ChemSusChem* **3**, 1048–1050 (2010).
19. Guerriero, A. *et al.* Hydrogen production by selective dehydrogenation of HCOOH catalyzed by Ru-biaryl sulfonated phosphines in aqueous solution. *ACS Catal.* **4**, 3002–3012 (2014).
20. Cui, X. *et al.* Selective Acceptorless Dehydrogenation of Primary Amines to Imines by Core–Shell Cobalt Nanoparticles. *Angew. Chemie Int. Ed.* **59**, 7501–7507 (2020).
21. Prechtl, M. H. G. *et al.* Synthesis and Characterisation of Nonclassical Ruthenium Hydride Complexes Containing Chelating Bidentate and Tridentate Phosphine Ligands. *Chem. - A Eur. J.* **13**, 1539–1546 (2007).
22. Sgro, M. J., Dahcheh, F. & Stephan, D. W. Synthesis and reactivity of ruthenium hydride complexes containing a tripodal aminophosphine ligand. *Organometallics* **33**, 578–586 (2014).
23. Lanorio, J. P., Mebi, C. A. & Frost, B. J. The Synthesis, Structure, and H/D Exchange Reactions of Water-Soluble Half-Sandwich Ruthenium(II) Hydrides of Indenyl and Dihydropentalenyl. *Organometallics* **38**, 2031–2041 (2019).



## Chapter 3 An efficient Pt nanoparticle-ionic liquid system for the hydrodeoxygenation of bio-derived phenols under mild conditions

### Overview

This chapter used a pseudo-homogeneous catalytic system for upgrading lignin derived phenols through hydrodeoxygenation (HDO). The pseudo-homogeneous catalytic system is formed by platinum nanoparticles (NPs) dispersed *in situ* in the ionic liquid (IL) [Emim]NTf<sub>2</sub> (1-Ethyl-3-methylimidazolium bis(trifluoromethylsulfonyl)imide) as well as in mixtures of [Emim]NTf<sub>2</sub> with a second IL, Lewis acid or Brønsted acid, but in the absence of additional stabilizers. The resulting NP/IL systems catalyze the hydrodeoxygenation of phenol under mild conditions (60 °C, 1.0 MPa H<sub>2</sub>), achieving full substrate conversion and high deoxygenation rate (over 95%) to cyclohexane and cyclohexene. The combination of [Emim]NTf<sub>2</sub> and [Bmim]PF<sub>6</sub> results in the best catalytic performance. The transformation of other substituted phenols and dimers such as catechol, guaiacol and diphenyl ether was studied in the Pt NP/[Emim]NTf<sub>2</sub>-[Bmim]PF<sub>6</sub> system and in most cases afforded cyclohexane in good yield.

This section is published as an article in *Green Chemistry* 19 (22), 5435-5441 (This article is part of the themed collection: 2017 Green Chemistry Hot Articles).

Graphic abstract:



### 3.1 Introduction

Bio-oil derived from lignocellulose biomass is a promising renewable liquid fuel that could substitute petroleum, although it cannot be used directly to replace diesel due to its lower heating value and thermal instability.<sup>1</sup> The heating value of bio-oil is less than half that of conventional fuels, with an energy density of 19 MJ/kg.<sup>2</sup> Because of the high oxygen content of bio-oil, upgrading by hydrodeoxygenation (HDO) could be beneficial, increasing the energy density and thermal stability.

In HDO reactions, the solvent has a pronounced effect on both the conversion rate and on the selectivity.<sup>3</sup> Therefore, an appropriate solvent is crucial for an efficient catalytic process. Many excellent aqueous- and organic phase catalytic systems for reducing phenolic compounds into alkanes have been reported.<sup>4,5</sup> However, the HDO of phenols in aqueous media is thermodynamically disfavored and additionally leads to the deactivation of heterogeneous catalysts due to the formation of carbon deposits on the catalysts' surface. These factors contribute to severe reaction conditions, resulting in high-energy consumption, even for the simplest compound, phenol. Since cyclohexanol is stable in aqueous solutions below 200 °C,<sup>6,7</sup> the formation of cyclohexane usually requires reaction temperatures above 200 °C, even in presence of a noble metal catalysts and under acidic conditions.<sup>8–10</sup> At reaction temperatures below 200 °C in aqueous media, the main products are cyclohexanol and cyclohexanone.<sup>7,11,12</sup> Noble metal catalysts in organic solvents give the desired selectivity below 150 °C,<sup>13,14</sup> but avoiding organic solvents would be advantageous. As an alternative to organic solvents, supercritical carbon dioxide (scCO<sub>2</sub>) has been used as a reaction medium for the HDO of phenol, which also allows lower reaction temperatures. Drawbacks for an industrial application are the modest preference of cyclohexane and involvement of high pressures.<sup>15,16</sup> Therefore, other solvents for the HDO of phenols are required, which ideally operate at low temperatures (<100 °C) and near-ambient pressures (1.0 MPa).

Ionic liquids (ILs) have been extensively investigated as solvents for the transformation of biomass into value-added products.<sup>17–19</sup> In downstream processes, the alkane products are essentially insoluble in the ILs, whereas the phenolic substrates are soluble. This is a clear advantages of a pseudo-homogeneous system which affords a biphasic system as the product is formed, shifting the reaction equilibrium towards to the product.

The NP/IL catalytic system is versatile on the hydrogenation processed.<sup>20–22</sup> The

reaction temperature for the HDO of phenol can be as low as 130 °C,<sup>23–26</sup> and clearly it would be advantageous to operate the reaction at lower temperatures. In our study we evaluated the performance of Pt NPs dispersed in ILs as a catalytic systems for the HDO of phenol (an abundant model/component of bio-oil).<sup>27</sup> The NPs were generated *in situ* and directly employed in the HDO of phenol under 1.0 MPa H<sub>2</sub> at 60 °C. To the best of our knowledge, this reaction has not previously been achieved under such mild reaction conditions. After optimization of the reaction conditions, the system was used to transform a series of more complex phenolic compounds and to the hydrogenolysis of C-O bonds.

## 3.2 Results and discussion

### 3.2.1 Characterizations of Pt NPs

A series of Pt NP solutions were prepared from H<sub>2</sub>PtCl<sub>6</sub> in [Emim]NTf<sub>2</sub> or [Emim]NTf<sub>2</sub> containing a second IL, Lewis acid or Brønsted acid, using H<sub>2</sub> as the reductant (see Table 1). In most cases the NPs form rapidly, as evidenced by the solution turning black, which is as expected as [Emim]NTf<sub>2</sub> is an excellent stabilizer for metal NPs.<sup>28,29</sup> TEM analysis of Pt NPs extracted from the [Emim]NTf<sub>2</sub> IL reveals NPs with an average diameter of 3.4 nm (Figure 3.1). TEM images of the Pt NPs isolated from all the other solutions are shown in Figure 3.2-3.6. The average diameter of Pt NPs in the [Emim]NTf<sub>2</sub> containing a second IL are all between 3.4 nm to 3.9 nm which shows the stability of [Emim]NTf<sub>2</sub> as the stabilizer for the Pt NPs. With only [Bmim]PF<sub>6</sub>, the mean diameter of Pt NPs is 5.5 nm, and that is larger than the one in [Emim]NTf<sub>2</sub>. The precursors PtO<sub>2</sub> or Pt<sub>2</sub>(dba)<sub>3</sub> (dba = bis-dibenzylidene acetone) yield upon reduction in [Bmim]PF<sub>6</sub> at 75 °C Pt NPs with an average size of 2.5 nm without any large agglomerates.<sup>20,21</sup> The precursors can either react with hydrophobic or hydrophilic regions of imidazolium ILs and the different reaction temperature that are possible explanations for obtaining Pt NPs of various size.<sup>30–32</sup>

The XRD data (Figure 3.7a) indicate that the crystal type of the Pt NPs prepared in [Emim]NTf<sub>2</sub> is face-centered cubic (fcc), based on the diffraction peaks at 111, 200 and 220. Using the Sherrer equation the mean diameter of Pt NPs is estimated to be approximately 5.4 nm from the 220 diffraction line, somewhat larger than the value

obtained from TEM. From the XPS data (Figure 3.7b), the Pt NPs have two valence states, the expected reduced state, Pt(0), and a lesser amount of an oxidized state, i.e. PtO<sub>2</sub>. The full XPS pattern shows the presence of O and F, implying interactions between the IL and Pt NPs.

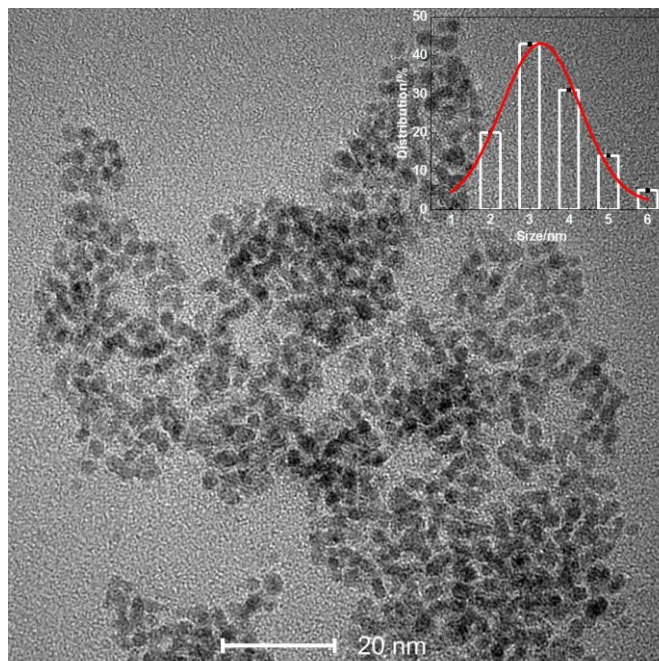


**Figure 3.1** TEM micrograph and histograms showing the size distribution of Pt NPs prepared in [Emim]NTf<sub>2</sub> ( $D_{\text{mean}} = 3.4$  nm)

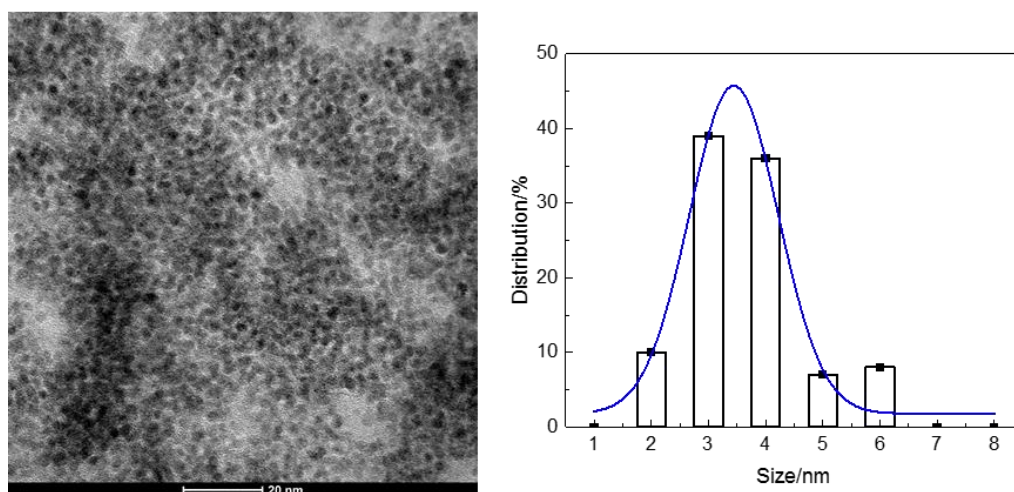


**Figure 3.2** TEM micrograph and histogram showing the size distribution of Pt NPs in [Emim]NTf<sub>2</sub>-[Bmmim]PF<sub>6</sub> ( $D_{\text{mean}} = 3.6$  nm)

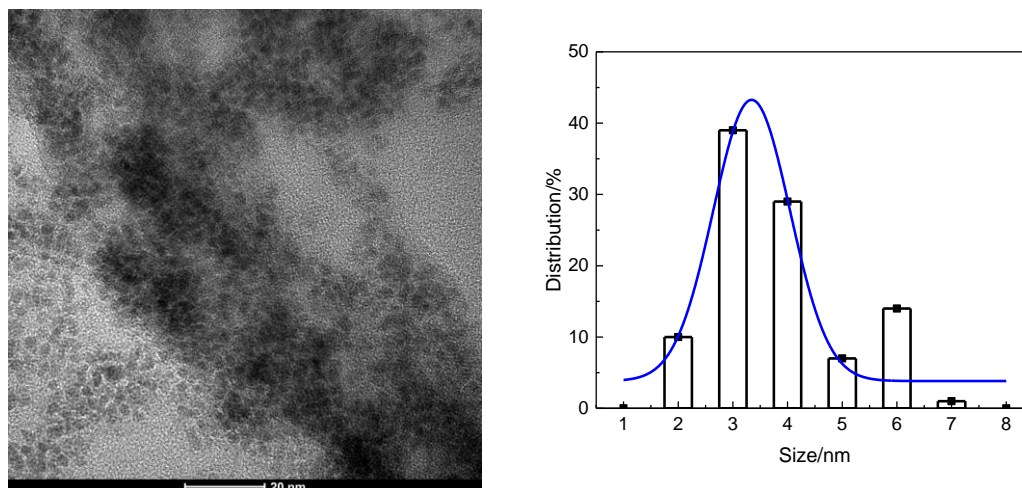


**Figure 3.3** TEM micrograph and histogram showing the size distribution of Pt NPs in [Emim]NTf<sub>2</sub>-[Bmpy]PF<sub>6</sub> ( $D_{\text{mean}} = 3.7$  nm)

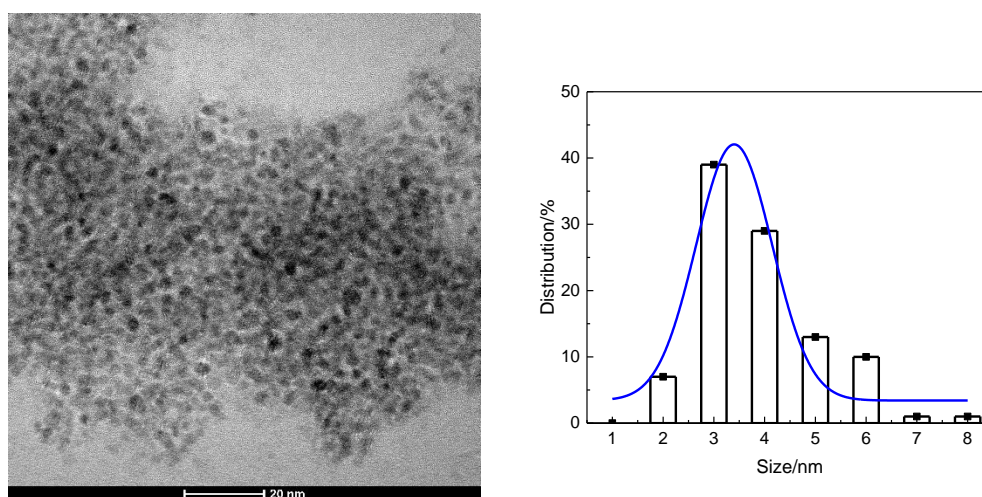


**Figure 3.4** TEM micrograph and histogram showing the size distribution of Pt NPs in [Emim]NTf<sub>2</sub>-[Bmim]OTf ( $D_{\text{mean}} = 3.5$  nm)



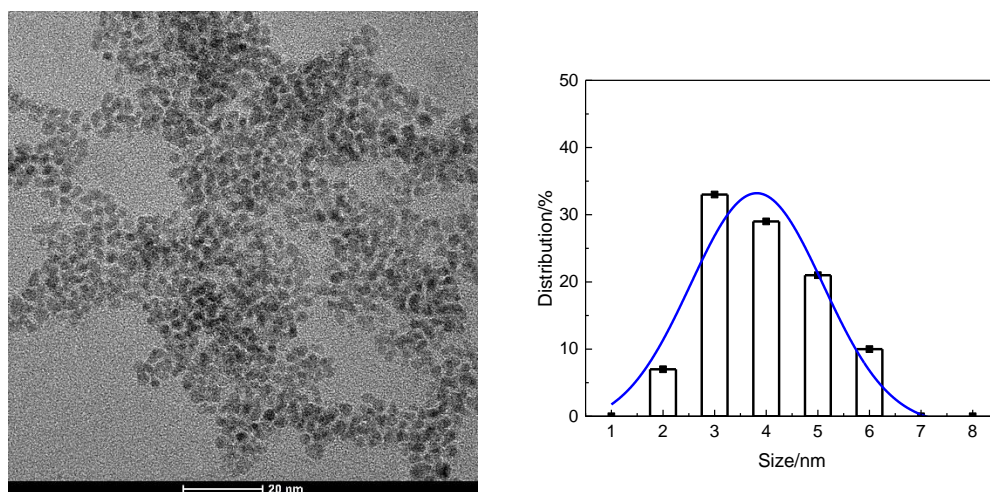


**Figure 3.5** TEM micrograph and histogram showing the size distribution of Pt NPs in [Emim]NTf<sub>2</sub>-[Bmim]BF<sub>4</sub> ( $D_{\text{mean}} = 3.9$  nm)

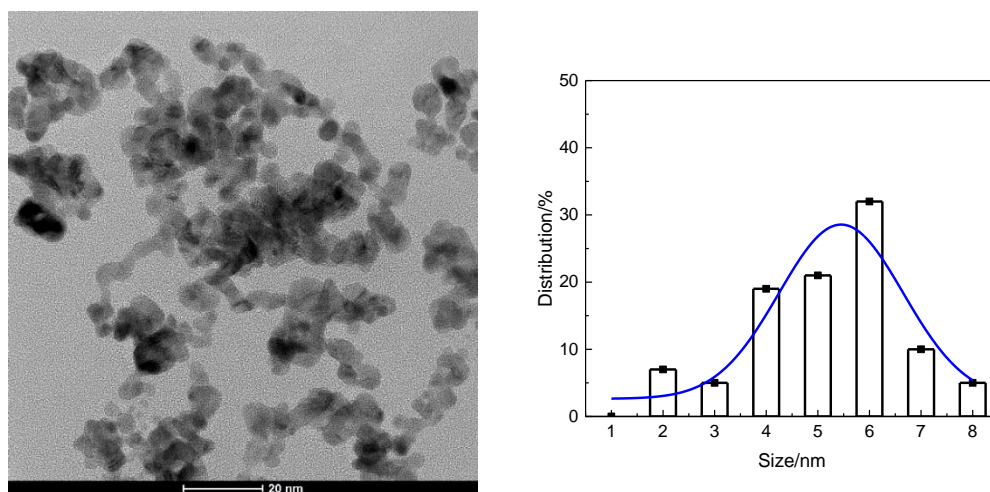


**Figure 3.6** TEM micrograph and histogram showing the size distribution of Pt NPs in [Bmim]PF<sub>6</sub> ( $D_{\text{mean}} = 5.5$  nm)

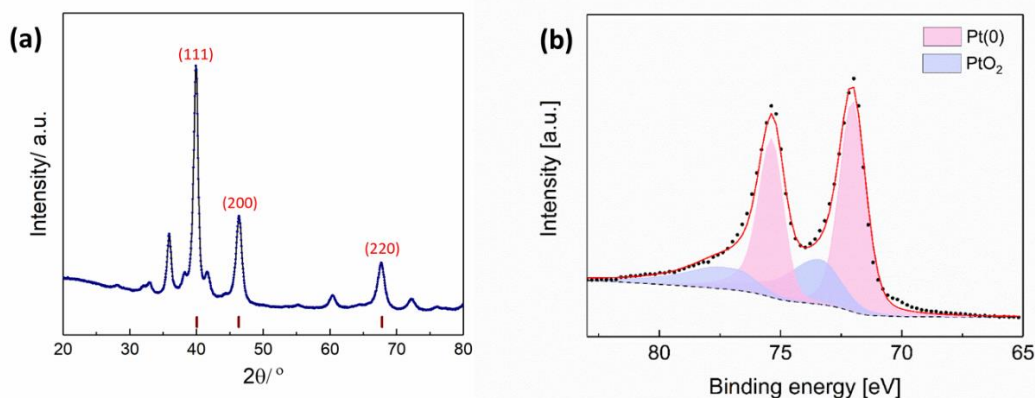


**Figure 3.7** (a) X-ray powder diffraction (XRD) of Pt NPs prepared in [Emim]NTf<sub>2</sub> (b) X-ray photoelectron spectroscopy (XPS) of Pt NPs prepared in [Emim]NTf<sub>2</sub>

### 3.2.2 Conversion of phenol

We evaluated the catalytic performance of the NP/IL systems in the HDO of phenol under 1.0 MPa of H<sub>2</sub> at 60 °C, for 15 h (Table 3.1). The reaction is highly depending on co-IL or acid used, although in most cases cyclohexane is obtained as the main product, accompanied by other C<sub>6</sub>-monoproducts such as cyclohexanol and cyclohexanone. Note that in the absence of Pt no reaction is observed (Table 3.1, entry 1). Cyclohexene is obtained in some of the reactions, i.e. those with a co-IL with a PF<sub>6</sub><sup>-</sup> or BF<sub>4</sub><sup>-</sup> anion (Table 3.1, entries 3, 4, 8, 13, 15, 16). Isolation of cyclohexene is probably due to its low solubility in the IL reaction medium, thus, once it is formed it is removed from the vicinity of the Pt NP catalyst and is not hydrogenated further. Differences in the solubility of substrates and partially hydrogenated products in ILs have previously been used to control reaction selectivity.<sup>24,33,34</sup> In addition, C<sub>12</sub>-dimers were detected in the reaction mixture, albeit at low yields. The formation of dimers presumably results from a stabilizing effect by the ILs on cyclohexyl cations which subsequently undergo dimerization via electrophilic aromatic substitution or aldol condensation reactions.<sup>23,35</sup>

The Pt NP/[Emim]NTf<sub>2</sub>-[Bmim]PF<sub>6</sub> system affords cyclohexane in highest yield, i.e. 86% together with 8% cyclohexene (Table 3.1, entry 3). The activity of this system is also superior to that of the well-studied heterogeneous catalysts Pt/C and Pt-Ni<sub>2</sub>P/C (Table 3.2, entries 4, 5). The Pt-Ni<sub>2</sub>P/C was synthesised followed by the reported method.<sup>36</sup> Compared to similar NP/IL catalytic systems, a reaction temperature of 60 °C as stated in this paper is lower than any reported previously.<sup>23,26</sup> Moreover, all in

literature described heterogeneous catalysts, also when based on noble metals, require reaction temperatures of over 130 °C for the same reaction.<sup>13,37–39</sup> The combination of the two hydrophobic anions,  $\text{Tf}_2\text{N}^-$  and  $\text{PF}_6^-$ , is critical and they presumably enhance the dehydration of cyclohexanol, facilitating the elimination of the water by-product. In [EMIM]OTf at 60 °C, NPs are not formed and the phenol is not converted (Table 3.1, entry 6), whereas at higher temperature of 130 °C, NPs formation takes place and some conversion of the substrate is observed (Table 3.1, entry 7).

As the Table 3.3 shows, after recycling once, the selectivity of cyclohexane is still high, while the conversion of phenol is decreasing. The inactivation of the catalyst may be caused by the increase of the size of the NPs after each reaction (Figure 3.8). The loss of NPs in each run may be another main reason.

Table 3.1 Yields of products and conversion of phenol over Pt NPs prepared in [Emim]NTf<sub>2</sub> with a second IL, Lewis acid or Brønsted acid

	ILs2/LA/BA	Con (%)	Selectivity (%)					DOR	TOF
			-ane	-ene	-nol	-one	Di		
1 <sup>a</sup>	[Bmim]PF <sub>6</sub>	0	0	0	0	0	0	0	0
2	-	100	45	0	53	1	1	45	1.5
3	[Bmim]PF <sub>6</sub>	100	86	8	0	0	6	94	2.9 (4.4) <sup>d</sup>
4 <sup>b</sup>	[Bmim]PF <sub>6</sub>	100	82	8	1	0	9	91	2.7
5	[Bmim]OTf	49	54	0	27	19	0	27	0.9
6 <sup>b</sup>	[Bmim]OTf	0	0	0	0	0	0	0	0
7 <sup>b,c</sup>	[Bmim]OTf	52	59	0	10	31	0	31	1.0
8	[Bmim]BF <sub>4</sub>	100	52	19	18	0	11	72	1.7
9 <sup>b</sup>	[Bmim]BF <sub>4</sub>	50	46	0	31	23	0	28	0.8
10	[Bmim]Cl	0	0	0	0	0	0	0	0
11 <sup>c</sup>	[Bmim]Cl	45	45	0	21	34	0	20	0.7
12	[Emim]OAc	0	0	0	0	0	0	0	0
13	[N(CH <sub>3</sub> ) <sub>4</sub> ]PF <sub>6</sub>	100	44	2	47	0	7	46	1.5
14	[N(CH <sub>3</sub> ) <sub>4</sub> ]ClO <sub>4</sub>	100	50	0	41	6	3	50	1.7
15	[Bmmim]PF <sub>6</sub>	100	61	13	17	3	6	84	2.0
16	[Bmpy]PF <sub>6</sub>	75	63	5	18	5	12	52	1.6
17	AlCl <sub>3</sub>	100	37	0	45	6		39	1.2
18	ZnCl <sub>2</sub>	100	43	0	36	0	21	44	1.5
19	Cu(OTf) <sub>2</sub>	10	71	12	0	0	17	9	0.2
20	H <sub>3</sub> PO <sub>4</sub>	100	56	0	42	0	2	56	1.9
21	HCl	55	45	0	39	15	1	25	0.8

ILs2: [Bmim]PF<sub>6</sub>; LA: Lewis acid; BA: Brønsted acid; Con: conversion; -ane: cyclohexane; -ene: cyclohexene; -nol: cyclohexanol; -one: cyclohexanone; Di: total dimers; DOR: deoxygenation rate. TOF: [mol cyclohexane]/[mol Pt][hour] and d: TOF for exposed metal site estimated according to ref 40<sup>40</sup>

a: without Pt; b: without [Emim]NTf<sub>2</sub>; c: 130 °C

Reaction conditions: [Emim]NTf<sub>2</sub> (2.0 g), ILs2/LA/BA (0.5 g/0.2 g/0.2 g), H<sub>2</sub>PtCl<sub>6</sub> (0.01 mmol), phenol (0.5 mmol), 1.0 MPa H<sub>2</sub>, 60 °C, 15 h. Reproducibility of results is ±5 %.

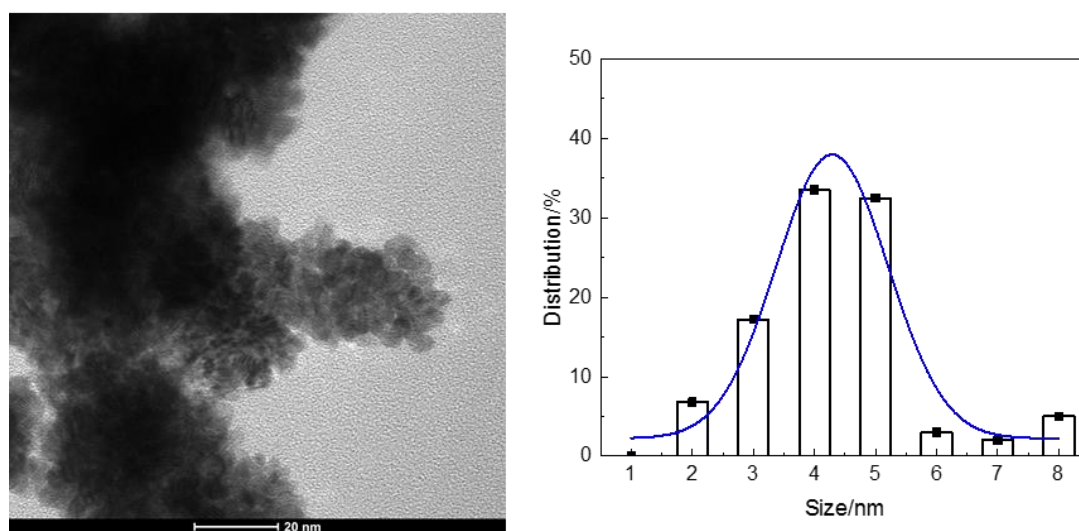
[Bmim]OTf: 1-Butyl-3-methylimidazolium trifluoromethanesulfonate; [Bmim]BF<sub>4</sub>: 1-Butyl-3-methylimidazolium tetrafluoroborate; [Bmim]Cl: 1-Butyl-3-methylimidazolium chloride; [Emim]OAc: 1-Ethyl-3-methylimidazolium acetate; [N(CH<sub>3</sub>)<sub>4</sub>]PF<sub>6</sub>: Tetraethylammonium hexafluorophosphate; [N(CH<sub>3</sub>)<sub>4</sub>]ClO<sub>4</sub>: Tetramethylammonium perchlorate; [Bmmim]PF<sub>6</sub>: 1-n-butyl-2,3-dimethylimidazolium hexafluorophosphate; [Bmpy]PF<sub>6</sub>: 1-butyl-4-methylpyridinium hexafluorophosphate.

Table 3.2 Yields of products and conversion of phenol over different NPs precursors in ILs

	NPs	Con (%)	Sel (%)				DOR
			-ane	-ene	-nol	-one	
1	H <sub>2</sub> PtCl <sub>6</sub>	100	86	8	0	0	94
2	K <sub>2</sub> PtCl <sub>4</sub>	100	63	18	13	0	81
3	PtO <sub>2</sub>	99	25	0	71	4	25
4	Pt/C	0	0	0	0	0	0
5	Pt-Ni <sub>2</sub> P/C	0	0	0	0	0	0
6	K <sub>2</sub> PdCl <sub>4</sub>	19	30	0	28	0	6
7	RuCl <sub>3</sub>	0	0	0	0	0	0
8	RhCl <sub>3</sub>	56	30	9	16	34	17

Con: conversion; Sel, selectivity; -ane: cyclohexane; -ene: cyclohexene; -nol: cyclohexanol; -one: cyclohexanone; DOR: deoxygenation rate

Reaction conditions: [Emim]NTf<sub>2</sub> (2.0 g), [Bmim]PF<sub>6</sub> (0.5 g), H<sub>2</sub>PtCl<sub>6</sub> (0.01 mmol), phenol (0.5 mmol), 1.0 MPa H<sub>2</sub>, 60 °C, 15 h. Reproducibility of results is  $\pm 5$  %.



**Figure 3.8** TEM micrograph and histogram showing the size distribution of Pt NPs after three times recycling in [Emim]NTf<sub>2</sub>-[Bmim]PF<sub>6</sub> ( $D_{\text{mean}} = 4.4$  nm)

Table 3.3 Catalyst recycling of Pt NPs/ILs for phenol

	Con (%)	Sel (%)						
		-ane	-ene	-nol	-one	Di-E	Bi-ane	Cy-one
1	100	86	8	0	0	5	1	0
2	71	84	5	0	0	7	2	2
3	53	84	5	2	0	5	1	3

Con: conversion; Sel, selectivity; -ane: cyclohexane; -ene: cyclohexene; -nol: cyclohexanol; -one: cyclohexanone; DOR: deoxygenation rate; Di-E: dicyclohexyl ether; Bi-ane: cyclohexylcyclohexane (bicyclohexane); Cy-one: cyclohexylcyclohexanone

---

Reaction conditions: [Emim]NTf<sub>2</sub> (2.0 g), [Bmim]PF<sub>6</sub> (0.5 g), H<sub>2</sub>PtCl<sub>6</sub> (0.01 mmol), phenol (0.5 mmol), 1.0 MPa H<sub>2</sub>, 60 °C, 15 h. Reproducibility of results is  $\pm 5$  %.

---

### 3.2.3 Influence of the IL anions

ILs are known to play a crucial role in dehydration step of HDO reactions, with performance of ILs is related to their acidity and hydrophobicity.<sup>18</sup> Hence, different combinations of cations and anions were evaluated (Table 3.1, entries 3-11). The performance of the ILs increases in the order: [Bmim]PF<sub>6</sub> > [Bmim]BF<sub>4</sub> > [Bmim]OTf >> [Bmim]Cl ~ [Emim]OAc. Essentially, the IL with the most hydrophobic anion, PF<sub>6</sub><sup>-</sup>, leads to the highest activity in combination with [Emim]NTf<sub>2</sub>. An obvious sign for that is that the ILs solutions (Table 3.1, entries 10, 12. [Bmim]Cl and [Emim]OAc) with the dissolved metal salt remain yellow, which indicates that no Pt NPs were formed and further, the conversion of phenol did not occur. The non-nucleophilic anions, Tf<sub>2</sub>N<sup>-</sup> or PF<sub>6</sub><sup>-</sup>, facilitate the formation of Pt NPs, since they interact only weakly with the Pt(IV) salt precursor, allowing reduction to take place, as noted previously.<sup>41</sup> Moreover, in keep with other studies, non-nucleophilic anions enable catalysts, surface of NP, as they can be displaced by the substrates more easily than strongly nucleophilic anions.<sup>42,43</sup>

Since both, Tf<sub>2</sub>N<sup>-</sup> and PF<sub>6</sub><sup>-</sup>, are hydrophobic and weak nucleophiles, it remains unclear why one outperforms the other. However, Katsyuba *et al.* revealed that the PF<sub>6</sub><sup>-</sup> anions form strong hydrogen bonds with the phenolic –OH groups on phenol,<sup>44</sup> which in consequence activates C–O bonds and facilitates hydrogenolysis. Another reason could be the formation of HF via partial decomposition of PF<sub>6</sub><sup>-</sup> in the presence of water,<sup>45</sup> which should, as a Brønsted acid, facilitate the dehydration step. The ESI-MS spectrum of the mixture after the reaction is shown in Figure 3.10. The peak found at 100.96 corresponds to the anion PO<sub>2</sub>F<sub>2</sub><sup>-</sup> (calc. 100.96), which would be the expected product of PF<sub>6</sub><sup>-</sup> after hydrolysis. Evaluation of a series of PF<sub>6</sub><sup>-</sup>-based ILs shows that the cation has little impact on the reaction Table 1, entries 13-16). Catalytic activity increases in the following order Bmim<sup>+</sup> > Bmmim<sup>+</sup> > N(CH<sub>3</sub>)<sub>4</sub><sup>+</sup> > Bmpy<sup>+</sup>. The small difference (< 25%) may be related to the hydrogen-bonding ability of the cation, with the acidic 2-proton in the Bmim<sup>+</sup> cation helping to activate the substrate.<sup>46</sup>

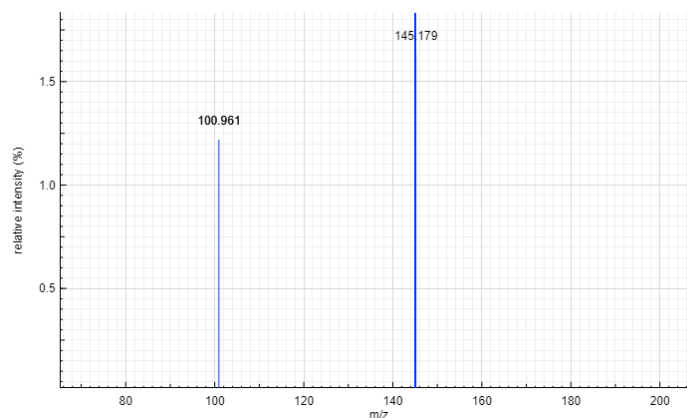


**Figure 3.9** The ESI-MS figure of the mixture after the reaction

### 3.2.4 Evaluation of acids as co-catalysts

The dehydration of cyclohexanol, which is apparently the rate-determining step,<sup>47,48</sup> usually proceeds more efficiently under acidic conditions. In addition, in the mechanism the keto/enol step is believed to require a considerably larger concentration of acid sites compared to the available metal sites for hydrogenation.<sup>6</sup> Therefore, we evaluated Lewis and Brønsted acid additives in the Pt NP/[Emim]NTf<sub>2</sub> catalytic system (Table 3.1, entries 17-21). None of the acids led to superior performances to the system containing [Bmim]PF<sub>6</sub>. This implies that the Pt NP/[Emim]NTf<sub>2</sub>-[Bmim]PF<sub>6</sub> system is sufficiently acidic so that the addition of further acid has little impact on the reaction. The reduction of the H<sub>2</sub>PtCl<sub>6</sub> results in the generation of HCl and consequently an intrinsically acid IL solution. Indeed, using other Pt salt precursors that do not generate acid upon reduction, e.g. PtO<sub>2</sub>, K<sub>2</sub>PtCl<sub>4</sub>, results in lower catalytic activities (Table 3.4).

In extension to the above work, further different metal NPs were tested for HDO of phenol to cyclohexane (Table 3.4). Based on our measurements, platinum is the best for HDO of phenol in terms of activity and yield, followed by rhodium, palladium, and ruthenium. The Pt NPs were more active than other metals, and provided the highest yield of cyclohexane. The reason for the inhibited activity of ruthenium is that RuCl<sub>3</sub> is not completely reduced at the given reaction conditions. In mechanistic terms, the decreased performance of Pd and Rh is directly linked to their ability to hydrogenate the aromatic ring of phenol.

The platinum salt precursors play a vital role in the reactions. Since the solubility of

H<sub>2</sub>PtCl<sub>6</sub> is the highest in ILs, the performance of H<sub>2</sub>PtCl<sub>6</sub> in HDO is better than K<sub>2</sub>PtCl<sub>4</sub> or PtO<sub>2</sub>. Our newly developed NPs/ILs systems has a notable better performance for hydrogenating phenol than the well-studied heterogeneous catalyst Pt/C and Pt-Ni<sub>2</sub>P/C. The Pt-Ni<sub>2</sub>P/C was synthesised followed by the reported method.<sup>36</sup>

Table 3.4 Yields of products and conversion of phenol over different NPs precursors in ILs

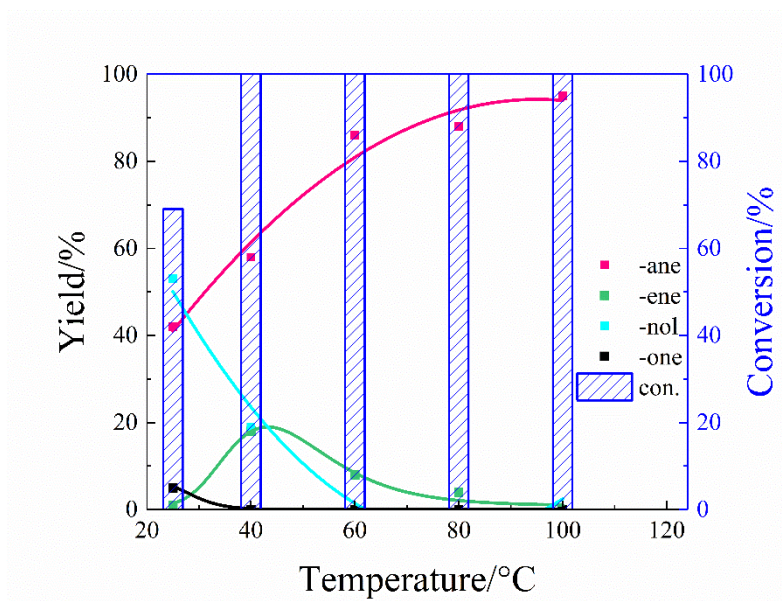
	NPs	Con (%)	Sel (%)				DOR
			-ane	-ene	-nol	-one	
1	H <sub>2</sub> PtCl <sub>6</sub>	100	86	8	0	0	94
2	K <sub>2</sub> PtCl <sub>4</sub>	100	63	18	13	0	81
3	PtO <sub>2</sub>	99	25	0	71	4	25
4	Pt/C	0	0	0	0	0	0
5	Pt-Ni <sub>2</sub> P/C	0	0	0	0	0	0
6	K <sub>2</sub> PdCl <sub>4</sub>	19	30	0	28	0	6
7	RuCl <sub>3</sub>	0	0	0	0	0	0
8	RhCl <sub>3</sub>	56	30	9	16	34	17

Con: conversion; Sel, selectivity; -ane: cyclohexane; -ene: cyclohexene; -nol: cyclohexanol; -one: cyclohexanone; DOR: deoxygenation rate

Reaction conditions: [Emim]NTf<sub>2</sub> (2.0 g), [Bmim]PF<sub>6</sub> (0.5 g), H<sub>2</sub>PtCl<sub>6</sub> (0.01 mmol), phenol (0.5 mmol), 1.0 MPa H<sub>2</sub>, 60 °C, 15 h. Reproducibility of results is ±5 %.

### 3.2.5 Reaction optimisation

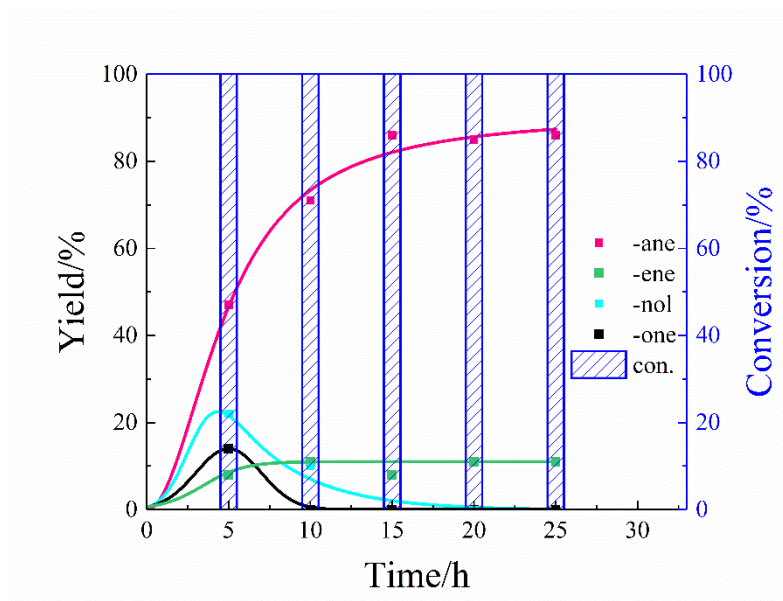
The Pt NP/[Emim]NTf<sub>2</sub>-[Bmim]PF<sub>6</sub> system was further optimized. The HDO of phenol to cyclohexane was executed within a temperature range from 25 °C to 100 °C, H<sub>2</sub> pressures ranging from 0.1 MPa to 10.0 MPa and reaction times from 5 h up to 25 h. Remarkably, even at room temperature (25 °C) the system catalyzes the HDO of phenol (Figure 3.10) at an acceptable rate. As the temperature is increased the yield of cyclohexane increases, reaching 96% at 100 °C.



**Figure 3.10** Yields of products and conversion of phenol over Pt NPs prepared in ILs ([Emim]NTf<sub>2</sub> (2.0 g), [Bmim]PF<sub>6</sub> (0.5 g), H<sub>2</sub>PtCl<sub>6</sub> (0.01 mmol), phenol (0.5 mmol), 1.0 MPa H<sub>2</sub>, 15 h. Reproducibility of results is  $\pm 5\%$ .) solid points: experiment data, line: curve for visualize tendency. -ane: cyclohexane; -ene: cyclohexene; -nol: cyclohexanol; -one: cyclohexanone; con.: conversion.

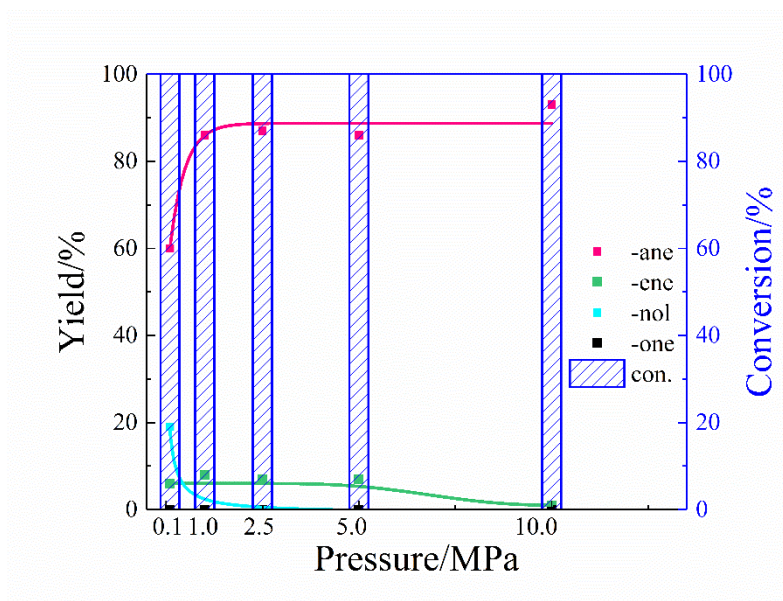
The hydrogenation products of phenol in Pt/ILs catalytic system is plotted in Figure 3.11 as a function of time at 60 °C and 1.0 MPa H<sub>2</sub>. The curve corresponding to the conversion of the substrate indicates that the Pt NP catalyst is generated in situ and consequently is not ideal for full analysis. In a first step, cyclohexanone and cyclohexanol are formed, then the ketone are rapidly hydrogenated to cyclohexanol. Subsequently, cyclohexanol dehydration directly leads to cyclohexene (acid catalysis) and ultimately metal-catalysed cyclohexene hydrogenation yields cyclohexane. Thus, cyclohexane became the major product with 86% selectivity.





**Figure 3.11** The products distributions and conversion of phenol over Pt NPs prepared in ILs ([Emim]NTf<sub>2</sub> (2.0 g), [Bmim]PF<sub>6</sub> (0.5 g), H<sub>2</sub>PtCl<sub>6</sub> (0.01 mmol), phenol (0.5 mmol), 1.0 MPa H<sub>2</sub>, 60 °C. Reproducibility of results is  $\pm 5\%$ .) solid points: experiment data, line: line: curve for visualize tendency.

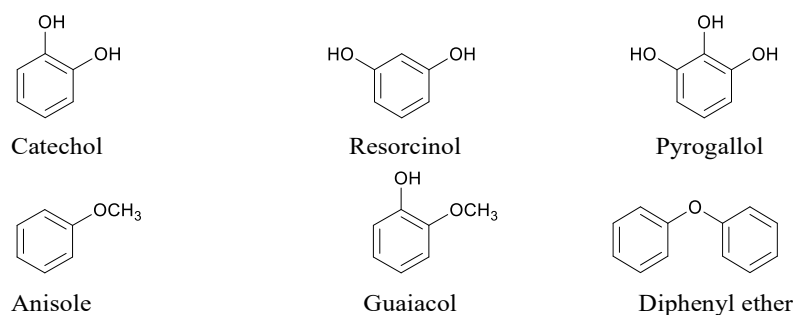
The catalytic activity was also studied as a function of the H<sub>2</sub> pressure (Figure 3.12). Even at 0.1 MPa H<sub>2</sub> the substrate was fully transformed although the selectivity to cyclohexane is lower than that observed at 1.0 MPa hydrogen pressure. At a pressure of 10.0 MPa only a slight increase in selectivity towards cyclohexane was observed. Although hydrogen gas solubility is low in ILs the rate of mass transfer of hydrogen into ILs seems to be fast,<sup>49</sup> showing why the hydrogen pressure has only minor influence on the reaction.



**Figure 3.12** Yields of products and conversion of phenol over Pt NPs prepared in ILs ([Emim]NTf<sub>2</sub> (2.0 g), [Bmim]PF<sub>6</sub> (0.5 g), H<sub>2</sub>PtCl<sub>6</sub> (0.01 mmol), phenol (0.5 mmol), 60 °C, 15 h. Reproducibility of results is  $\pm 5\%$ .) solid points: experiment data, line: line: curve for visualize tendency.

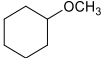
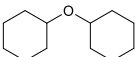
### 3.2.6 Substrate scope

A series of more complex substrates (Figure 3.13) with one or more hydroxyl or methoxide groups were evaluated. Catechol, for example, is one of the major components found in lignin depolymerisation products and bio-oil.<sup>50,51</sup> Aromatic alcohols with two or more hydroxyl groups such as catechol, resorcinol or pyrogallol were completely converted, showing a high selectivity for cyclohexane (Table 3.5). The number and position of phenolic hydroxyl groups does not reduce the catalytic activity of the Pt NP/[Emim]NTf<sub>2</sub>-[Bmim]PF<sub>6</sub> system.



**Figure 3.13** Substrates employed

Table 3.5 Yields of products and conversion of substituted phenol over Pt NPs in ILs

	Substrates	Con (%)	Sel (%)				TOF
			-ane	-ene	-nol	-one	
1	Benzene	100	93	7	0	0	3.1
2	Catechol	100	85	4	8	0	2.8
3	Resorcinol	100	85	5	2	0	2.8
4	Pyrogallol	100	83	8	2	0	2.8
			-ane	-ene	-nol		
5	Anisole	100	56	3	0	40	1.8
6	Guaiacol	38	62	5	0	21	0.8
			-ane	-ene	-nol		
7 <sup>a</sup>	Diphenyl ether	100	50	10	15	25	1.7
8	Diphenyl ether	100	68	11	6	13	2.3

Con: conversion; Sel, selectivity; -ane: cyclohexane; -ene: cyclohexene; -nol: cyclohexanol; -one: cyclohexanone; Di: total dimers; DOR: deoxygenation rate; TOF: [mol main product]/[mol Pt][hour]

Reaction conditions: [Emim]NTf<sub>2</sub> (2.0 g), [Bmim]PF<sub>6</sub> (0.5 g), H<sub>2</sub>PtCl<sub>6</sub> (0.01 mmol), substrate (0.5 mmol), 1.0 MPa H<sub>2</sub>, 60 °C, 15 h. Reproducibility of results is ±5 %.

<sup>a</sup>: 40 °C.

With substrates with methoxy substituents, the selectivity of the HDO reaction decreases substantially. For example, anisole afforded two main products, i.e. cyclohexane and cyclohexyl methyl ether. The reductive removal of methoxy groups is less effective than dehydration of cyclohexanol. Since the bond dissociation energy of C-O for methoxide groups is with 290 kJ/mol considerably higher than 190 kJ/mol for phenolic hydroxyl groups, their elimination is also more demanding.<sup>37</sup> Guaiacol, which is a major fraction in bio-oil and a typical lignin-derived monomer, contains three different types of C-O bonds. Moreover, the steric hindrance exerted by methoxide groups is more pronounced than for hydroxyl groups. As a result, the conversion and selectivity for cyclohexane of guaiacol are lower than for phenol.

The Pt NP/[Emim]NTf<sub>2</sub>-[Bmim]PF<sub>6</sub> system was also evaluated as a catalyst for the hydrogenolysis of diphenyl ether (DPE), which possesses a very strong C-O bond. Cyclohexane was obtained in 68% yield, the main by-product is the aliphatic ether oxydicyclohexane.

### 3.3 Conclusions

In summary, the Pt NP/[Emim]NTf<sub>2</sub>-[Bmim]PF<sub>6</sub> systems is an excellent catalyst for the HDO of bio-oil type compounds. The system operates under remarkable mild conditions and is stable allowing several recycling. The selectivity towards cyclohexane remains high in recycling experiments only the conversion of phenol progresses more tempered. The observed slow-down of catalytic activity might be caused by aggregation processes of NPs during the reaction. The current systems leaves room for optimization, especially stable and high TOFs throughout multiple re-uses of the catalyst is one of the most appealing starting-points for future work.

### 3.4 Methods

#### 3.4.1 Materials and methods

The ILs used in this study were dried under vacuum at 60 °C for 24 h before use. The ILs were characterised using NMR spectroscopy recorded by Bruker 400 MHz instrument (see Supporting Information). Other chemicals, including phenol (CP, Acros), guaiacol (CP, Fluka), diphenyl ether (CP, VWR International SA) and substituted phenols were obtained from Acros or Sigma-Aldrich and used without further purification.

#### 3.4.2 Pt NPs characterisation

The Pt NPs were isolated by centrifugation (5000 rpm) for 15 minutes, then were washed by dichloromethane (3 × 5 mL) and ethanol (3 × 5 mL). The final re-suspended ethanolic solution was ultra-sonicated for 1 h. Subsequently, the ethanol suspension of nanoparticles was deposited on a carbon film coated copper grid and then examined by trans-mission electron microscopy (TEM). (FEI Talos, operated at 200 keV).

#### 3.4.3 Catalyst Testing and Product Analysis

The experiments were performed in a 45 mL batch reactor. For a typical experiment,

the reactor was loaded with substrate (0.5 mmol),  $\text{H}_2\text{PtCl}_6$  (0.01 mmol),  $[\text{EMIM}]\text{NTF}_2$  (2.0 g) and  $[\text{BMIM}]\text{PF}_6$  (0.5 g). After purging with  $\text{H}_2$  (1.0 MPa) three times, the mixture was stirred at 700 rpm and heated to 60 °C for 15 h. Thereafter, the autoclave was allowed to cool to room temperature and the  $\text{H}_2$  gas was released. Upon that, the products were extracted with 8 ml diethyl ether. The final products were identified by GC-MS using a Agilent 7890B Gas Chromatograph equipped with an Agilent 7000C GC/MS triple quad detector and a capillary column from Agilent (30 m  $\times$  0.25 mm  $\times$  0.25  $\mu\text{m}$ ) with a connected flame ionization detector (FID) for quantification.

### 3.5 References

- (1) M. Saidi; F. Samimi; D. Karimipourfard; T. Nimmanwudipong; B. C. Gates; M. R. Rahimpour. Upgrading of Lignin-Derived Bio-Oils by Catalytic Hydrodeoxygenation. *Energy Environ. Sci.* **2014**, 7 (1), 103–129.
- (2) D. Mohan; C. U. Pittman; P. H. Steele. Pyrolysis of Wood/Biomass for Bio-Oil: A Critical Review. *Energy and Fuels* **2006**, 20 (3), 848–889.
- (3) J. He; C. Zhao; J. A. Lercher. Impact of Solvent for Individual Steps of Phenol Hydrodeoxygenation with Pd/C and HZSM-5 as Catalysts. *J. Catal.* **2014**, 309, 362–375.
- (4) C. Zhao; J. A. Lercher. Upgrading Pyrolysis Oil over Ni/HZSM-5 by Cascade Reactions. *Angew. Chemie - Int. Ed.* **2012**, 51 (24), 5935–5940.
- (5) J. Zakzeski; P. C. A. Bruijninx; A. L. Jongerius; B. M. Weckhuysen. The Catalytic Valorization of Ligning for the Production of Renewable Chemicals. *Chem. Rev.* **2010**, 110, 3552–3599.
- (6) C. Zhao; J. He; A. A. Lemonidou; X. Li; J. A. Lercher. Aqueous-Phase Hydrodeoxygenation of Bio-Derived Phenols to Cycloalkanes. *J. Catal.* **2011**, 280 (1), 8–16.
- (7) C. Zhao; Y. Kou; A. A. Lemonidou; X. Li; J. A. Lercher. Highly Selective Catalytic Conversion of Phenolic Bio-Oil to Alkanes. *Angew. Chemie - Int. Ed.* **2009**, 48 (22), 3987–3990.
- (8) Q. Guan; Y. Zeng; J. Shen; X. S. Chai; J. Gu; R. Miao; B. Li; et al. Selective Hydrogenation of Phenol by Phosphotungstic Acid Modified Pd/Ce-AlO<sub>x</sub> Catalyst in High-Temperature Water System. *Chem. Eng. J.* **2016**, 299, 63–73.
- (9) C. Zhao; W. Song; J. A. Lercher. Aqueous Phase Hydroalkylation and Hydrodeoxygenation of Phenol by Dual Functional Catalysts Comprised of Pd/C and H/La-BEA. *ACS Catal.* **2012**, 2 (12), 2714–2723.
- (10) D. Y. Hong; S. J. Miller; P. K. Agrawal; C. W. Jones. Hydrodeoxygenation and Coupling of Aqueous Phenolics over Bifunctional Zeolite-Supported Metal Catalysts. *Chem Commun* **2010**, 46 (7), 1038–1040.
- (11) X. Cui; A.-E. Surkus; K. Junge; C. Topf; J. Radnik; C. Kreyenschulte; M. Beller. Highly Selective Hydrogenation of Arenes Using Nanostructured Ruthenium Catalysts Modified with a Carbon–Nitrogen Matrix. *Nat. Commun.* **2016**, 7 (6), 11326.
- (12) H. Liu; T. Jiang; B. Han; S. Liang; Y. Zhou. Selective Phenol Hydrogenation to Cyclohexanone Over a Dual Supported Pd-Lewis Acid Catalyst. *Science (80-. )*.

- 2009**, 326 (5957), 1250–1252.
- (13) S. Xu; H. Sheng; T. Ye; D. Hu; S. Liao. Hydrophobic Aluminosilicate Zeolites as Highly Efficient Catalysts for the Dehydration of Alcohols. *Catal. Commun.* **2016**, 78, 75–79.
- (14) K. L. Luska; P. Migowski; S. El Sayed; W. Leitner. Synergistic Interaction within Bifunctional Ruthenium Nanoparticle/SILP Catalysts for the Selective Hydrodeoxygenation of Phenols. *Angew. Chemie - Int. Ed.* **2015**, 54 (52), 15750–15755.
- (15) M. Chatterjee; A. Chatterjee; T. Ishizaka; H. Kawanami. Rhodium-Mediated Hydrogenolysis/Hydrolysis of the Aryl Ether Bond in Supercritical Carbon Dioxide/Water: An Experimental and Theoretical Approach. *Catal. Sci. Technol.* **2015**, 5 (3), 1532–1539.
- (16) H. Ohde; M. Ohde; C. M. Wai. Swelled Plastics in Supercritical CO<sub>2</sub> as Media for Stabilization of Metal Nanoparticles and for Catalytic Hydrogenation. **2004**, 1 (1), 930–931.
- (17) S. Siankevich; Z. Fei; N. Yan; P. J. Dyson. Application of Ionic Liquids in the Downstream Processing of Lignocellulosic Biomass. *Chimia (Aarau)*. **2015**, 69 (10), 592–596.
- (18) A. S. Amarasekara. Acidic Ionic Liquids. *Chem. Rev.* **2016**, 116 (10), 6133–6183.
- (19) B. M. Upton; A. M. Kasko. Strategies for the Conversion of Lignin to High-Value Polymeric Materials: Review and Perspective. *Chem. Rev.* **2015**, 116, 2277.
- (20) C. W. Scheeren; J. B. Domingos; G. Machado; J. Dupont. Hydrogen Reduction of Adams' Catalyst in Ionic Liquids: Formation and Stabilization of Pt(0) Nanoparticles. *J. Phys. Chem. C* **2008**, 112 (42), 16463–16469.
- (21) C. W. Scheeren; G. Machado; J. Dupont; P. F. P. Fichtner; S. R. Teixeira. Nanoscale Pt(0) Particles Prepared in Imidazolium Room Temperature Ionic Liquids: Synthesis from an Organometallic Precursor, Characterization, and Catalytic Properties in Hydrogenation Reactions. *Inorg. Chem.* **2003**, 42 (15), 4738–4742.
- (22) Y. Wang; S. De; N. Yan. Rational Control of Nano-Scale Metal-Catalysts for Biomass Conversion. *Chem. Commun.* **2016**, 52 (37), 6210–6224.
- (23) L. Chen; J. Xin; L. Ni; H. Dong; D. Yan; X. Lu; S. Zhang. Conversion of Lignin Model Compounds under Mild Conditions in Pseudo-Homogeneous Systems. *Green Chem.* **2016**, 18 (8), 2341–2352.
- (24) A. Banerjee; R. W. J. Scott. Optimization of Transition Metal Nanoparticle-Phosphonium Ionic Liquid Composite Catalytic Systems for Deep Hydrogenation and Hydrodeoxygenation Reactions. *Green Chem.* **2015**, 17 (3),

- 1597–1604.
- (25) K. Barta; M. H. G. Precht; P. J. Deuss; J. G. de Vries; M. Scott. New Insights into the Catalytic Cleavage of the Lignin  $\beta$ -O-4 Linkage in Multifunctional Ionic Liquid Media. *Catal. Sci. Technol.* **2015**, 6, 1882–1891.
- (26) N. Yan; Yuan; R. Dykeman; Y. Kou; P. J. Dyson. Hydrodeoxygenation of Lignin-Derived Phenols into Alkanes by Using Nanoparticle Catalysts Combined with Brønsted Acidic Ionic Liquids. *Angew. Chemie - Int. Ed.* **2010**, 49 (32), 5549–5553.
- (27) D. Li; X. Li; J. Gong. Catalytic Reforming of Oxygenates: State of the Art and Future Prospects. *Chem. Rev.* **2016**, 116 (19), 11529–11653.
- (28) K. L. Luska; A. Moores. Ruthenium Nanoparticle Catalysts Stabilized in Phosphonium and Imidazolium Ionic Liquids: Dependence of Catalyst Stability and Activity on the Ionicity of the Ionic Liquid. *Green Chem.* **2012**, 14 (6), 1736.
- (29) J. Dupont. From Molten Salts to Ionic Liquids: A “Nano” Journey. *Acc. Chem. Res.* **2011**, 44 (11), 1223–1231.
- (30) J. Dupont. From Molten Salts to Ionic Liquids: A “Nano” Journey. *Acc. Chem. Res.* **2011**, 44 (11), 1223–1231.
- (31) P. Migowski; J. Dupont. Catalytic Applications of Metal Nanoparticles in Imidazolium Ionic Liquids. *Chem. - A Eur. J.* **2007**, 13 (1), 32–39.
- (32) J. Dupont; J. D. Scholten. On the Structural and Surface Properties of Transition-Metal Nanoparticles in Ionic Liquids. *Chem. Soc. Rev.* **2010**, 39 (5), 1780.
- (33) M. Ruta; G. Laurenczy; P. J. Dyson; L. Kiwi-Minsker. Pd Nanoparticles in a Supported Ionic Liquid Phase: Highly Stable Catalysts for Selective Acetylene Hydrogenation under Continuous-Flow Conditions. *J. Phys. Chem. C* **2008**, 112 (46), 17814–17819.
- (34) M. Crespo-Quesada; R. R. Dykeman; G. Laurenczy; P. J. Dyson; L. Kiwi-Minsker. Supported Nitrogen-Modified Pd Nanoparticles for the Selective Hydrogenation of 1-Hexyne. *J. Catal.* **2011**, 279 (1), 66–74.
- (35) J. W. Lee; J. Y. Shin; Y. S. Chun; H. Bin Jang; C. E. Song; S. G. Lee. Toward Understanding the Origin of Positive Effects of Ionic Liquids on Catalysis: Formation of More Reactive Catalysts and Stabilization of Reactive Intermediates and Transition States in Ionic Liquids. *Acc. Chem. Res.* **2010**, 43 (7), 985–994.
- (36) J. Chang; L. Feng; C. Liu; W. Xing; X. Hu. An Effective Pd-Ni<sub>2</sub>P/C Anode Catalyst for Direct Formic Acid Fuel Cells. *Angew. Chemie - Int. Ed.* **2014**, 53 (1), 122–126.



- (37) M. Ishikawa; M. Tamura; Y. Nakagawa; K. Tomishige. Demethoxylation of Guaiacol and Methoxybenzenes over Carbon-Supported Ru-Mn Catalyst. *Appl. Catal. B Environ.* **2016**, *182*, 193–203.
- (38) H. Xu; K. Wang; H. Zhang; L. Hao; J. Xu; Z. Liu. Ionic Liquid Modified Montmorillonite-Supported Ru Nanoparticles: Highly Efficient Heterogeneous Catalysts for the Hydrodeoxygenation of Phenolic Compounds to Cycloalkanes. *Catal. Sci. Technol.* **2014**, *4* (8), 2658.
- (39) B. Güvenatam; O. Kurşun; E. H. J. Heeres; E. A. Pidko; E. J. M. Hensen. Hydrodeoxygenation of Mono- and Dimeric Lignin Model Compounds on Noble Metal Catalysts. *Catal. Today* **2014**, *233*, 83–91.
- (40) B. J. Hornstein; J. D. Aiken; R. G. Finke. Nanoclusters in Catalysis: A Comparison of CS<sub>2</sub> Catalyst Poisoning of Polyoxoanion- and Tetrabutylammonium-Stabilized 40 ± 6 Å Rh(0) Nanoclusters to 5 Rh/Al<sub>2</sub>O<sub>3</sub>, Including an Analysis of the Literature Related to the CS<sub>2</sub> to Metal Stoichiometry Issue. *Inorg. Chem.* **2002**, *41* (6), 1625–1638.
- (41) A. Strádi; M. Molnár; M. Óvári; G. Dibó; F. U. Richter; L. T. Mika. Rhodium-Catalyzed Hydrogenation of Olefins in  $\gamma$ -Valerolactone-Based Ionic Liquids. *Green Chem.* **2013**, *15* (7), 1857.
- (42) C. Chiappe; D. Pieraccini; D. Zhao; Z. Fei; P. J. Dyson. Remarkable Anion and Cation Effects on Stille Reactions in Functionalised Ionic Liquids. *Adv. Synth. Catal.* **2006**, *348* (1–2), 68–74.
- (43) C. Chiappe; G. Imperato; E. Napolitano; D. Pieraccini. Ligandless Stille Cross-Coupling in Ionic Liquids. *Green Chem.* **2004**, *6* (1), 33–36.
- (44) S. A. Katsyuba; M. V. Vener; E. E. Zvereva; Z. Fei; R. Scopelliti; G. Laurenczy; N. Yan; et al. How Strong Is Hydrogen Bonding in Ionic Liquids? Combined x-Ray Crystallographic, Infrared/Raman Spectroscopic, and Density Functional Theory Study. *J. Phys. Chem. B* **2013**, *117* (30), 9094–9105.
- (45) G. S. Fonseca; A. P. Umpierre; P. F. P. Fichtner; S. R. Teixeira; J. Dupont. The Use of Imidazolium Ionic Liquids for the Formation and Stabilization of Ir<sup>0</sup> and Rh<sup>0</sup> Nanoparticles: Efficient Catalysts for the Hydrogenation of Arenes. *Chemistry - A European Journal*. 2003, pp 3263–3269.
- (46) T. Gutel; C. C. Santini; K. Philippot; A. Padua; K. Pelzer; B. Chaudret; Y. Chauvin; et al. Organized 3D-Alkyl Imidazolium Ionic Liquids Could Be Used to Control the Size of in Situ Generated Ruthenium Nanoparticles? *J. Mater. Chem.* **2009**, *19* (22), 3624.
- (47) W. Zhang; J. Chen; R. Liu; S. Wang; L. Chen; K. Li. Hydrodeoxygenation of Lignin-Derived Phenolic Monomers and Dimers to Alkane Fuels over Bifunctional Zeolite-Supported Metal Catalysts. *ACS Sustain. Chem. Eng.* **2014**,

- 2 (4), 683–691.
- (48) F. E. Massoth; P. Politzer; M. C. Concha; J. S. Murray; J. Jakowski; J. Simons. Catalytic Hydrodeoxygenation of Methyl-Substituted Phenols: Correlations of Kinetic Parameters with Molecular Properties. *J. Phys. Chem. B* **2006**, *110* (29), 14283–14291.
- (49) P. J. Dyson; G. Laurenczy; C. André Ohlin; J. Vallance; T. Welton. Determination of Hydrogen Concentration in Ionic Liquids and the Effect (or Lack of) on Rates of Hydrogenation. *Chem. Commun.* **2003**, No. 19, 2418–2419.
- (50) M. P. Pandey; C. S. Kim. Lignin Depolymerization and Conversion: A Review of Thermochemical Methods. *Chem. Eng. Technol.* **2011**, *34* (1), 29–41.
- (51) A. Maximov; A. Zolotukhina; V. Murzin; E. Karakhanov; E. Rosenberg. Ruthenium Nanoparticles Stabilized in Cross-Linked Dendrimer Matrices: Hydrogenation of Phenols in Aqueous Media. *ChemCatChem* **2015**, *7* (7), 1197–1210.

## Chapter 4 Selective hydrogenation of lignin-derived model compounds and sawdust under mild conditions

### Overview

The chapter starts with an introduction to the challenge in the production of lignin-derived chemicals is to reduce the energy intensive processes used in their production. Here, we show that well-defined Rh nanoparticles dispersed in sub-micrometer size carbon hollow spheres, are able to hydrogenate lignin derived products under mild conditions (30°C, 5 bar H<sub>2</sub>), in water. The optimum catalyst exhibits excellent selectivity and activity in the conversion of phenol to cyclohexanol and other related substrates including aryl ethers and real lignin.

First part of this section is published as an article in *Green Chemistry* 22 (10), 3069-3073 (This article is part of the themed collection: Celebrating our 2020 Prize and Award winners) and the second part of this section is ready to submit.

Front cover:



## 4.1 Introduction

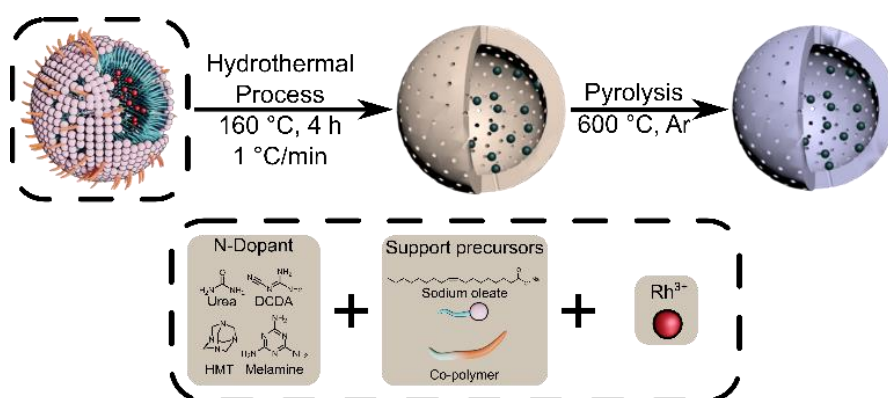
Chemicals and fuels are mainly fossil based and consequently are the major contributor of CO<sub>2</sub> emissions and, hence, the development of renewable alternatives is urgently required. The utilization of inedible lignocellulosic biomass should help to decrease dependency on fossil resources while avoiding competition with food production.<sup>1,2</sup> Lignin, one of the three main components of lignocellulosic biomass, is the only renewable polymer composed of phenolic units (an important component in petrochemicals). Lignin depolymerization typically affords a large number of products, although recently approaches that afford 2-4 main monomeric products and broad range of dimeric and oligomeric products have been reported.<sup>3-7</sup> Nevertheless, the phenolic mixture usually needs to be further upgraded into fuels or platform chemicals,<sup>2</sup> and selective hydrogenation of the aromatic rings present in the compounds is one such approach.<sup>8,9</sup> Such an approach affords products with a large range of applications, e.g. solvents, fuels, polymer precursors, etc.<sup>10,11</sup>

Nanoparticles (NPs) based on noble metals such as Pd,<sup>12,13</sup> Pt,<sup>14,15</sup> Rh<sup>16,17</sup> and Ru<sup>18,19</sup> have been extensively explored as hydrogenation catalysts.<sup>20,21</sup> For the hydrogenation of phenols, these catalysts tend to operate under forcing conditions (i.e. above 80 °C and/or 10 bar H<sub>2</sub>) in environmentally detrimental solvents.<sup>22,23</sup> Such harsh conditions hamper the viability of the process and, therefore, the development of catalysts that operate under comparatively mild conditions and in an environmentally benign solvent are of considerable interest. Small, uniformly dispersed noble metal NPs are generally the most active,<sup>24-26</sup> and by employing N-doped, carbon-based supports the size and dispersion of the NPs can be modulated.<sup>27,28</sup> Another approach is to use well-defined sub-micrometer sized supports, such as hollow carbon spheres, to increase the dispersion of deposited NPs.<sup>29</sup> Therefore, we decided to combine these strategies and evaluate different N-dopants in the synthesis of hollow carbon spheres (HCSs), and study their influence on the size distribution and dispersion of rhodium NPs. The resulting catalysts were evaluated as hydrogenation catalysts and exhibit high activity in the hydrogenation of aromatic compounds, including substrates derived from lignin.

## 4.2 Results and discussion

### 4.2.1 Characterizations of Rh@HCS

The catalysts were prepared by a hydrothermal polymerization process followed by a pyrolysis step (Scheme 4.1). Sodium oleate (SO) and the block co-polymer (P123, EO<sub>20</sub>–PO70–EO20) were used as soft templates, 2,4-dihydroxybenzoic acid (DA) as a carbon source, dicyandiamide (DCDA), melamine, hexamethylenetetramine (HMT) or urea as the N source and RhCl<sub>3</sub> as the nanoparticle precursor. The resulting Rh@HCS (Rh nanoparticles on hollow carbon spheres) catalysts were named according to the N-dopant used, i.e. Rh-D (DCDA), Rh-M (melamine), Rh-H (HMT) and Rh-U (urea).



**Scheme 4.1** Synthesis of the catalysts, Rh-D, Rh-M, Rh-H and Rh-U.

The thickness and the size of the spheres differ depending upon the N-dopant used. HMT (Figure 4.1c) affords the smallest spheres (363 nm of diameter) with the thinnest shell (50 nm), whereas DCDA (Figure 4.1a) and urea (Figure 4.1d) afford the largest spheres (diameter = 492 and 474 nm, respectively). The spheres obtained with melamine (Figure 4.1b) are of intermediate size (diameter = 409 nm). The characteristics of the Rh NPs are also modified by the dopant (Figure 4.1). The particles form small aggregates mostly on the inner layer of the sphere in Rh-D and Rh-U. In Rh-H they are more homogeneously dispersed with some of the NPs also observed on the outside of the sphere. The NPs in Rh-M form larger aggregates and are located throughout the sphere, possibly due to the low solubility of melamine that may interfere with the formation of the micelles. Previously, the solubility of dopants was shown to influence the characteristics of catalysts,<sup>30</sup> and here the N-dopant strongly influences

the size distribution of Rh NPs, varying from a mean value of 1.0 nm in Rh-H to 6.1 nm in Rh-M (Figure 4.1c and b, respectively). The NPs in Rh-U and Rh-D (Figure 4.1a and d, respectively) are small, but with a relatively large size distribution.

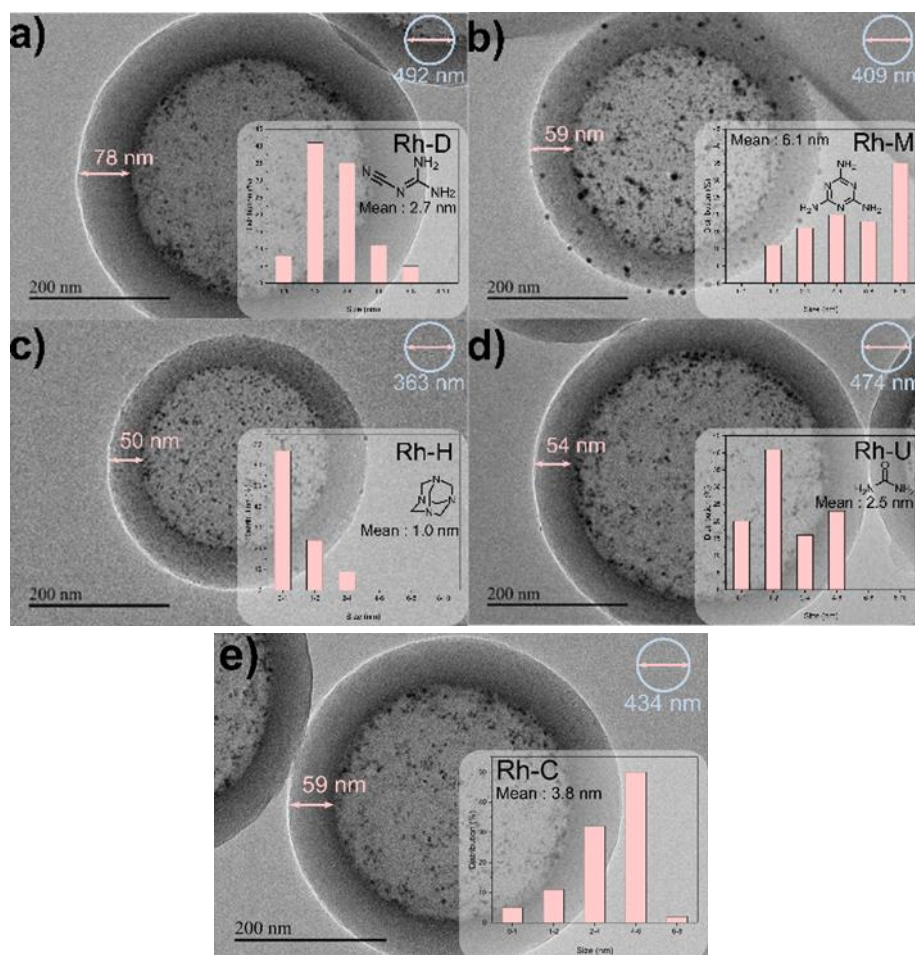


**Figure 4.1** TEM images of (a) Rh-D, (b) Rh-M, (c) Rh-H, (d) Rh-U and (e) Rh-C prepared at 160 °C. The insert shows the corresponding size distribution and mean diameter of the Rh NPs as well as the structure of the N-dopant. The blue circle represents the average outer diameter of the carbon support. The pink scale indicates the average thickness of the shell.

X-ray photoemission spectroscopy (XPS) of Rh-H (Figure 4.2a, b) confirms the presence of carbon, rhodium, oxygen and nitrogen. The Rh NPs are difficult to detect by XPS, which indicates that they are mostly present on the inside of the sphere. The narrow scan Rh 3d spectrum (Figure 4.2a) reveals the presence of metallic Rh(0) (83 %) and a small amount of Rh<sub>2</sub>O<sub>3</sub> phase (17%) due to surface oxidation,<sup>31</sup> and the N spectrum (Figure 4.2b) shows that the N atoms are linked to both Rh and C atoms.<sup>32,33</sup> The XRD patterns of all the catalysts (Figure 4.2c) contain a characteristic peak for graphitic carbon at 23°. The shape of the BET adsorption isotherm of the Rh-H catalyst

corresponds to that of a mesoporous material, with a surface area of 540 m<sup>2</sup>/g and an average pore diameter of 4 nm (Figure 4.2d), i.e. a pore size sufficient size to allow a variety of substrates to enter the shell.

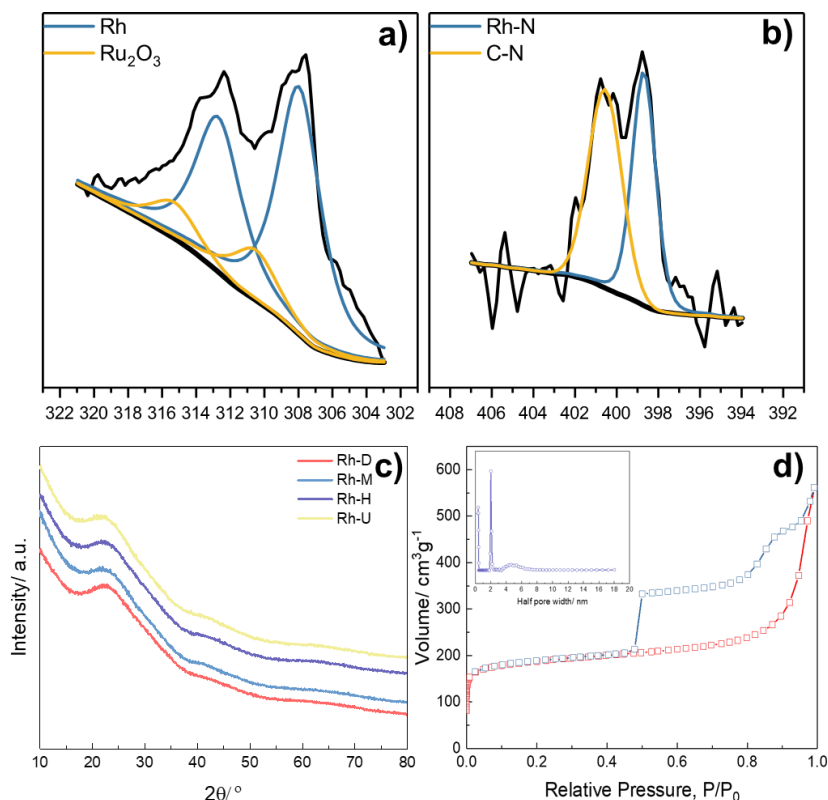


**Figure 4.2** X-ray photoelectron spectroscopy (XPS) of the Rh-H catalyst. (a) Rh 3d<sub>5/2</sub> region (b) N 1s region (c) Powder X-ray diffraction (XRD) profiles of the catalysts with different N-doping agents. (d) N<sub>2</sub> physisorption isotherms of Rh-H. The specific surface areas of 540 m<sup>2</sup>/g, and the mean diameter of pores 4 nm. The pore size distribution curves were obtained by analysing the isotherm desorption branch using the Barrett–Joyner–Halenda (BJH) model.

#### 4.2.2 Catalytic activity tests of Rh@HCS in lignin model compounds

The catalytic activity of Rh-D, Rh-M, Rh-H and Rh-U was assessed in the hydrogenation of phenol in H<sub>2</sub>O at 30°C under H<sub>2</sub> (5 bar), see Figure 4.3. The N-doped catalysts are more active than the non-doped control catalyst (Rh-C, Figure 4.1e), with the activity correlating with the average size of the NPs present in the different catalysts, i.e. the Rh-H catalyst which has the smallest NPs (Rh NP mean diameter = 1.0 nm) leads to a conversion of 100% and a yield of cyclohexanol of 99%, demonstrating high



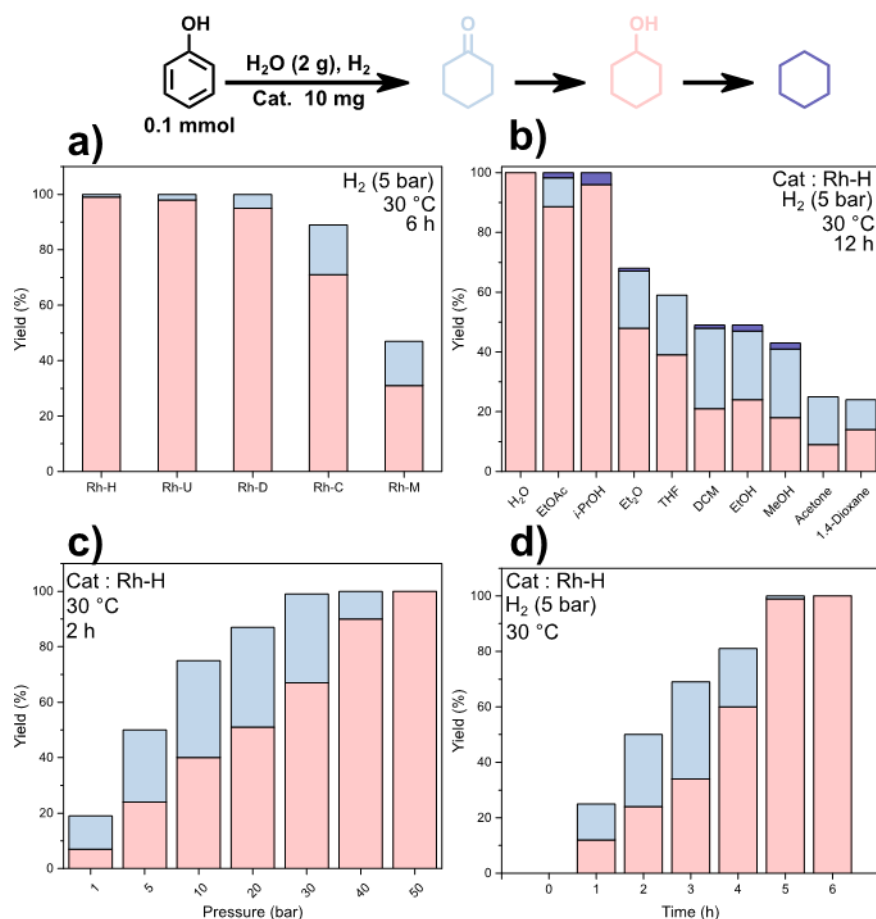
selectivity for ring hydrogenation over hydrogenolysis. The least active catalyst is Rh-M with the largest NPs (Rh NP mean diameter = 6.1 nm) with a conversion of only 47 % and a poorer selectivity.

The solvent influences the Rh-H catalyst (Figure 4.3b), with the activity correlating well with the solubility of phenol in the solvent, i.e. with highest conversion in water, ethyl acetate and isopropanol (100% conversion). The selectivity to cyclohexanol is lower in ethyl acetate and isopropanol compared to water, which might be due, at least in part, to the higher solubility of the product in these two solvents, leading to further reduction. Moreover, electrophilic aromatic substitution products, e.g. [1,1'-bi(cyclohexan)]-2-one or 1,1'-bi(cyclohexane), which are often detected with reactions operating at higher temperatures,<sup>34,35</sup> were not observed. Previously, Shirai et al showed that using 5 wt% Rh/C commercial catalyst the hydrogenation of phenol is incomplete under 30 bar of H<sub>2</sub> in supercritical carbon dioxide at 80°C.<sup>36</sup> The Rh-H catalyst is considerably more active than commercial Rh/C which can be attributed to the small size of the Rh NPs and the N-dopant.

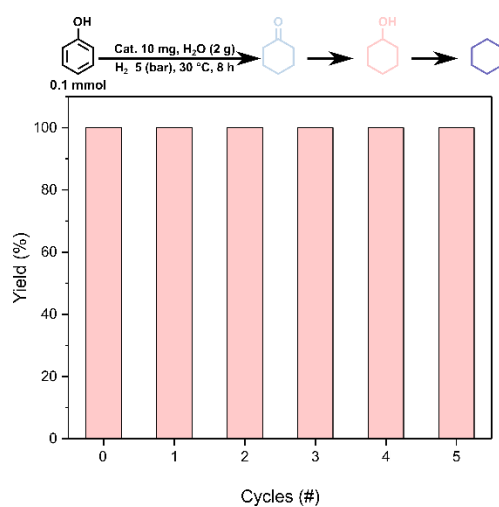
The reaction pressure and reaction time were further optimized (Figures 4.3c and d, respectively), with the Rh-H catalyst even able to slowly hydrogenate phenol at 30°C and an atmospheric pressure of H<sub>2</sub>. The recyclability and stability of the catalyst was assessed and with product yield decreasing slightly over five batches (Figure 4.4). No rhodium was detected in the product phase.

The activity of Rh-H was compared with a series of commercial catalysts (Table 4.1), demonstrating the superiority of the Rh-H catalyst. With the commercial Rh/C, the lower activity may be attributed to the larger mean diameter of the Rh NPs (5.7 nm, Figure 4.5),<sup>27,28</sup> which is considerable larger than the Rh NPs in the Rh-H catalyst (mean diameter 1.0 nm). Moreover, the Rh-H catalyst operates under lower H<sub>2</sub> pressures and temperatures than reported noble metal catalysts.<sup>9,37-39</sup> Ni/C with mean diameter 4.3 nm (Figure 4.6) are inactive under the mild reaction conditions whereas Raney nickel hydrogenates phenol to cyclohexanol at 80 °C using 2-PrOH as a hydrogen donor.<sup>40</sup>

Note that the solubility of phenol and cyclohexanol in H<sub>2</sub>O at 30 °C is 0.084 and 0.043 g/ml, respectively, and therefore under our conditions the system is monophasic. However, as the phenol: Rh molar ratio is increased, i.e. 588:1, 1470:1, 2940:1 (Table 4.1, entries 8-10), full converted to cyclohexanol is achieved, albeit at extended reaction times, and the system becomes biphasic.

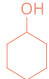



**Figure 4.3** **a)** Product distributions for the different catalysts in H<sub>2</sub>O. Reaction conditions: phenol (1.0 mmol), cat. (10 mg), H<sub>2</sub>O (2.0 g), 5 bar H<sub>2</sub>, 30 °C, 6 h. **b)** Influence of solvent on the reaction. Reaction conditions: phenol (1.0 mmol), Rh-H (10 mg, Rh 3.5 wt% in Rh-H), solvent (2.0 g) 5 bar H<sub>2</sub>, 30 °C, 12 h. **c)** Effect of H<sub>2</sub> pressure on the reaction. Reaction conditions: phenol (1.0 mmol), Rh-H (10 mg), H<sub>2</sub>O (2.0 g), 30 °C, 2 h. **d)** Product distribution as a function of reaction time. Reaction conditions: phenol (1.0 mmol), Rh-H (10 mg), H<sub>2</sub>O (2.0 g), 5 bar H<sub>2</sub>, 30 °C. Colour bars refer to the colour of the products shown in the scheme.



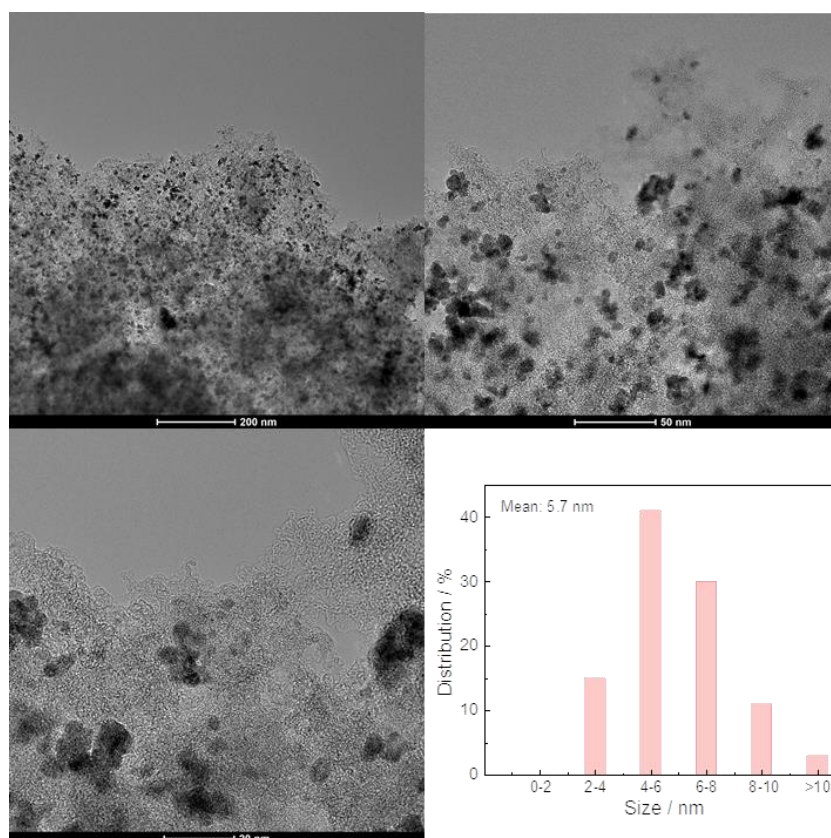
**Figure 4.4** Recycling experiments. Reaction conditions: phenol (1.0 mmol), Rh-H (10 mg), H<sub>2</sub>O (2.0 g) 5 bar H<sub>2</sub>, 30 °C, 8 h.

**Table 4.1** Comparison of the Rh-H catalyst with other widely used carbon supported metal NP hydrogenation catalysts.

Entry	Catalyst	Conversion %			TOF
			(Yield %)	(Yield %)	
1	Rh-H	100	100	0	49.0
2 <sup>a</sup>	Rh-H	93	92	1	5.7
3	5 wt% Rh/C	90	69	21	44.1
4	5 wt% Ru/C	43	27	16	20.1
5	5 wt% Pt/C	66	44	22	32.4
6 <sup>b</sup>	5 wt% Pd/C	0	0	0	0
7	5 wt% Ni/C	0	0	0	0

Reaction conditions: phenol (1.0 mmol), Rh-H (10 mg) (or 5 wt% Rh/C (7 mg), or 5 wt% Ru/C (7 mg), or 5 wt% Pt/C (13 mg), or 5 wt% Pd/C (7 mg), or 5 wt% Ni/C (4 mg)), H<sub>2</sub>O (2.0 g) 5 bar H<sub>2</sub>, 30 °C, 6 h. [a] 1 bar H<sub>2</sub>, 48 h. [b] 5 wt% Ni/C was synthesized using a typical impregnation method.<sup>41</sup> TOF: [mol phenol]/[mol metal]/[hour]

The rhodium content in the Rh-H catalyst is 3.5 wt% according to the ICP (Inductively Coupled Plasma) test.

**Figure 4.5** TEM images and size distribution of the Rh/C.

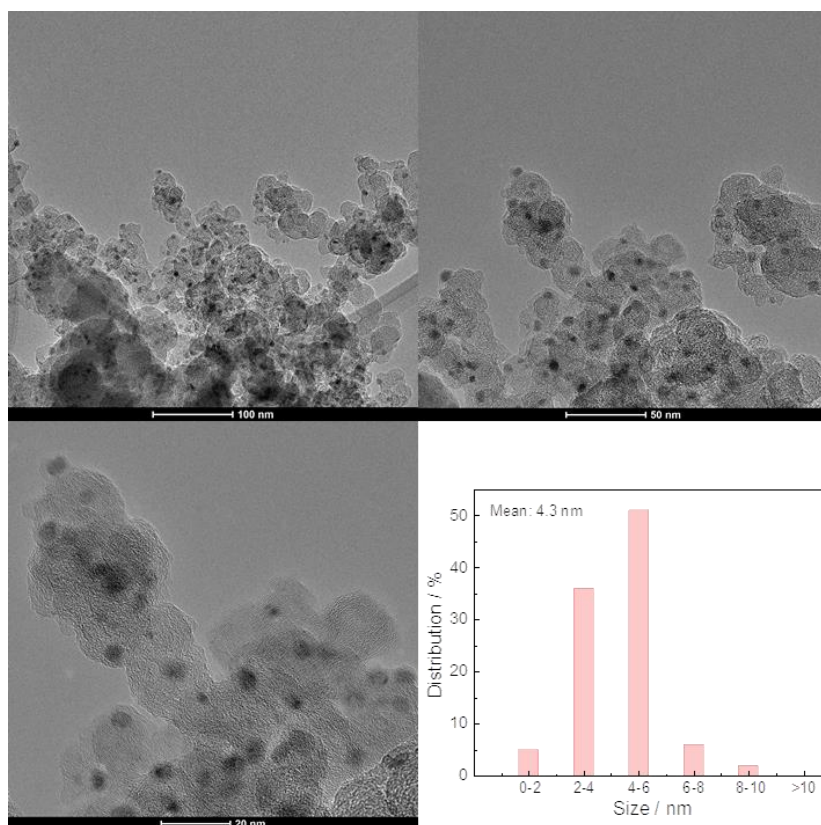


Figure 4.6 TEM images and size distribution of the Ni/C.

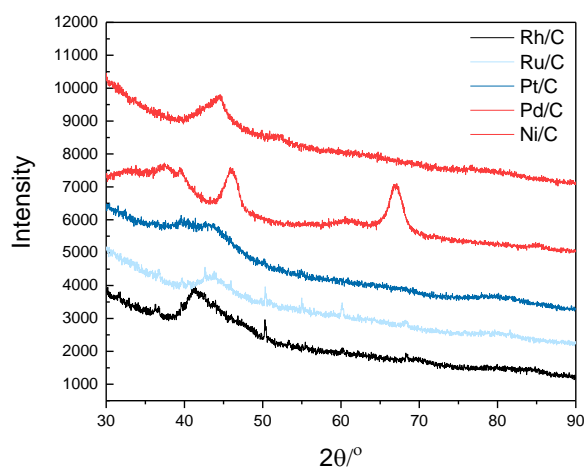


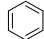
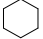
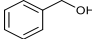
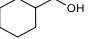
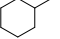
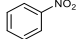
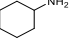
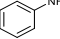
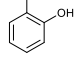
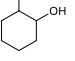
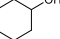
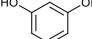
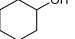
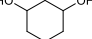
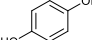
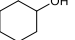
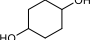
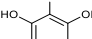
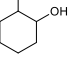
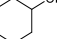
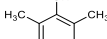
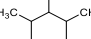
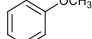
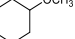
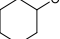
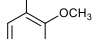
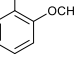
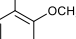
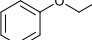
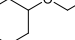
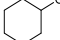
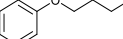
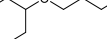
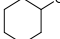
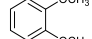
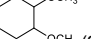
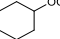
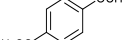
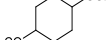
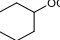
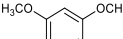
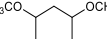
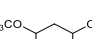
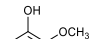
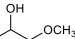
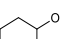
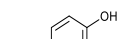
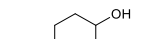
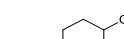
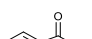
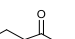
Figure 4.7 XRD of the Rh/C, Ru/C, Pt/C, Pd/C and Ni/C.

The substrate scope of the Rh-H catalyst was evaluated (Table 4.2), with substrates containing electron withdrawing groups (i.e. Table 4.2, entries 2, 18 and 19) most efficiently hydrogenated, whereas substrates with two or three electron donating groups (i.e. Table 4.2, entries 13-15) less efficiently hydrogenated. The presence of two alcohol groups leads to cleavage of one of the C-O bonds in the substrate, which potentially reduces the complexity of the products when mixtures of phenolic compounds are transformed simultaneously (Table 4.2, entries 3-6). Notably, as the temperature is increased to 60 °C, hydroquinone is fully converted to cyclohexanol, i.e. the same product obtained from phenol hydrogenation (Table 4.2, entry 6). The hydrogenation of lignin derived compounds guaiacol and 4-propylguaiacol (Table 4.2, entries 16 and 17), was also efficiently achieved.

The selectivity for hydrogenation (relative to hydrogenolysis and hydrolysis) was assessed using various aryl ether substrates (Table 4.3). The Rh-H catalyst mostly provides hydrogenation products without (or with only limited) cleavage of C-O bonds either via hydrogenolysis or hydrolysis. Only hydrolysis of benzyl phenyl ether (Table 4.3 entry 6) and aryl-ethers (Table 4.3 entries 1-4) were detected without any hydrogenolysis products (i.e. cyclic compounds without oxygen atoms). Only xanthene (Table 4.3, entry 5) showed 2% of a hydrogenolysis product. Therefore, our catalyst has a remarkable selectivity for hydrogenation over hydrogenolysis with only limited hydrolysis, leading to the high catalytic activity for hydrogenation (Note that it was shown that hydrolysis of aryl ethers takes place in two steps via an enol ether intermediate that is rapidly hydrolysed).<sup>42</sup>

In summary, the Rh-H catalyst, comprising finely dispersed Rh NPs immobilized within N-doped hollow carbon spheres, exhibits excellent selectivity and activity in the conversion of phenol to cyclohexanol under ambient conditions. High activity was also observed for a wide and diverse range of related substrates including aryl ethers. Importantly, the catalyst operates in water without additives and under mild reaction conditions.

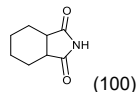
**Table 4.2** Evaluation of the substrate scope of the Rh-H catalyst in H<sub>2</sub>O.

Entry	Substrate	Con. %	Products (Yield %)	
1 <sup>a</sup>		100	 (100)	-
2 <sup>a</sup>		100	 (99)	 (1)
3 <sup>a</sup>		100	 (99)	 (1)
4 <sup>a</sup>		100	 (58)	 (42)
5 <sup>a</sup>		100	 (81)	 (19)
6 <sup>a</sup>		100	 (81)	 (19)
7		100	 (61)	 (33)
8		100	 (100)	-
9		99	 (98)	 (1)
10		100	 (98)	 (2)
11		99	 (98)	 (1)
12		95	 (98)	 (1)
13		94	 (92)	 (2)
14		94	 (90)	 (4)
15		88	 (80)	 (8)
16		100	 (87)	 (8)
17		100	 (94)	 (6)
18		100	 (100)	

19



100



Reaction conditions: Substrate (1.0 mmol), Rh-H (10 mg), H<sub>2</sub>O (2.0 g) 10 bar H<sub>2</sub>, 60 °C, 24 h. Conversion and yields determined by GC. [a] 30 °C, 5 bar H<sub>2</sub>, 12 h.

**Table 4.3** Hydrogenations of lignin dimer model compounds using Rh-H in H<sub>2</sub>O (only the two major products are shown, details of all products are provided in Table S1 in the SI).

Entry	Substrate	Con. %	Products (Yield %)	
1	4-O-5	100	(82)	(18)
2	4-O-5	100	(85)	(15)
3	4-O-5	100	(85)	(15)
4	4-O-5	95	(90)	(5)
5	5-O-6	100	(98)	(2)
6	$\alpha$ -O-4	83	(21)	(15)
7	$\beta$ -O-4	84	(67)	(17)
8 <sup>a</sup>	$\beta$ -5	80	(77)	(3)
9 <sup>a</sup>	$\beta$ -5	79	(76)	(3)
10 <sup>a</sup>	$\beta$ -5	100	(75)	(25)
11	$\alpha$ -1	100	(98)	(2)
12	5-5	100	(98)	(2)

Reaction conditions: phenol (1.0 mmol), Rh-H (20 mg), H<sub>2</sub>O (2.0 g) 15 bar H<sub>2</sub>, 80 °C, 24 h. Conversion and yields determined by GC.

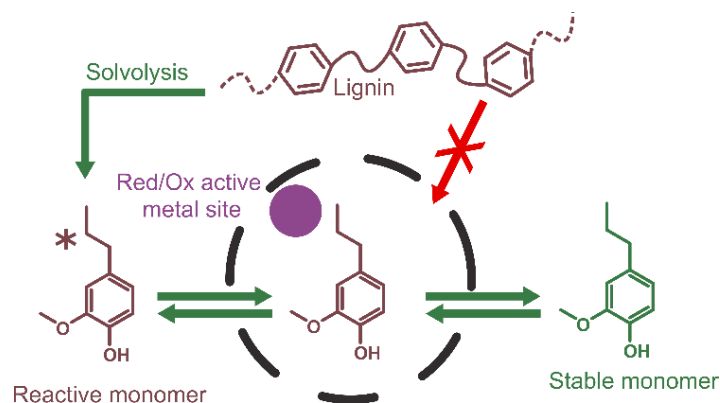
[a] 100 °C.

### 4.2.3 Catalytic activity tests of Rh@HCS in lignin conversion

Reductive catalytic fractionation (RCF) is one of the key ways used to valorise lignin.<sup>43–46</sup> In the presence of a metal catalyst and a reductant (usually H<sub>2</sub>), essentially all the  $\beta$ -O-4 motifs can be cleaved in native lignin present in woody biomass, affording up to 50-60 % of monomeric phenolic compounds.<sup>7,47,48</sup> The transformation comprises three steps, including solvolysis fractionation of lignin from cellulose and hemicellulose by breaking the lignin-sugar linkages, followed by fragmentation of polymeric lignin into monomers and oligomers via C-O bond cleavage, and finally stabilisation of the reactive allyl species by hydrogenation.<sup>49</sup> However, the exact role of the catalyst in RCF remains a matter of intensive debate. Using a catalyst basket strategy, Sels et al. elegantly provided strong evidence that the solvent (a protic one i.e. MeOH) is almost entirely responsible for both fractionation and fragmentation of lignin.<sup>50</sup> However, the basket used to confine the catalyst pellets consisted of 40 mesh (0.4 mm pore diameter) and therefore the possibility of lignin fragmentation over the metal catalyst in solubilized polymeric form cannot be excluded. Indeed, other studies suggest that the metal catalyst contributes to breaking the ether linkages in lignin via hydrogenolysis.<sup>51–55</sup> As a result of this uncertainty, many efforts to improve catalysts for RCF continue to be focused on enhancing  $\beta$ -O-4 bond cleavage in lignin model compounds.

To unambiguously address whether metal catalysts actively participate in the lignin depolymerisation step, or only play a role in the stabilization step, a catalyst encapsulated within a porous shell that prevents the lignin polymer from entering and interacting with the catalyst would be ideal. Comparing the performance of the encapsulated metal catalyst with an exposed catalyst would provide quantitative understanding on the contribution of the metal catalyst in RCF. Herein we used Rh nanoparticles (NPs) embedded in porous hollow carbon spheres (Rh@HCS) to test this hypothesis.





**Scheme 4.2** Strategy adopted to probe the mechanism of reductive catalytic fractionation. 4-n-propyl guaiacol was used as a representative monomer. Lignin is depicted as a polymer composed of aromatic rings, the linkages and methoxy groups are omitted for clarity.

The catalyst (termed Rh@HCS – Figure 4.8) was prepared by a modified solvothermal procedure (see Experimental for details).<sup>56</sup> Electron microscopy shows that the carbon spheres are uniform in size (~178 nm) and thickness (~42 nm) (Figure 4.8a). The Rh NPs are completely embedded within the interior of the carbon spheres and have a narrow size distribution (~1.4 nm average diameter) (Figure 4.8b). The Rh loading was determined by ICP-OES as 3.5 wt%. The Rh region of the XPS confirms the absence of Rh on the outer surface of the carbon spheres (Figure 4.9 a-c), i.e. exhibiting a broad carbon peak without any evidence of surface bound Rh (Figure 4.9 d). Physisorption analysis reveals a mesoporous material with pore diameter of 4 nm and a surface area of 540 m<sup>2</sup>/g (Figure 4.8d). Commercial Rh/C was used as a control catalyst and was characterised by TEM (Figure 4.10) with the Rh NPs having a mean diameter was of 5.7 nm unevenly distributed over the support material. Due to the larger size of the Rh NPs in the Rh/C catalyst compared to the Rh@HCS catalyst, the Rh/C catalyst is expected to be less active and to compensate for this a higher catalyst loading was used in the studies.

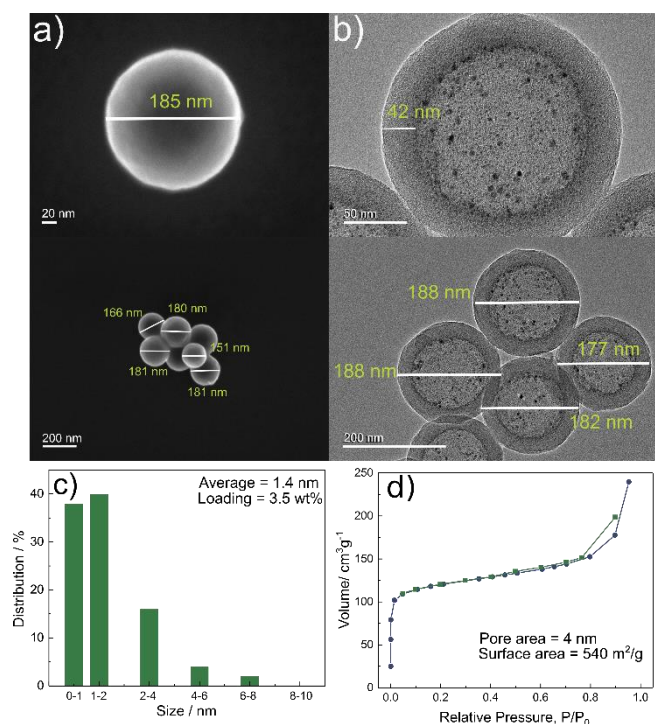


**Figure 4.8** a) SEM images of the Rh@HCS catalyst. b) TEM images of the Rh@HCS catalyst. c) Rh particles size distribution in the Rh@HCS catalyst. d) Physiosorption curves. Relative pressure  $P/P_0$ ,  $P_0$  is the saturated vapour pressure of N<sub>2</sub> at -196 °C.

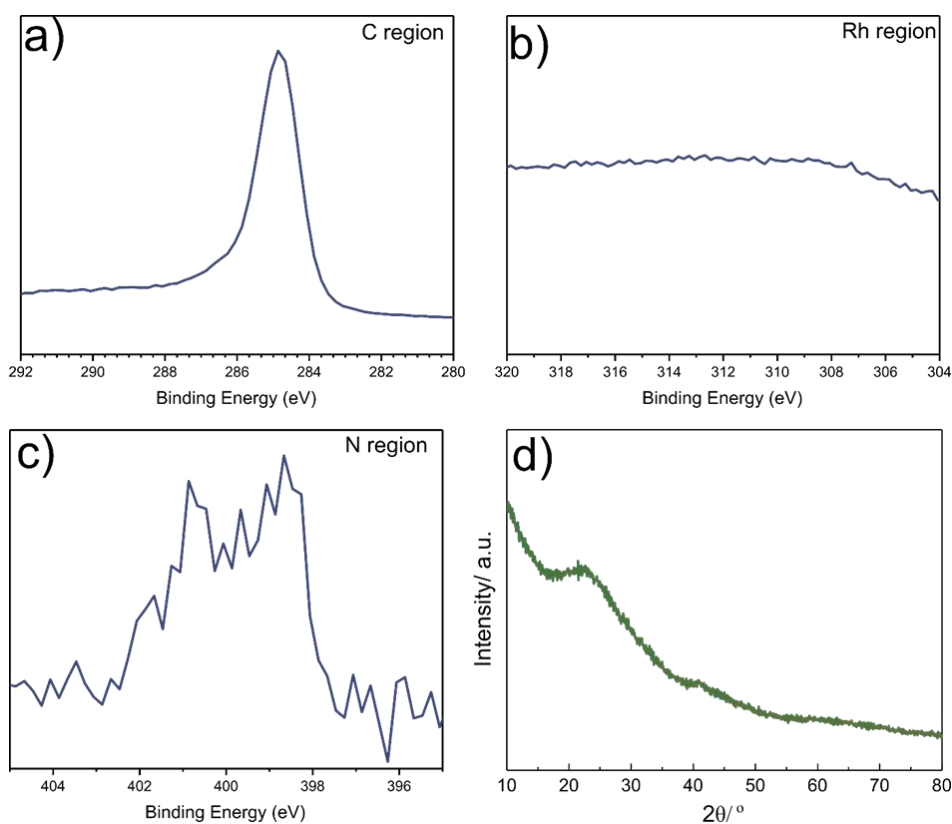


**Figure 4.9** (a, b and c) XPS multiplex of the C, Rh and N region. (d) XRD spectra of Rh@HCS

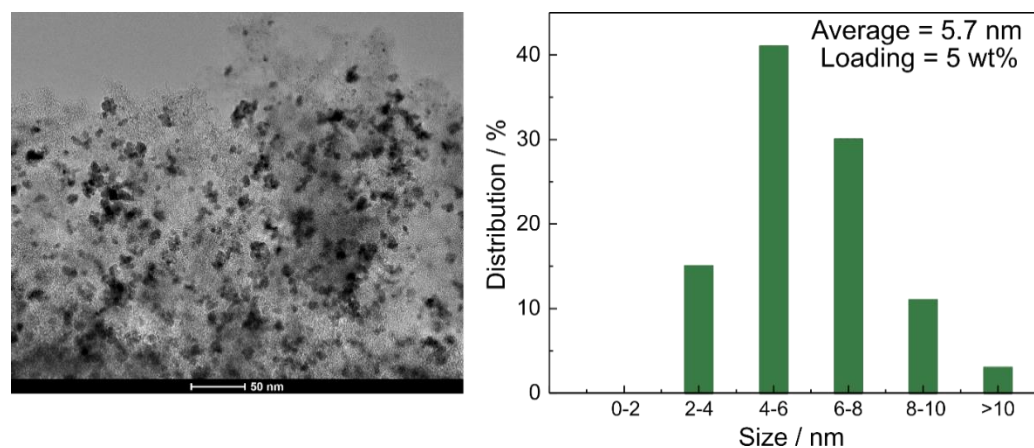


**Figure 4.10** TEM characterization of the Rh/C catalyst. (left) TEM image and (right) particle size distribution.

Polystyrene was used as a probe compound to determine whether the Rh NPs in the Rh@HCS catalyst can react with polymers. The C-C bonds connecting the styrene cannot be cleaved but the aromatic rings can be hydrogenated by Rh NPs.<sup>57</sup> Polystyrene with three different molecular weights were tested, one low (1300 g/mol), one close to the molecular weight typical of lignin (13000 g/mol) and a larger one (30000 g/mol). The polystyrene was dissolved in THF and reacted under forcing conditions to ensure hydrogenation in the presence of Rh NPs, i.e. 200 °C, 4 MPa H<sub>2</sub>, 15 h. After reaction, the solvent was removed and FT-IR spectra were recorded (Figure 4.11 for 13000 g/mol polystyrene and Figure 4.12 for a comparison of all three polymers). The FT-IR spectra show the disappearance of the aromatic signal of the polymers from the reaction with the Rh/C catalyst, whereas the FT-IR spectra remain unchanged when the Rh@HCS catalyst is used. The peaks corresponding to the C=C bending vibrations (1500 to 1600 cm<sup>-1</sup>), C-H aromatic bending (660-800 cm<sup>-1</sup>) and C-H stretching (3000-3100 cm<sup>-1</sup>) are highlighted in the figures to illustrate the differences. Thus, the Rh NPs encapsulated within the porous shell are unable to access the polystyrene, i.e. the polystyrene cannot traverse the nanoscale shell, and it can be expected that lignin would also not be able to access the Rh NPs in the Rh@HCS catalyst. As a positive control, toluene was used as a substrate in place of polystyrene and the toluene was hydrogenated to afford methyl cyclohexane in near-quantitative yield by both catalysts under the same reaction conditions.

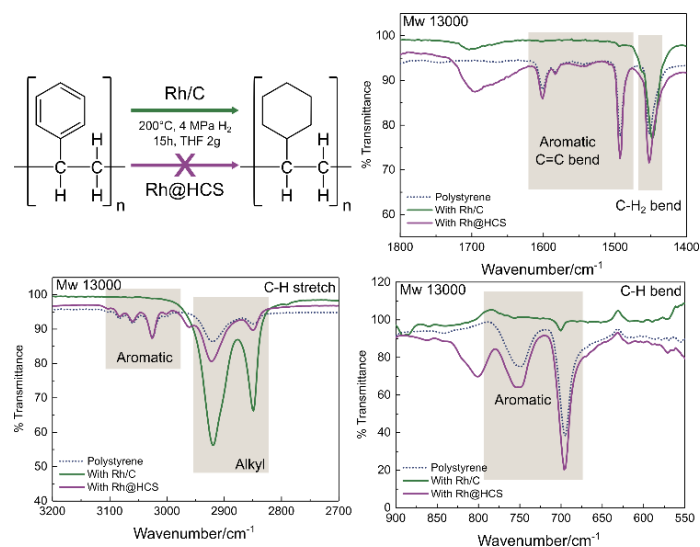


**Figure 4.11** Relevant regions of the FT-IR spectra of polystyrene (13000 g/mol) before and after reaction with the Rh/C and Rh@HCS catalysts. Pristine polystyrene – grey dots. Polystyrene after the reaction with the Rh/C catalyst – green. Polystyrene after the reaction with the Rh@HCS catalyst – purple. Conditions: polystyrene (10 mg), catalyst (Rh@HCS, 3.5 wt%, 20 mg or Rh/C, 5 wt%, 14 mg.), THF (2 ml), H<sub>2</sub> (4 MPa), 200 °C, 15 h.

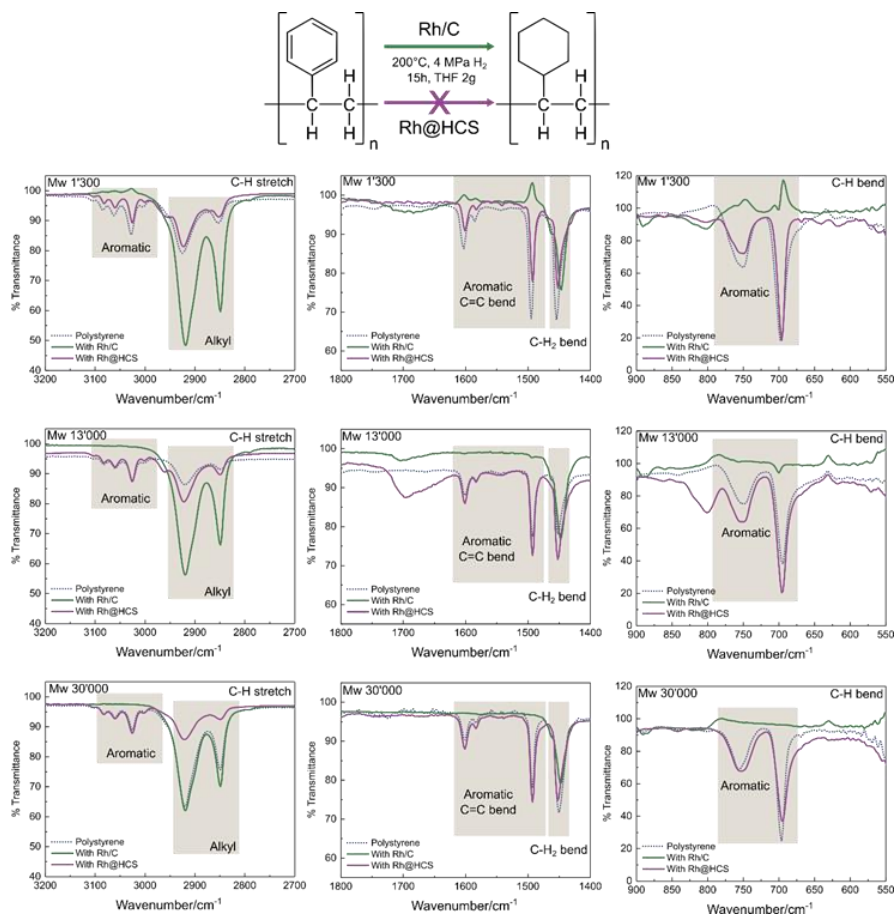


**Figure 4.12** FT-IR spectra of polystyrene with different molecular weights.

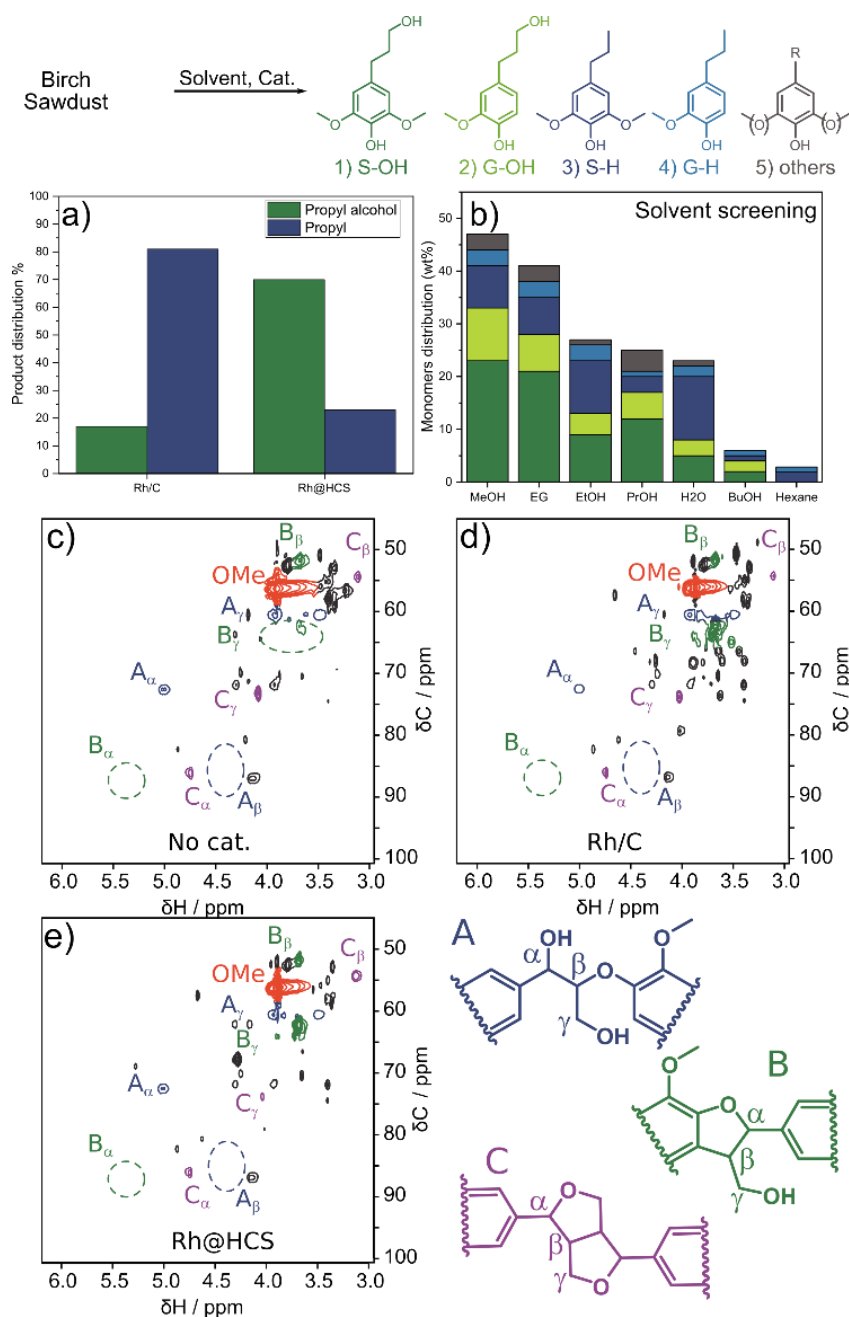


**Figure 4.13** a) Comparison between the Rh/C and Rh@HCS catalysts under RCF conditions. b) Protic solvent screening. c-e) 2D HSQC NMR spectra of the liquid products after RCF. c) Without catalyst. d) Using the Rh/C catalyst. e) Using the Rh@HCS catalyst. Motifs are colour coded.  $\beta$ -O-4 labelled as A (in blue). Phenylcoumaran labelled as B (in green). Resinol labelled as C (in purple). Conditions: Rh@HCS, (3.5 wt%, 20 mg) or Rh/C (5 wt%, 14 mg), sawdust (100 mg), MeOH (5 g), H<sub>2</sub> (4 MPa), 200 °C, 15 h.

Birch sawdust was reacted in MeOH with H<sub>2</sub> (4 MPa) at 200°C in the presence of the Rh/C or Rh@HCS catalysts, both affording monomers in ~47 % yield, confirming solvolysis is responsible for both fractionation and fragmentation of lignin. Analysis of the post-reaction solution revealed a Rh content of 40 ppm which would have a negligible influence on the reaction.

Notably, there is a difference in the product distribution depending on the catalyst used (Figure 4.13a). The Rh@HCS catalyst affords more n-propyl alcohol monomers than n-propyl monomers, whereas the Rh/C catalyst results in the opposite selectivity. This difference may be attributed to the support materials rather than the Rh NPs, with the N-doped support in the Rh@HCS catalyst being less acidic than the pure carbon support in the Rh/C catalyst.<sup>46,58</sup> Nevertheless, the product distribution of the Rh@HCS catalyst can be tuned such that more n-propyl monomers obtained under more forcing conditions (Figure 4.14a,b).

2D HSQC NMR spectra of the liquid products obtained from both catalysts and under catalyst-free conditions confirm that cleavage of the  $\beta$ -O-4 motifs leads to depolymerisation via solvolysis as peaks corresponding to A $_{\beta}$  carbons are absent in all the spectra. The absence of peaks corresponding to B $_{\alpha}$  carbons suggest that  $\beta$ -5 dimers are produced from the phenylcoumaran motifs in lignin. Notably, in the catalyst-free reaction, the peaks corresponding to B $_{\gamma}$  carbons are of very low relative intensity, indicative of re-condensation. All three carbons signals (i.e. C $_{\alpha}$ , C $_{\beta}$  and C $_{\gamma}$ ) corresponding to the resinol motifs are present.<sup>59</sup>

Common protic solvents used in RCF were also evaluated (Figure 4.13b),<sup>60</sup> with longer chain alcohols retarding solvolysis whereas adding another OH function increases it. Hexane was used as a non-protic solvent with monomers obtained 2% yield, further confirming the mechanism.

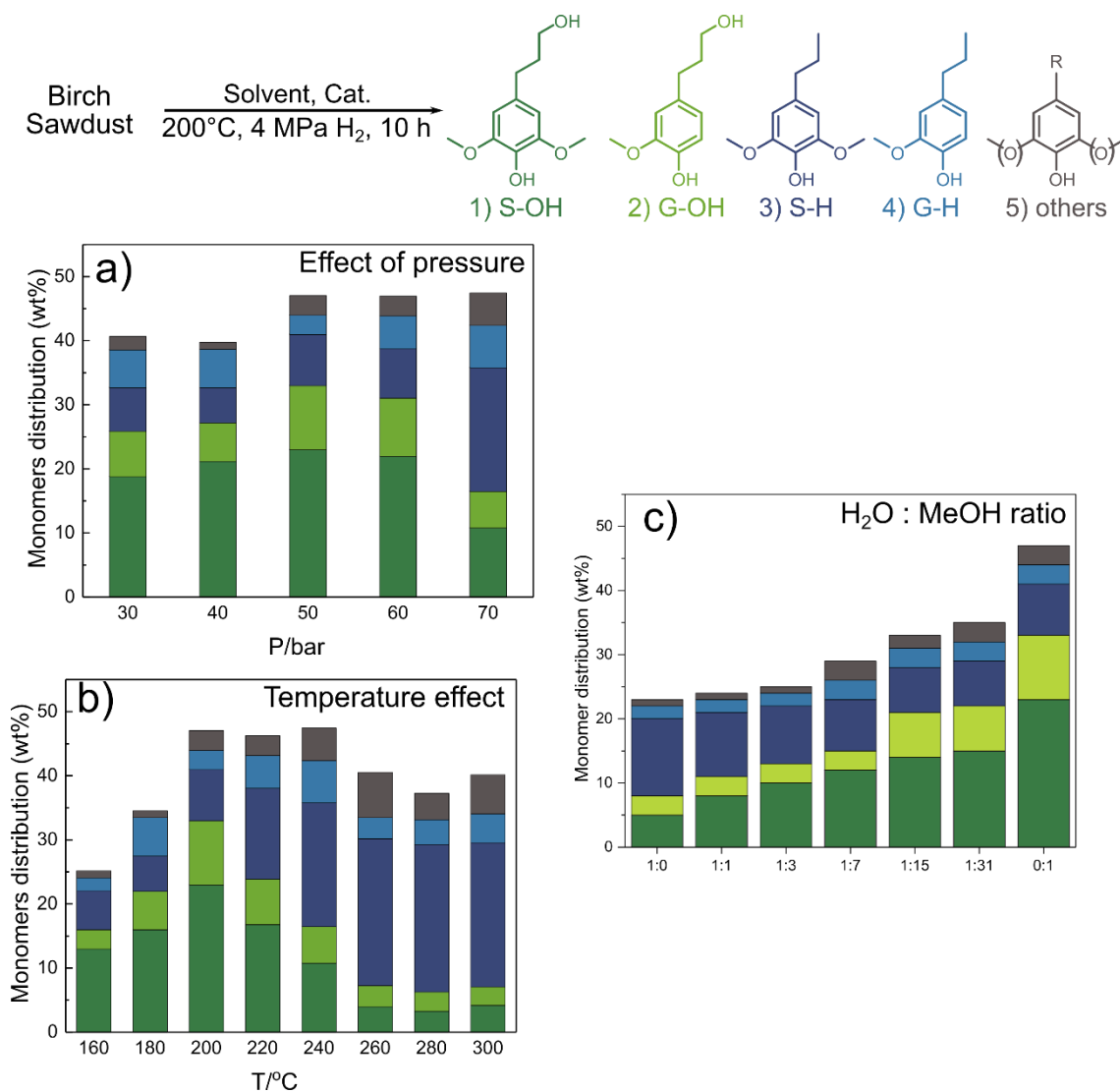


**Figure 4.14** Effect of pressure, temperature and water on the reaction. a) Pressure screening to highlight the ability of Rh@HCS to dehydrate the propyl alcohol moiety under more forcing. Temperature screening to highlight the ability of Rh@HCS to dehydrate the propyl alcohol moiety under more forcing conditions. c) Presence of water extracts sugar and forms humins leading to a loss in activity even with 1:31 ratios. Conditions: Sawdust (100 mg), MeOH (5 g), cat. (Rh@HCS, 3.5 wt%, 20 mg, Rh/C, 5 wt%, 14 mg.), 200 °C, H<sub>2</sub> (4 MPa).

### 4.3 Conclusions

In conclusion, we designed a catalyst, comprising Rh NPs immobilized within hollow nanoscale shells, to confirm the mechanism of reductive catalytic fractionation (RCF) of biomass. Initially we demonstrated that polymers cannot come into contact with the

Rh NPs located at the interior of the hollow shell catalyst, whereas monomers can come into contact with the Rh NPs. The catalyst was then evaluated under typical RCF conditions and was shown to have similar activity to a Rh/C catalyst where the Rh NPs are exposed to all reagents, thus demonstrating that hydrogenolysis is not responsible for the cleavage of the  $\beta$ -O-4 motif, and providing unambiguous evidence to support Sels mechanism<sup>49</sup> that RCF involves initial solvolysis, occurring spontaneously under the harsh reaction conditions, followed by stabilisation of the reactive species generated via hydrogen by the Rh NPs.

## 4.4 Methods

### 4.4.1 Synthesis of the catalysts

In a typical experiment, 2,4-dihydroxybenzoic acid (DA) (1.0 mmol), hexamethylenetetramine HMT (0.5 mmol) and the N-dopant (0.5 mmol) were dissolved in deionized water (60 ml) to form Solution 1. EO20-PO70-EO20 Pluronic (P123) (0.01 mmol), sodium oleate (SO) (0.25 mmol) and  $\text{RhCl}_3 \cdot 3\text{H}_2\text{O}$  (0.05 mmol) were dissolved in deionized (DI) water (20 mL), to form Solution 2. Next, Solution 2 was added to Solution 1 dropwise, and then the mixture was transferred into a Teflon-lined cell, and loaded into a stainless steel autoclave (120 ml). The autoclave was heated from 30 °C to 160 °C with a heating rate of 1 °C min<sup>-1</sup> and maintained at 160 °C for 4 h. After cooling to room temperature, the solid was separated by centrifugation and washed three times with DI water. The obtained solid was dried under vacuum at 60 °C. The resulting powder was heated from 30 °C to 600 °C at a heating rate of 2 °C min<sup>-1</sup> under an argon atmosphere and maintained at 600 °C for 3 h.

### 4.4.2 Catalyst Testing

The substrate (1 mmol), catalyst (10 mg), and  $\text{H}_2\text{O}$  (2.0 g) were introduced into a 20 mL glass vial and loaded in an autoclave (75 ml). After flushing the autoclave with  $\text{H}_2$  three times, the autoclave was pressurized to the desired pressure and placed in a heating block maintained at the desired temperature with stirring at 800 rpm. After reaction, the products were extracted with diethyl ether and analysed by gas



chromatography-mass spectrometry (GC-MS).

#### 4.4.3 Lignin product analysis

The reaction mixture was filtered and washed with MeOH. The solid residues were dried in an oven at 80 °C overnight. The MeOH was evaporated and the resulting brown oil was subjected to a liquid-liquid extraction (3 x 10 mL DCM/H<sub>2</sub>O (1:1)) to separate the sugar-derived products from the lignin derived products. The dichloromethane (DCM) was evaporated to afford the lignin derived products (used for the calculation of “delignification”). To analyze the mixture, it was diluted in ethyl acetate (EtOAc) and dodecane (internal standard) was added.

#### 4.4.4 Analytical methods

##### **FT-IR analysis**

After the reaction, centrifuged the final mixture for at 6000 rpm 15 min. The result solution was removed by rotary evaporation, and finally collected the solid. IR spectra of the result solid was recorded on a Varian 800 FT-IR spectrometer.

##### **GC-MS analysis**

GC-MS were recorded on an Agilent 7890B equipped with an Agilent 7000C MS triple quad detector and a capillary column from Agilent (l x d x f: 25 m x 0.25 mm x 0.25 µm) using He as carrier gas. The conversions and yield were obtained using dodecane as an internal standard. The following parameters were used: 45 °C hold for 5 min; heat to 240 °C with a ramp of 5 °C/min and hold 10 min at 240 °C.

##### **TEM analysis**

TEM and HAADF STEM-EDX were obtained on a FEI Tecnai Osiris equipped with an 80-200 kV high brightness XFEG, A-Twin pole piece with Super-X EDX and a 4k x 2.6k Gatan Orius CCD camera (<https://cime.epfl.ch/osiris> for full detail of the device).

##### **ICP-OES**

Inductively coupled plasma optical emission spectrometry (ICP-OES) was conducted on an ICP-OES 5110 instrument (Agilent) using standard metal solutions as reference

for each measurement.

### **XPS analysis**

Analysis were performed using a monochromatic Al K $\alpha$  X-ray source of 24.8 W power with a beam size of 100  $\mu\text{m}$ . The spherical capacitor analyzer was set at 45° take-off angle with respect to the sample surface. The pass energy was 46.95 eV yielding a full width at half maximum of 0.91 eV for the Ag 3d 5/2 peak. Curve fitting was performed using the PHI Multipack software.

### **XRD analysis**

All measurements were recorded in Bragg Brentano geometry on a Bruker D8 Discover diffractometer, equipped with a Lynx Eye XE detector, using non-monochromated Cu-K $\alpha$  radiation.

### **HSQC-2D-NMR acquisition**

Heteronuclear Single Quantum Coherence (HSQC) NMR spectra of extracted lignin oil samples were recorded at room temperature on a Bruker 500 MHz nuclear magnetic resonance (NMR) spectrometer with a 5 mm BBO probe. The pulse program was hsqcetgpsi2. Lignin oil sample (20 mg) was dissolved in deuterated chloroform (0.5 mL). Spectra were acquired with a sweep width of 15 ppm in the F2 ( $^1\text{H}$ ) dimension and 140 ppm in the F1 ( $^{13}\text{C}$ ) dimension. The acquisition time was 71.2 ms for  $^1\text{H}$  and 9.0 ms for  $^{13}\text{C}$ . The relaxation delay is 1.5 s. The solvent peak of chloroform was used as an internal reference ( $\delta\text{H}$  7.24,  $\delta\text{C}$  77.23 ppm).

## 4.5 References

- (1) J. Zakzeski; P. C. A. Bruijninx; A. L. Jongerius; B. M. Weckhuysen. The Catalytic Valorization of Lignin for the Production of Renewable Chemicals. *Chem. Rev.* **2010**, *110*, 3552–3599.
- (2) W. Schutyser; T. Renders; S. Van Den Bosch; S.-F. Koelewijn; G. T. Beckham; B. F. Sels. Chemicals from Lignin: An Interplay of Lignocellulose Fractionation, Depolymerisation, and Upgrading. *Chem. Soc. Rev.* **2018**.
- (3) N. Yan; Yuan; R. Dykeman; Y. Kou; P. J. Dyson. Hydrodeoxygenation of Lignin-Derived Phenols into Alkanes by Using Nanoparticle Catalysts Combined with Brønsted Acidic Ionic Liquids. *Angew. Chemie - Int. Ed.* **2010**, *49* (32), 5549–5553.
- (4) L. Chen; J. Xin; L. Ni; H. Dong; D. Yan; X. Lu; S. Zhang. Conversion of Lignin Model Compounds under Mild Conditions in Pseudo-Homogeneous Systems. *Green Chem.* **2016**, *18* (8), 2341–2352.
- (5) M. P. Pandey; C. S. Kim. Lignin Depolymerization and Conversion: A Review of Thermochemical Methods. *Chem. Eng. Technol.* **2011**, *34* (1), 29–41.
- (6) M. Kleinert; T. Barth. Phenols from Lignin. *Chem. Eng. Technol.* **2008**, *31* (5), 736–745.
- (7) Z. Sun; B. Fridrich; A. De Santi; S. Elangovan; K. Barta. Bright Side of Lignin Depolymerization: Toward New Platform Chemicals. *Chem. Rev.* **2018**, *118* (2), 614–678.
- (8) S. C. Qi; L. Zhang; H. Einaga; S. Kudo; K. Norinaga; J. ichiro Hayashi. Nano-Sized Nickel Catalyst for Deep Hydrogenation of Lignin Monomers and First-Principles Insight into the Catalyst Preparation. *J. Mater. Chem. A* **2017**, *5* (8), 3948–3965.
- (9) X. Cui; A.-E. Surkus; K. Junge; C. Topf; J. Radnik; C. Kreyenschulte; M. Beller. Highly Selective Hydrogenation of Arenes Using Nanostructured Ruthenium Catalysts Modified with a Carbon–Nitrogen Matrix. *Nat. Commun.* **2016**, *7* (6), 11326.
- (10) J. Dijkmans; W. Schutyser; M. Dusselier; B. F. Sels. Sn $\beta$ -Zeolite Catalyzed Oxido-Reduction Cascade Chemistry with Biomass-Derived Molecules. *Chem. Commun.* **2016**, *52* (40), 6712–6715.
- (11) W. Schutyser; S. Van Den Bosch; J. Dijkmans; S. Turner; M. Meledina; G. Van Tendeloo; D. P. Debecker; et al. Selective Nickel-Catalyzed Conversion of Model and Lignin-Derived Phenolic Compounds to Cyclohexanone-Based Polymer Building Blocks. *ChemSusChem* **2015**, *8* (10), 1805–1818.

- 
- (12) Q. Meng; M. Hou; H. Liu; J. Song; B. Han. Synthesis of Ketones from Biomass-Derived Feedstock. *Nat. Commun.* **2017**, 8, 14190.
- (13) H. Liu; T. Jiang; B. Han; S. Liang; Y. Zhou. Selective Phenol Hydrogenation to Cyclohexanone over a Dual Supported Pd-Lewis Acid Catalyst. *Science* **2009**, 326 (5957), 1250–1252.
- (14) C. Zhao; J. He; A. A. Lemonidou; X. Li; J. A. Lercher. Aqueous-Phase Hydrodeoxygenation of Bio-Derived Phenols to Cycloalkanes. *J. Catal.* **2011**, 280 (1), 8–16.
- (15) Y. Yoon; R. Rousseau; R. S. Weber; D. Mei; J. A. Lercher. First-Principles Study of Phenol Hydrogenation on Pt and Ni Catalysts in Aqueous Phase. *J. Am. Chem. Soc.* **2014**, 136 (29), 10287–10298.
- (16) C. V. Rode; U. D. Joshi; O. Sato; M. Shirai. Catalytic Ring Hydrogenation of Phenol under Supercritical Carbon Dioxide. *Chem. Commun.* **2003**, 0 (15), 1960.
- (17) H. Wang; F. Zhao; S. Fujita; M. Arai. Hydrogenation of Phenol in ScCO<sub>2</sub> over Carbon Nanofiber Supported Rh Catalyst. *Catal. Commun.* **2008**, 9 (3), 362–368.
- (18) F. Lu; J. Liu; J. Xu. Synthesis of Chain-like Ru Nanoparticle Arrays and Its Catalytic Activity for Hydrogenation of Phenol in Aqueous Media. *Mater. Chem. Phys.* **2008**, 108 (2–3), 369–374.
- (19) J. Wildschut; M. Iqbal; F. H. Mahfud; I. M. Cabrera; R. H. Venderbosch; H. J. Heeres. Insights in the Hydrotreatment of Fast Pyrolysis Oil Using a Ruthenium on Carbon Catalyst. *Energy Environ. Sci.* **2010**, 3 (7), 962.
- (20) N. Yan; C. Zhao; P. J. Dyson; C. Wang; L. Liu; Y. Kou. Selective Degradation of Wood Lignin over Noble-Metal Catalysts in a Two-Step Process. *ChemSusChem* **2008**, 1 (7), 626–629.
- (21) Z. Li; R. S. Assary; A. C. Atesin; L. A. Curtiss; T. J. Marks. Rapid Ether and Alcohol C–O Bond Hydrogenolysis Catalyzed by Tandem High-Valent Metal Triflate + Supported Pd Catalysts. *J. Am. Chem. Soc.* **2014**, 136 (1), 104–107.
- (22) H. Liu; T. Jiang; B. Han; S. Liang; Y. Zhou. Selective Phenol Hydrogenation to Cyclohexanone Over a Dual Supported Pd-Lewis Acid Catalyst. *Science* (80-. ). **2009**, 326 (5957), 1250–1252.
- (23) Q. Meng; M. Hou; J. Song; H. Liu; B. Han. Synthesis of Ketones from Biomass-Derived Feedstock. *Nat. Commun.* **2017**, 8, 1–8.
- (24) R. Nie; H. Jiang; X. Lu; D. Zhou; Q. Xia. Highly Active Electron-Deficient Pd Clusters on N-Doped Active Carbon for Aromatic Ring Hydrogenation. *Catal. Sci. Technol.* **2016**, 6 (6), 1913–1920.
- (25) Z. Dong; C. Dong; Y. Liu; X. Le; Z. Jin; J. Ma. Hydrodechlorination and Further

- Hydrogenation of 4-Chlorophenol to Cyclohexanone in Water over Pd Nanoparticles Modified N-Doped Mesoporous Carbon Microspheres. *Chemical Engineering Journal*. 2015, pp 215–222.
- (26) H. Jiang; X. Yu; R. Nie; X. Lu; D. Zhou; Q. Xia. Selective Hydrogenation of Aromatic Carboxylic Acids over Basic N-Doped Mesoporous Carbon Supported Palladium Catalysts. *Applied Catalysis A: General*. 2016, pp 73–81.
- (27) Z. Xu; F.-S. Xiao; S. K. Purnell; O. Alexeev; S. Kawi; S. E. Deutsch; B. C. Gates. Size-Dependent Catalytic Activity of Supported Metal Clusters. *Nature* **1994**, 372 (6504), 346–348.
- (28) B. C. Gates. Supported Metal Clusters: Synthesis, Structure, and Catalysis Contents Supported Metal Catalysts Structure-Sensitive and Structure-Insensitive Reactions Catalyzed by Metals Molecular Metal Clusters and Supported Metal Clusters Classes of Supported Metal C. *Chem. Rev* **1995**, 95, 511–522.
- (29) G.-H. Wang; J. Hilgert; F. H. Richter; F. Wang; H. Bongard; B. Spliethoff; C. Weidenthaler; et al. Platinum-Cobalt Bimetallic Nanoparticles in Hollow Carbon Nanospheres for Hydrogenolysis of 5-Hydroxymethylfurfural. *Nat. Mater.* **2014**, 13 (3), 293–300.
- (30) W. R. Crowell; O. König. Hexamethylenetetramine as a Reagent for Microscopic Tests for Gold and the Platinum Metals. *Mikrochemie Ver. mit Mikrochim. Acta* **1948**, 33 (4), 303–309.
- (31) C. V. Rode; U. D. Joshi; T. Sato; O. Sato; M. Shirai. Phenol Hydrogenation over Supported Metal Catalysts under Supercritical Carbon Dioxide. In *Journal of Catalysis*; 2004; Vol. 48, pp 385–388.
- (32) T. Kondo; D. Guo; T. Shikano; T. Suzuki; M. Sakurai; S. Okada; J. Nakamura. Observation of Landau Levels on Nitrogen-Doped Flat Graphite Surfaces without External Magnetic Fields. *Sci. Rep.* **2015**, 5 (November), 1–8.
- (33) M. Xu; G. He; Z. Li; F. He; F. Gao; Y. Su; L. Zhang; et al. A Green Heterogeneous Synthesis of N-Doped Carbon Dots and Their Photoluminescence Applications in Solid and Aqueous States. *Nanoscale* **2014**, 6 (17), 10307–10315.
- (34) P. Giannoccaro; M. Gargano; A. Fanizzi; C. Ferragina; M. Aresta. Rh-Ions and Rh-Complexes Intercalated in ??-Titanium or ??-Zirconium Hydrogen Phosphate as Highly Efficient Catalysts for Arene Hydrogenation. *Appl. Catal. A Gen.* **2005**, 284 (1–2), 77–83.
- (35) J. He; C. Zhao; J. A. Lercher. Impact of Solvent for Individual Steps of Phenol Hydrodeoxygenation with Pd/C and HZSM-5 as Catalysts. *J. Catal.* **2014**, 309, 362–375.

- (36) L. Giraldo; M. Bastidas-Barranco; J. C. Moreno-Piraján. Vapour Phase Hydrogenation of Phenol over Rhodium on SBA-15 and SBA-16. *Molecules* **2014**, *19* (12), 20594–20612.
- (37) V. Vinokurov; A. Glotov; Y. Chudakov; A. Stavitskaya; E. Ivanov; P. Gushchin; A. Zolotukhina; et al. Core/Shell Ruthenium–Haloysite Nanocatalysts for Hydrogenation of Phenol. *Ind. Eng. Chem. Res.* **2017**, *56* (47), 14043–14052.
- (38) N. Singh; M.-S. Lee; S. A. Akhade; G. Cheng; D. M. Camaioni; O. Y. Gutiérrez; V.-A. Glezakou; et al. Impact of PH on Aqueous-Phase Phenol Hydrogenation Catalyzed by Carbon-Supported Pt and Rh. *ACS Catal.* **2019**, *9* (2), 1120–1128.
- (39) W.-Y. Lu; S. Bhattacharjee; B.-X. Lai; A.-B. Duh; P.-C. Wang; C.-S. Tan. Hydrogenation of Bisphenol A-Type Epoxy Resin (BE186) over Vulcan XC72-Supported Rh and Rh–Pt Catalysts in Ethyl Acetate-Containing Water. *Ind. Eng. Chem. Res.* **2019**, *58* (36), 16326–16337.
- (40) X. Wang; R. Rinaldi. Exploiting H-Transfer Reactions with RANEY® Ni for Upgrade of Phenolic and Aromatic Biorefinery Feeds under Unusual, Low-Severity Conditions. *Energy Environ. Sci.* **2012**, *5* (8), 8244–8260.
- (41) S. Wang; G. Q. Lu. Effects of Acidic Treatments on the Pore and Surface Properties of Ni Catalyst Supported on Activated Carbon. *Carbon N. Y.* **1998**, *36* (3), 283–292.
- (42) M. Wang; H. Shi; D. M. Camaioni; J. A. Lercher. Palladium-Catalyzed Hydrolytic Cleavage of Aromatic C–O Bonds. *Angew. Chemie - Int. Ed.* **2017**, *56* (8), 2110–2114.
- (43) C. Li; X. Zhao; A. Wang; G. W. Huber; T. Zhang. Catalytic Transformation of Lignin for the Production of Chemicals and Fuels. *Chemical Reviews*. American Chemical Society 2015, pp 11559–11624.
- (44) G. T. Beckham; C. W. Johnson; E. M. Karp; D. Salvachúa; D. R. Vardon. Opportunities and Challenges in Biological Lignin Valorization. *Current Opinion in Biotechnology*. Elsevier Ltd December 1, 2016, pp 40–53.
- (45) A. J. Ragauskas; G. T. Beckham; M. J. Biddy; R. Chandra; F. Chen; M. F. Davis; B. H. Davison; et al. Lignin Valorization: Improving Lignin Processing in the Biorefinery. *Science*. American Association for the Advancement of Science May 16, 2014.
- (46) A. Narani; R. K. Chowdari; C. Cannilla; G. Bonura; F. Frusteri; H. J. Heeres; K. Barta. Efficient Catalytic Hydrotreatment of Kraft Lignin to Alkylphenolics Using Supported NiW and NiMo Catalysts in Supercritical Methanol. *Green Chem.* **2015**, *17* (11), 5046–5057.
- (47) T. Renders; G. Van den Bossche; T. Vangeel; K. Van Aelst; B. Sels. Reductive

- Catalytic Fractionation: State of the Art of the Lignin-First Biorefinery. *Curr. Opin. Biotechnol.* **2019**, *56*, 193–201.
- (48) W. Schutyser; T. Renders; S. Van Den Bosch; S. F. Koelewijn; G. T. Beckham; B. F. Sels. Chemicals from Lignin: An Interplay of Lignocellulose Fractionation, Depolymerisation, and Upgrading. *Chem. Soc. Rev.* **2018**, *47* (3), 852–908.
- (49) T. Renders; S. Van Den Bosch; S. F. Koelewijn; W. Schutyser; B. F. Sels. Lignin-First Biomass Fractionation: The Advent of Active Stabilisation Strategies. *Energy Environ. Sci.* **2017**, *10* (7), 1551–1557.
- (50) S. Van Den Bosch; T. Renders; S. Kennis; S. F. Koelewijn; G. Van Den Bossche; T. Vangeel; A. Deneyer; et al. Integrating Lignin Valorization and Bio-Ethanol Production: On the Role of Ni-Al<sub>2</sub>O<sub>3</sub> catalyst Pellets during Lignin-First Fractionation. *Green Chem.* **2017**, *19* (14), 3313–3326.
- (51) E. M. Anderson; M. L. Stone; R. Katahira; M. Reed; G. T. Beckham; Y. Román-Leshkov. Flowthrough Reductive Catalytic Fractionation of Biomass. *Joule* **2017**, *1* (3), 613–622.
- (52) E. M. Anderson; M. L. Stone; M. J. Hülsey; G. T. Beckham; Y. Román-Leshkov. Kinetic Studies of Lignin Solvolysis and Reduction by Reductive Catalytic Fractionation Decoupled in Flow-Through Reactors. *ACS Sustain. Chem. Eng.* **2018**, *6* (6), 7951–7959.
- (53) J. N. Chheda; Y. Román-Leshkov; J. A. Dumesic. Production of 5-Hydroxymethylfurfural and Furfural by Dehydration of Biomass-Derived Mono- and Poly-Saccharides. *Green Chem.* **2007**, *9* (4), 342–350.
- (54) H. Xu; B. Yu; H. Zhang; Y. Zhao; Z. Yang; J. Xu; B. Han; et al. Reductive Cleavage of Inert Aryl C-O Bonds to Produce Arenes. *Chem. Commun.* **2015**, *51* (61), 12212–12215.
- (55) H. Wu; J. Song; C. Xie; C. Wu; C. Chen; B. Han. Efficient and Mild Transfer Hydrogenolytic Cleavage of Aromatic Ether Bonds in Lignin-Derived Compounds over Ru/C. *ACS Sustain. Chem. Eng.* **2018**, *6* (3), 2872–2877.
- (56) G. H. Wang; J. Hilgert; F. H. Richter; F. Wang; H. J. Bongard; B. Spliethoff; C. Weidenthaler; et al. Platinum-Cobalt Bimetallic Nanoparticles in Hollow Carbon Nanospheres for Hydrogenolysis of 5-Hydroxymethylfurfural. *Nat. Mater.* **2014**, *13* (3), 293–300.
- (57) T. Maegawa; A. Akashi; H. Sajiki. A Mild and Facile Method for Complete Hydrogenation of Aromatic Nuclei in Water. *Synlett* **2006**, *2006* (9), 1440–1442.
- (58) S. Kasakov; H. Shi; D. M. Camaioni; C. Zhao; E. Baráth; A. Jentys; J. A. Lercher. Reductive Deconstruction of Organosolv Lignin Catalyzed by Zeolite Supported Nickel Nanoparticles. *Green Chem.* **2015**, *17* (11), 5079–5090.

- (59) J. Ralph; K. Lundquist; G. Brunow; F. Lu; H. Kim; P. F. Schatz; J. M. Marita; et al. Lignins: Natural Polymers from Oxidative Coupling of 4-Hydroxyphenyl-Propanoids. *Phytochemistry Reviews*. Springer January 2004, pp 29–60.
- (60) W. Schutyser; S. Van Den Bosch; T. Renders; T. De Boe; S. F. Koelewijn; A. Dewaele; T. Ennaert; et al. Influence of Bio-Based Solvents on the Catalytic Reductive Fractionation of Birch Wood. *Green Chem.* **2015**, 17 (11), 5035–5045.

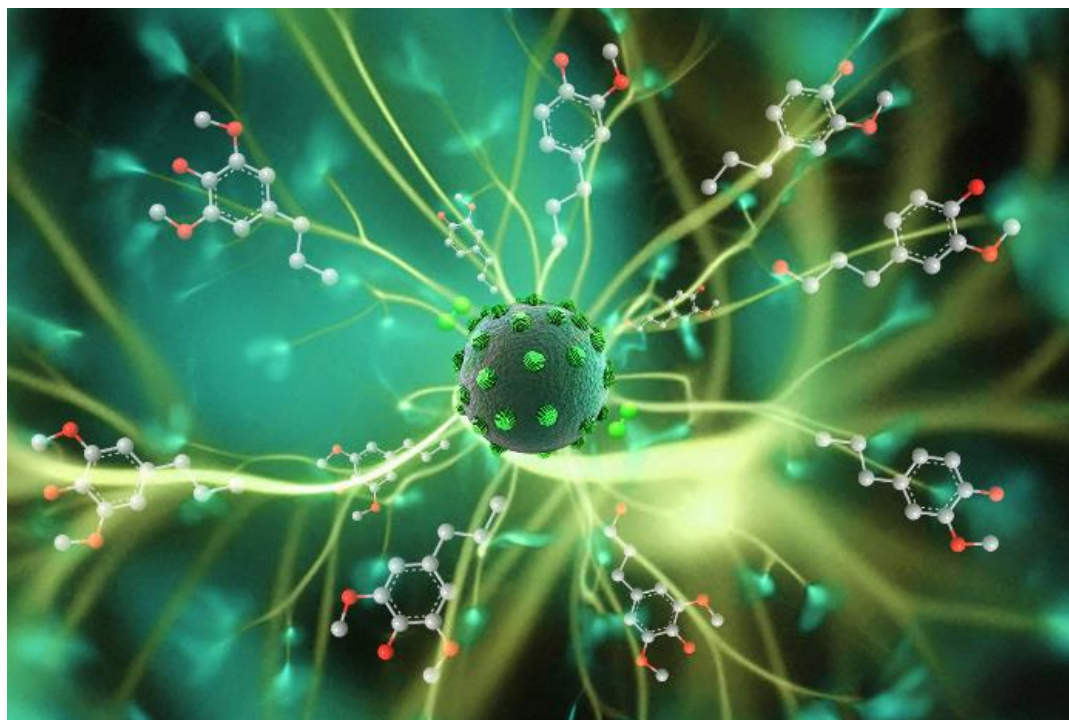


# **Chapter 5 Embedding single platinum atoms into nickel nanoparticles to afford a highly selective catalyst for lignin conversion**

## **Overview**

The chapter introduces that using atomically dispersed catalysts in the reductive lignin depolymerization. Lignin is an abundant biomass source that can potentially be converted into value-added aromatic platform chemicals. Due to the highly complex polyphenol-structure of lignin, depolymerisation without a prior chemical treatment is challenging, and new, superior catalysts are required. Atomically dispersed catalysts containing isolated atoms are able to maximize the atomic efficiency of noble metals in a catalytic process, simultaneously providing an alternative strategy to tune the activity and selectivity by alloying with other abundant metal supports. Herein, we report a highly active catalyst comprising monodispersed (single) Pt atoms on Ni nanoparticles supported on carbon (denoted as Pt<sub>1</sub>Ni/C where Pt<sub>1</sub> represent single Pt atoms), designed for the reductive depolymerization of lignin. At 200 °C under 5 MPa of H<sub>2</sub> in methanol, after 18 h the yield of total lignin monomers is 37%, which is significantly higher than that obtained using single component Pt single atoms or Ni nanoparticles as the catalysts. The increased activity of the engineered Pt<sub>1</sub>Ni/C catalyst in the reductive depolymerization of lignin is attributed to synergistic effects between the Ni nanoparticles that promote dissociation of H<sub>2</sub> and supply the absorbed hydrogen to the single Pt atoms where cleavage of the C-O bonds takes place.

Graphic abstract:



## 5.1 Introduction

To utilize biomass to its fullest, the challenges involved in valorizing lignin need to be overcome.<sup>1,2</sup> Conventional lignocellulose delignification methods, such as Kraft and Organosolv pulping, require complete breakdown of the C-O bonds in a series of steps.<sup>3-5</sup> However, the ability to deconstruct lignin directly from raw biomass has transformed the conventional concept of the biorefinery by capturing high-value products from lignin in the first step,<sup>6</sup> a process that is particularly effective under reductive conditions.<sup>2,7-9</sup> The lignin is depolymerized and selectively converted to monomers with high retention of carbohydrates in the pulp.<sup>10-12</sup> The monomers obtained are valuable platform chemicals with a range of applications. Further utilization of remaining cellulose and hemicellulose provides additional value-added chemicals.<sup>13-15</sup>

Using noble metal catalysts, e.g. Rh, Ru, Pd and Pt, the yields of lignin monomers can reach close to the theoretical maximum.<sup>16-18</sup> However, these noble metal catalysts are expensive and can be susceptible to poisoning by CO or coking.<sup>19</sup> Efforts to maximize the efficiency of these noble metal catalysts with improved selectivity has led to the development of atomically dispersed heterogeneous catalysts.<sup>20-22</sup> All reaction steps take place at single atom sites and, compared with metal nanoparticles, the reaction kinetics with single atoms catalysts are rate-limited by the low concentration of H atoms available in the active atomic sites.

Progress towards catalyst design to combine the activity of noble metals and low cost of earth abundant metals is popular.<sup>23</sup> Some earth abundant metals such as Ni have low energy barriers for both the dissociation of H<sub>2</sub> and the diffusion of H atoms.<sup>24</sup> If H<sub>2</sub> dissociation on Ni nanoparticles and diffusion to active single noble metal atoms is facile, then the rate limiting addition of H atoms to substrate should be accelerated, improving the overall reaction kinetics and reducing the amount of the precious metal required. Such a single atom alloy (SAA) concept has been described for a PdCu system in which facile hydrogen dissociation and spillover takes place.<sup>25</sup> Because the dissociation of H<sub>2</sub> and reaction sites on SAAs are decoupled, SAAs may not be confined to linear scaling relationships, exceeding the reactivity limit and selectivity of many catalysts.

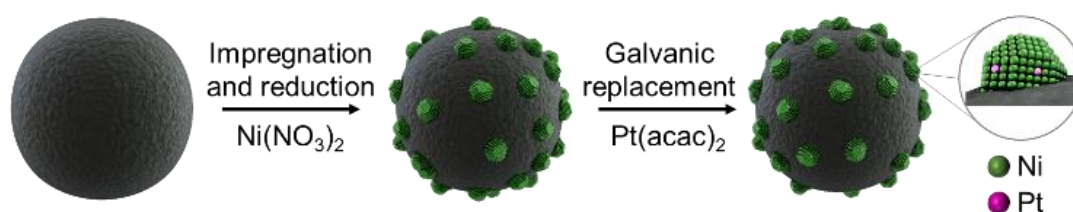
Despite numerous reports of SAAs, their application is mostly limited to catalytic

process involving small substrates, and in reactions such as C-C coupling, hydrogenation and electrocatalytic processes.<sup>20,26–31</sup> There are only limited studies describing SAAs as catalysts for biomass transformations, with the focus on lignin model compounds as substrates.<sup>32,33</sup> Direct depolymerization of lignin using SAAs has not, to the best of our knowledge, been reported.

Herein, we describe a highly active catalyst for reductive lignin depolymerization based on Pt single atoms embedded into Ni nanoparticles supported on carbon (denoted as Pt<sub>1</sub>Ni/C, where Pt<sub>1</sub> represent single Pt atoms). Using this catalyst, a yield of lignin monomers of 37% for birch sawdust was achieved under 5 MPa H<sub>2</sub> in methanol (MeOH) at 200 °C, which is significantly higher than that using single Pt atoms supported on active carbon Pt<sub>1</sub>/C or Ni NPs on active carbon Ni/C.

## 5.2 Results and discussion

The Pt<sub>1</sub>Ni/C catalyst was obtained by embedding Pt atoms on Ni nanoparticles supported on carbon (Ni/C) through galvanic replacement (Scheme 5.1). In the synthesis, Pt(acac)<sub>2</sub> dissolved in toluene was added to a suspension of Ni/C in ethanol. Carbon was chosen as the support as it is inexpensive and has a high surface area and cavities where H<sub>2</sub> can be adsorbed.<sup>34</sup> Following washing with ethanol and hexane, the Pt<sub>1</sub>Ni/C catalyst was obtained as black powder. Inductively coupled plasma-atomic emission spectroscopy (ICP-AES) analysis of the Pt<sub>1</sub>Ni/C catalyst gives weight percentages of the Pt and Ni as 0.3 and 4.4 wt%, respectively. Thermogravimetric analysis (TGA) of Pt<sub>1</sub>Ni/C in air (Figure 5.7B) confirmed that the loading of Ni NPs is around 5%. Using Transmission electron microscopy (TEM), the diameter of the Ni NPs was found to be approximately 6.9 nm with a narrow size distribution (Figure 5.2).

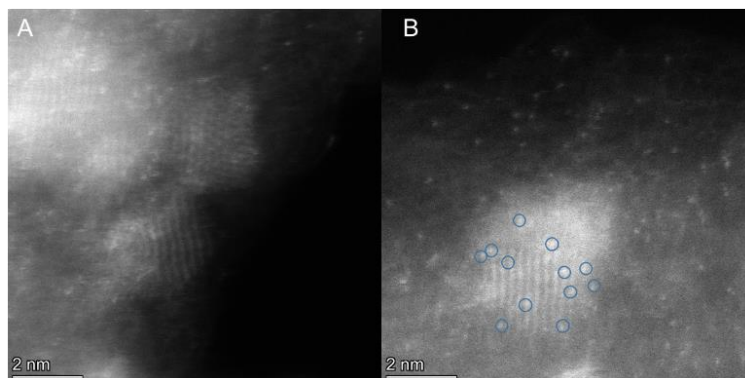


**Scheme 5.1** Synthesis route for Pt<sub>1</sub>Ni/C.

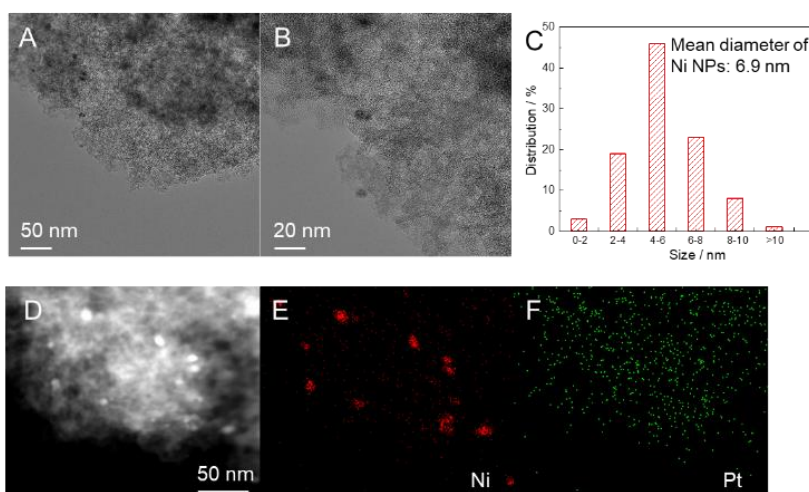
The distribution of Pt on Ni/C within the Pt<sub>1</sub>Ni/C matrix was analyzed by high-angle annular dark-field scanning transmission electron microscopy (HAADF-STEM) (Figure 5.1), which confirms that the Pt atoms are highly dispersed (the isolated Pt atoms are manifested by brightness and marked by circles, Figure 5.1B). The Pt single atoms in the surface of Ni/C were further identified by the extended X-ray absorption fine structure (EXAFS) analysis in the R space (Figure 5.5A). The oscillation manners of the Pt L<sub>3</sub>-edge in the R space for the Pt<sub>1</sub>Ni/C differ to those of Pt foil. The Pt–Pt bond at 2.76 Å was not observed in Pt<sub>1</sub>Ni/C. Compared to the Pt L<sub>3</sub>-edge of Pt foil in the X-ray absorption near-edge spectroscopy (XANES) spectra (Figure 5.5B), the adsorption edge for Pt<sub>1</sub>Ni/C is around 11570 eV, indicative of Pt(II) species. Indeed, the X-ray photoelectron spectroscopy (XPS) spectra of Ni 2p and Pt 4f indicate that the majority of surface Ni and Pt species are in the oxidation state (Figure 5.6).<sup>35</sup>

The X-ray diffraction (XRD) profile of the Pt<sub>1</sub>Ni/C catalyst shows a characteristic peak at 44° corresponding to (111) reflections of face-centered cubic Ni NPs (Figure 5.7A), at the identical position observed in Ni/C, presumably as the low content of highly dispersed Pt does not influence the XRD pattern.

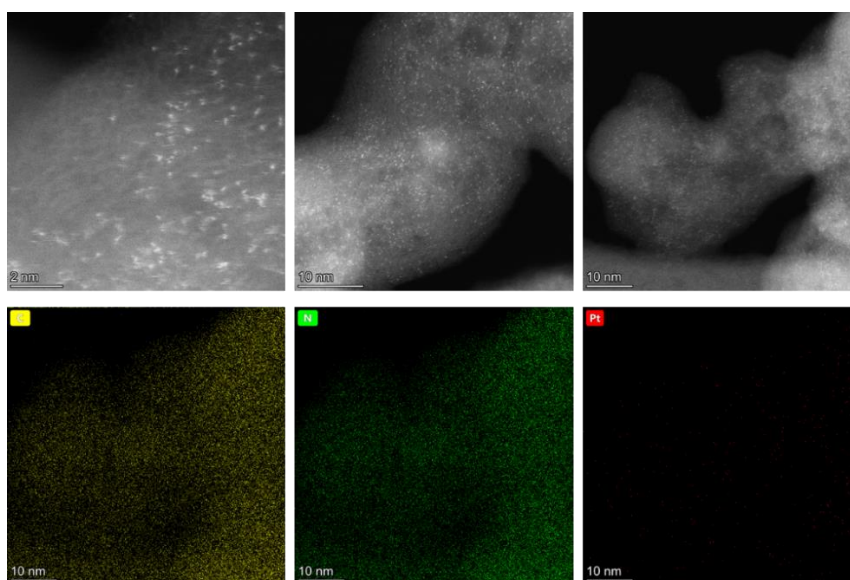
The H<sub>2</sub>-temperature-programmed reaction (TPR) profiles (Figure 5.5C) indicate that alloying takes place in the Pt<sub>1</sub>Ni/C catalyst. With the addition of single Pt atoms, the reduction temperature of Pt<sub>1</sub>Ni/C (275 °C) is shifted to lower regions compared with Ni/C (261 °C). The adsorption of H<sub>2</sub> on the surface of the Pt<sub>1</sub>Ni/C catalyst was investigated through H<sub>2</sub>-temperature-programmed desorption (TPD) measurements (Figure 5.5D). The first peak (at 425 °C) in the Pt<sub>1</sub>Ni/C catalyst is at a much lower temperature than that observed for Ni/C (at 698 °C), indicating that the Pt atoms provide low-barrier exit routes for H<sub>2</sub> during the desorption process.

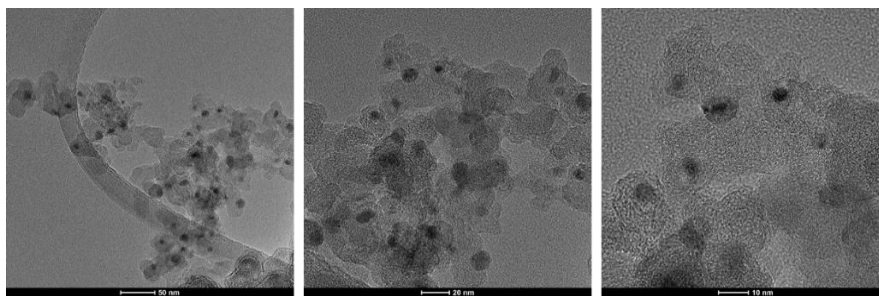
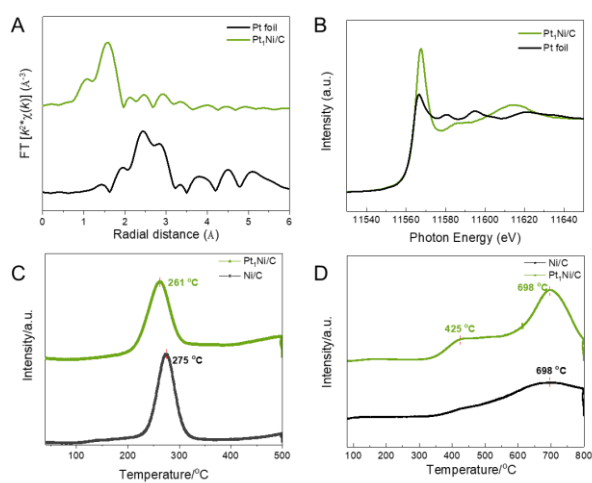
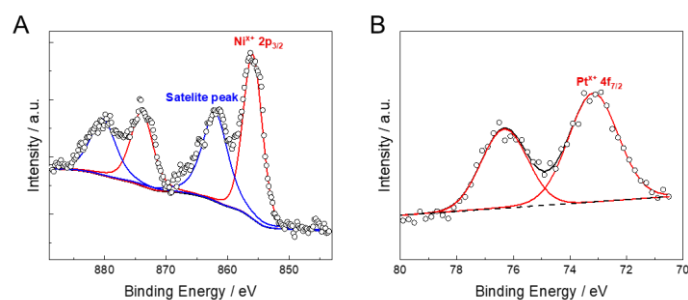


**Figure 5.1** (A) HAADF-STEM image of Pt<sub>1</sub>Ni/C. (B) HAADF-STEM image of an individual Pt<sub>1</sub>Ni nanoparticle. The Pt single atoms marked in blue circles were uniformly embedded in the surface of Ni NPs.



**Figure 5.2** (A-B) TEM images, (C) size distribution of Ni NPs, and (D-F) elements mapping of Pt<sub>1</sub>Ni/C



**Figure 5.3** HAADF-STEM images and elements mapping of Pt/C**Figure 5.4** TEM images of Ni/C**Figure 5.5** (A) Pt L3-edge EXAFS spectra in R space of Pt foil and Pt<sub>1</sub>Ni/C. Pt foil was used as the reference; (B) Pt L3-edge XANES profiles of Pt foil and Pt<sub>1</sub>Ni/C; (C) H<sub>2</sub>-temperature-programmed reaction (TPR) profiles of Pt<sub>1</sub>Ni/C; (D) H<sub>2</sub>-temperature-programmed desorption (TPD) profiles of Pt<sub>1</sub>Ni/C.**Figure 5.6** X-ray photoelectron spectroscopy (XPS) spectra of (A) Ni 2p and (B) Pt 4f for Pt<sub>1</sub>Ni/C



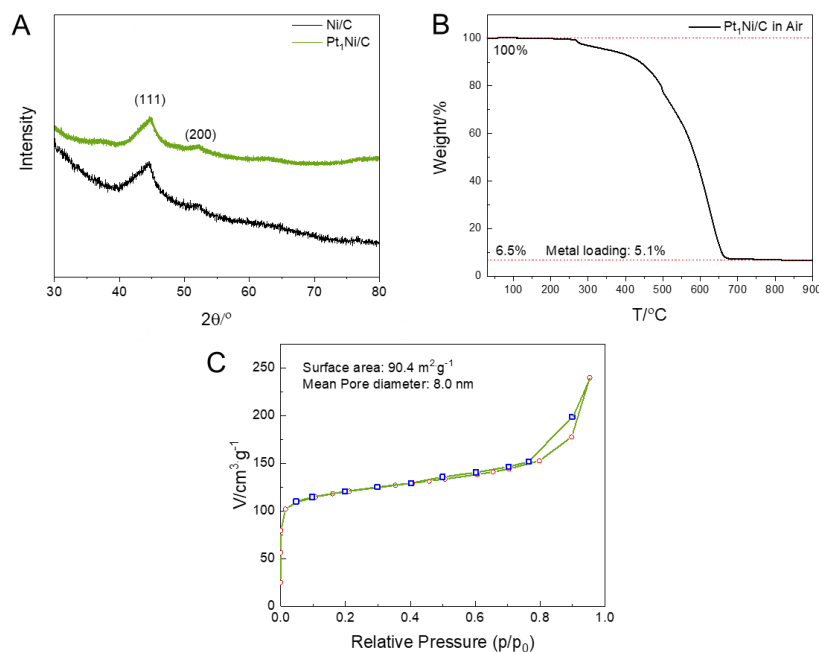


**Figure 5.7** (A) Powder X-ray diffraction (XRD) profiles of Pt<sub>1</sub>Ni/C and Ni/C; (B) Thermal gravimetric analysis (TGA) of Pt<sub>1</sub>Ni/C in air; (C) N<sub>2</sub> physisorption isotherms of Pt<sub>1</sub>Ni/C. The specific surface areas of 90.4 m<sup>2</sup>/g, and the mean diameter of pores 8 nm.

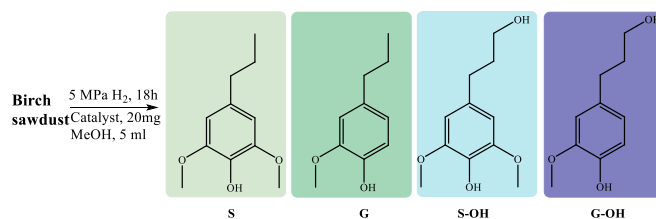
The performance of the Pt<sub>1</sub>Ni/C catalyst was investigated in the depolymerization of lignin using birch sawdust as the substrate. For comparison, single Pt atoms and nickel nanoparticles supported on carbon (Pt<sub>1</sub>/C and Ni/C) were prepared and applied in the same depolymerization reaction under identical conditions (Table 5.1). The monomer yields are used as a measure of depolymerization efficiency of the catalysts. Under 5 MPa H<sub>2</sub> in methanol at 200 °C, the yield of total monomers with the Pt<sub>1</sub>Ni/C catalyst is 37% after 18 h (Table 5.1, entry 1), close to the theoretical maximum monomer yield which is between 44 and 56 wt%.<sup>36</sup> The yield of total monomers is significantly higher than that with the control catalysts (Table 5.1, entries 2 and 3) and reported Ni/C, with monomer yields of 28.3% at 200 °C in methanol.<sup>37</sup> Further analysis of the product distribution shows that a combined selectivity towards 4-n-propylsyringol (S) and 4-n-propylguaiacol (G) exceeding 90% within the monomer fractions, whereas 4-n-propanolguaiacol (G-OH) and 4-n-propanolsyringol (S-OH) accounts for less than 5% of the monomers (Table 1, entry 1). It has been previously shown that Pt NPs are more active hydrogenolysis catalysts than Ni NPs.<sup>38</sup> As hydrogenolysis of C–O bonds is highly metal dependent,<sup>39</sup> the overall yield in S and G may be attributed to high activity of Pt atoms. Note that in the absence of the carbon support the monomer yield is very low (Table 5.1, entry 4).



The mechanism of reductive fractionation involves solvolysis of the C-O bonds with the catalyst hydrogenating the reactive intermediate products generated, preventing re-polymerization.<sup>40,41</sup> Compare with Pt<sub>1</sub>/C which is less active with hydrogen dissociation as the rate-limiting step, both Ni NPs and single Pt atoms in Pt<sub>1</sub>Ni/C served as active sites in H<sub>2</sub> dissociation and adsorption of H atoms, so that a more abundant amount of H atoms can be produced on the surface of Pt<sub>1</sub>Ni/C. Compare with Ni/C, better performance of Pt<sub>1</sub>Ni/C owns to lower hydrogen binding energy of Pt atoms than Ni atoms. As suggested by the H<sub>2</sub>-TPD analysis, single Pt atoms in the Pt<sub>1</sub>Ni/C can serve as active sites in the addition of H atoms to intermediate products is facilitating the addition step. Moreover, due to the single atom nature of the Pt in the Pt<sub>1</sub>Ni/C, the aromatic structure of the phenyl rings of lignin monomers are preserved without further hydrogenation. Since ring hydrogenation requires coordination of the aromatic ring over a trimetal face, single Pt atoms can achieve hydrogenolysis of the C-O bonds without the hydrogenation of the phenyl ring.<sup>42</sup> As such, Pt single atoms played a pivotal role in Pt<sub>1</sub>Ni/C in enhancing the catalytic activity while keeping the high selectivity in the lignin depolymerization, a benefit that can not be achieved by using Ni/C only.

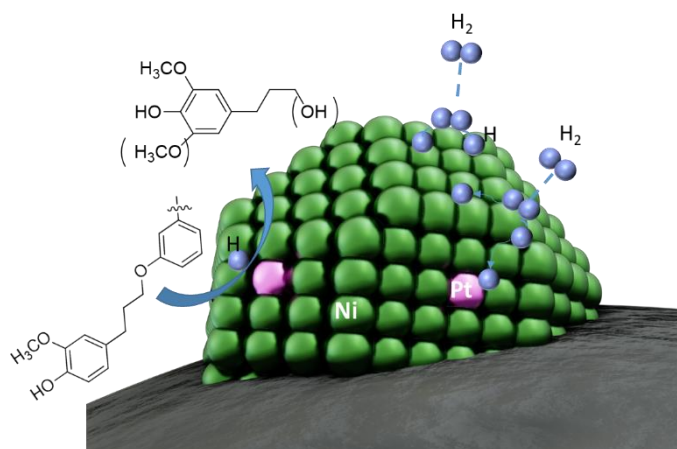
The reaction conditions were optimized to obtain monophenolic compounds in higher yields (Figure 5.8). The yield of monophenolic compounds increased from 12 wt % at 150 °C to 43 wt% at 300 °C at a H<sub>2</sub> pressure of 5 MPa in methanol after 18 h (Figure 5.8a), with high selectivity to S and G (>90%, Figure 5.8b). At lower H<sub>2</sub> pressures (and in the absence of H<sub>2</sub>), G-OH and S-OH are preferentially formed instead of G and S (Figure 5.8c).

A comparison of product distributions in water, methanol, ethanol, 1-propanol, 1-butanol and ethylene glycol (Figure 5.8d) shows that solvent has remarkable impact on the monomer yield as well as the product distribution, as observed elsewhere.<sup>43,44</sup> The solubility of lignin in different solvents has been extensively studied,<sup>45</sup> with the solubility in ethylene glycol being the highest followed by methanol, ethanol, 1-propanol, 1-butanol and H<sub>2</sub>O.<sup>46</sup> The monomer yields basically decrease with the decreasing solubility of lignin in the solvent. As in our case, comparably lower yield of 32% in the pure ethylene glycol was obtained than that from methanol, probably due to the high viscosity and low solubility of H<sub>2</sub> in ethylene glycol.

**Table 5.1.** Lignin monomers distribution with different catalysts

Entry	Catalyst	Total yield of monomers (%)	S	G	S-OH	G-OH
1	Pt <sub>1</sub> Ni/C (This work)	37	23	12	0.1	0.5
2	Pt <sub>1</sub> /C	14	3	2	5	2
3	Ni/C	24	9	6	5	3
4	C	6	1	-	-	-

Reaction conditions: 0.1 g birch sawdust, 0.02 g catalyst, 5 mL MeOH, 5 MPa H<sub>2</sub>, 200 °C and 18 h.

**Scheme 5.2** Schematic illustration of H<sub>2</sub> dissociation and H diffusion on Pt<sub>1</sub>Ni/C

A comparison of product distributions in water, methanol, ethanol, 1-propanol, 1-butanol and ethylene glycol (Figure 5d) shows that solvent has remarkable impact on the yield of monomers as well as the products distribution.<sup>43,44</sup> It has been reported that high solubility of lignin will allow faster interaction with the active catalyst.<sup>47</sup> The solubility of lignin in different solvents including alcohols, cyclic ethers and

hydrocarbons has been extensively studied using UV-Vis spectroscopy.<sup>45</sup> In general, the solubility of lignin in alcohols decreases with the increased alkyl chain. The ethylene glycol gives the best solubility and followed by MeOH, because the hydroxyl groups may weaken the hydrogen bonding network through hydrogen bonding formation.<sup>46</sup> Reactions in ethanol, 1-propanol and 1-butanol are less effective than in methanol. As the length of the alkyl chains in the alcohols increases, the yield of the monomers decreases (Figure 5d) probably due to the decreased solubility of lignin. In the pure ethylene glycol, the high viscosity and low H<sub>2</sub> solubility may be the reason for the lower yield compared with methanol (Figure 5d). Apart from being an efficient solvent, MeOH is also an active hydrogen source.<sup>48,49</sup> The solvent effect has been studied<sup>44</sup> with the more polar and Lewis acidic solvent being able to induce swelling of the lignin, facilitating faster interactions of the lignin with catalysts for increased yield of monomers.

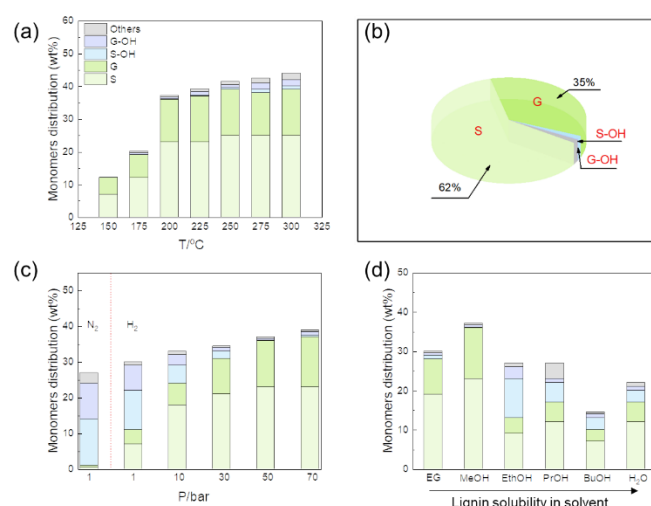


**Figure 5.8** (a) Yields of lignin monomers obtained from birch sawdust as a function of temperature. Reaction conditions: 0.1 g birch sawdust, 0.02 g Pt<sub>1</sub>Ni/C, 5 mL MeOH, 5 MPa H<sub>2</sub>, 200 °C and 18 h. (b) Monomer distribution at 200 °C in MeOH. Reaction conditions are the same as those in (a). (c) Yields of lignin monomers obtained from birch sawdust as a function of H<sub>2</sub> pressure. Reaction conditions: 0.1 g birch sawdust, 0.02 g Pt<sub>1</sub>Ni/C, 5 mL MeOH, H<sub>2</sub>, 200 °C and 18 h. (d) Yields of lignin monomers obtained from birch sawdust in various solvents. Reaction conditions: 0.1 g birch sawdust, 0.02 g Pt<sub>1</sub>Ni/C, 5 mL solvent, 5 MPa H<sub>2</sub>, 200 °C and 18 h. Abbreviations: methanol (MeOH), ethanol (EtOH), 1-propanol (PrOH), 1-butanol (BuOH), ethylene glycol (EG), water (H<sub>2</sub>O).

## 5.3 Conclusions

We describe a selective hydrogenation catalyst in which monodispersed Pt atoms are embedded within the surface of Ni NPs supported on active carbon. The Pt<sub>1</sub>Ni/C catalyst affords monophenolic compounds in 37 wt% yield at 200°C which is close to the theoretical maximum yield which is between 44 and 56 wt%. The remarkable selectivity of Pt<sub>1</sub>Ni/C attributed to the inability of single Pt atoms to hydrogenate aromatic rings, hence enabling C-O bond hydrogenolysis without ring hydrogenation.

## 5.4 Methods

### 5.4.1 Synthesis of Ni/C and Pt<sub>1</sub>Ni/C

Carbon powder (Vulcan XC 72R, 1 g) was mixed with 50 mL of 5 M nitric acid at 80 °C and stirred for 18 h. The solids were separated by centrifugation and were washed with distilled water until constant pH. The pre-treated activated carbon (200 mg) was dispersed in ethanol (20 mL) under vigorous stirring at room temperature. To the resulting suspension, a solution containing Ni(NO<sub>3</sub>)<sub>2</sub> (50 mg, 0.2 mmol) in ethanol (5 mL) was slowly added and stirring was continued for 12 h at room temperature. The reaction mixture was further heated at 40 °C under stirring until all the solvent had evaporated. The remaining the solid was heated to 400°C for 1 h under H<sub>2</sub> in a tube furnace, to afford Ni/C.

The Pt<sub>1</sub>Ni/C catalyst was prepared via galvanic replacement between Ni NPs and Pt(acac)<sub>2</sub>. Ni/C was dispersed in ethanol (50 mL), and resulting suspension was heated at 50 °C for 10 min. To the reaction mixture, a solution of Pt(acac)<sub>2</sub> (6 mg, 0.015 mmol) dissolved in toluene (5.2 mL) was added slowly. After stirring for 6 h at 50 °C, the solution was cooled to room temperature, then the sample was collected by centrifugation, and washed with ethanol (3 x 10 mL) and hexane (3 x 10 mL). After drying in vacuum at 40 °C for 24 h, the Pt<sub>1</sub>Ni/C catalyst was obtained as a black powder.

### 5.4.2 Synthesis of Pt<sub>1</sub>/C

Carbon powder (Vulcan XC 72R, 1 g) was mixed with 50 mL of 5 M nitric acid at 80 °C and stirred for 18 h. The solids were separated by centrifugation and were washed with distilled water until constant pH. This pre-treated activated carbon (100 mg) was

dispersed in water (20 mL) under magnetic stirring.  $\text{K}_2\text{PtCl}_4$  aqueous solution (10 mL, 0.043 mg/mL) was slowly added to the resulting reaction mixture. After stirring at room temperature for 30 min, the solid was collected by centrifugation. The isolated solid was washed with water (3x 10 mL) and dried at 60 °C in vacuum for 24h. The  $\text{Pt}_1/\text{C}$  was obtained as a black powder.

#### 5.4.3 XAFS analysis

XAFS data were recorded under fluorescence mode with a 32-element Ge solid state detector. The energy was calibrated according to the absorption edge of pure Pt foil.

#### 5.4.4 TEM, XPS, XRD measurements

The  $\text{Pt}_1\text{Ni}/\text{C}$  powders were suspended in acetone and the resulting suspension was ultrasonicated for 1 h. Subsequently, the acetone suspension of nanoparticles was deposited on a carbon film coated with copper grid and then analyzed by transmission electron microscopy (TEM). (FEI Talos, operated at 200 keV). XPS analysis were performed using a monochromatic Al  $\text{K}\alpha$  X-ray source of 24.8 W power with a beam size of 100  $\mu\text{m}$ . XRD measurements were recorded in Bragg Brentano geometry on a Bruker D8 Discover diffractometer, equipped with a Lynx Eye XE detector, using non-monochromated Cu- $\text{K}\alpha$  radiation.

#### 5.4.5 Catalytic tests

In a typical reaction, birch sawdust (0.1 g, size 0.25–0.5 mm),  $\text{Pt}_1\text{Ni}/\text{C}$  (0.02 g) in MeOH (5 mL) were added into a 100 mL stainless steel batch reactor with a glass liner. The reactor was sealed, was flushed with  $\text{H}_2$  three times and then pressurized to 5 MPa at room temperature. The reaction mixture was heated at 100 °C for 3h under stirring at 800 rpm, and then heated to 200 °C. After 18 h, the autoclave was cooled in water and then depressurized.

## 5.5 References

- (1) B. M. Upton; A. M. Kasko. Strategies for the Conversion of Lignin to High-Value Polymeric Materials: Review and Perspective. *Chem. Rev.* **2015**, *116*, 2277.
- (2) W. Schutyser; T. Renders; S. Van Den Bosch; S.-F. F. Koelewijn; G. T. Beckham; B. F. Sels. Chemicals from Lignin: An Interplay of Lignocellulose Fractionation, Depolymerisation, and Upgrading. *Chem. Soc. Rev.* **2018**, *47* (3), 852–908.
- (3) J. Hu; Q. Zhang; D. J. Lee. Kraft Lignin Biorefinery: A Perspective. *Bioresour. Technol.* **2018**, *247*, 1181–1183.
- (4) S. Gillet; M. Aguedo; L. Petitjean; A. R. C. Morais; A. M. Da Costa Lopes; R. M. Łukasik; P. T. Anastas. Lignin Transformations for High Value Applications: Towards Targeted Modifications Using Green Chemistry. *Green Chemistry*. Royal Society of Chemistry 2017, pp 4200–4233.
- (5) C. Xu; R. A. D. Arancon; J. Labidi; R. Luque. Lignin Depolymerisation Strategies: Towards Valuable Chemicals and Fuels. *Chemical Society Reviews*. Royal Society of Chemistry November 21, 2014, pp 7485–7500.
- (6) T. Parsell; S. Yohe; J. Degenstein; T. Jarrell; I. Klein; E. Gencer; B. Hewetson; et al. A Synergistic Biorefinery Based on Catalytic Conversion of Lignin Prior to Cellulose Starting from Lignocellulosic Biomass. *Green Chem.* **2015**, *17* (3), 1492–1499.
- (7) Z. Sun; B. Fridrich; A. de Santi; S. Elangovan; K. Barta. Bright Side of Lignin Depolymerization: Toward New Platform Chemicals. *Chem. Rev.* **2018**, *118* (2), 614–678.
- (8) B. M. Upton; A. M. Kasko. Strategies for the Conversion of Lignin to High-Value Polymeric Materials: Review and Perspective. *Chem. Rev.* **2016**, *116* (4), 2275–2306.
- (9) D. M. Alonso; S. G. Wettstein; J. A. Dumesic. Bimetallic Catalysts for Upgrading of Biomass to Fuels and Chemicals. *Chemical Society Reviews*. December 21, 2012, pp 8075–8098.
- (10) N. Yan; C. Zhao; P. J. Dyson; C. Wang; L. T. Liu; Y. Kou. Selective Degradation of Wood Lignin over Noble-Metal Catalysts in a Two-Step Process. *ChemSusChem* **2008**, *1* (7), 626–629.
- (11) S. Van den Bosch; W. Schutyser; S.-F. Koelewijn; T. Renders; C. M. Courtin; B. F. Sels. Tuning the Lignin Oil OH-Content with Ru and Pd Catalysts during Lignin Hydrogenolysis on Birch Wood. *Chem. Commun.* **2015**, *51* (67), 13158–13161.

- 
- (12) Z. Sun; B. Fridrich; A. De Santi; S. Elangovan; K. Barta. Bright Side of Lignin Depolymerization: Toward New Platform Chemicals. *Chemical Reviews*. American Chemical Society January 24, 2018, pp 614–678.
- (13) A. M. Ruppert; K. Weinberg; R. Palkovits. Hydrogenolysis Goes Bio: From Carbohydrates and Sugar Alcohols to Platform Chemicals. *Angew. Chemie Int. Ed.* **2012**, *51* (11), 2564–2601.
- (14) J. B. Binder; R. T. Raines. Simple Chemical Transformation of Lignocellulosic Biomass into Furans for Fuels and Chemicals. *J. Am. Chem. Soc.* **2009**, *131* (5), 1979–1985.
- (15) W. Liu; Y. Chen; H. Qi; L. Zhang; W. Yan; X. Liu; X. Yang; et al. A Durable Nickel Single-Atom Catalyst for Hydrogenation Reactions and Cellulose Valorization under Harsh Conditions. *Angew. Chemie* **2018**, *130* (24), 7189–7193.
- (16) M. V. Galkin; J. S. M. Samec. Selective Route to 2-Propenyl Aryls Directly from Wood by a Tandem Organosolv and Palladium-Catalysed Transfer Hydrogenolysis. *ChemSusChem* **2014**, *7* (8), 2154–2158.
- (17) I. Kumaniaev; E. Subbotina; J. Sävmärker; M. Larhed; M. V. Galkin; J. S. M. Samec. Lignin Depolymerization to Monophenolic Compounds in a Flow-through System. *Green Chem.* **2017**, *19* (24), 5767–5771.
- (18) X. Huang; J. Zhu; T. I. Korányi; M. D. Boot; E. J. M. Hensen. Effective Release of Lignin Fragments from Lignocellulose by Lewis Acid Metal Triflates in the Lignin-First Approach. *ChemSusChem* **2016**, *9* (23), 3262–3267.
- (19) P. Albers; J. Pietsch; S. F. Parker. Poisoning and Deactivation of Palladium Catalysts. *J. Mol. Catal. A Chem.* **2001**, *173* (1–2), 275–286.
- (20) L. Liu; A. Corma. Metal Catalysts for Heterogeneous Catalysis: From Single Atoms to Nanoclusters and Nanoparticles. *Chem. Rev.* **2018**, *118* (10), 4981–5079.
- (21) G. Giannakakis; M. Flytzani-Stephanopoulos; E. C. H. Sykes. Single-Atom Alloys as a Reductionist Approach to the Rational Design of Heterogeneous Catalysts. *Acc. Chem. Res.* **2019**, *52* (1), 237–247.
- (22) A. Wang; J. Li; T. Zhang. *Heterogeneous Single-Atom Catalysis*; Nature Publishing Group, 2018; Vol. 2, pp 65–81.
- (23) M. Sankar; N. Dimitratos; P. J. Miedziak; P. P. Wells; C. J. Kiely; G. J. Hutchings. Designing Bimetallic Catalysts for a Green and Sustainable Future. *Chem. Soc. Rev.* **2012**, *41* (24), 8099–8139.
- (24) M. Pozzo; D. Alfè. Hydrogen Dissociation and Diffusion on Transition Metal (= Ti, Zr, V, Fe, Ru, Co, Rh, Ni, Pd, Cu, Ag)-Doped Mg(0001) Surfaces. *Int. J.*

*Hydrogen Energy* **2009**, 34 (4), 1922–1930.

- (25) G. Kyriakou; M. B. Boucher; A. D. Jewell; E. A. Lewis; T. J. Lawton; A. E. Baber; H. L. Tierney; et al. Isolated Metal Atom Geometries as a Strategy for Selective Heterogeneous Hydrogenations. *Science* (80-. ). **2012**, 335 (6073), 1209–1212.
- (26) Y. Chen; S. Ji; C. Chen; Q. Peng; D. Wang; Y. Li. Single-Atom Catalysts: Synthetic Strategies and Electrochemical Applications. *Joule* **2018**, 2 (7), 1242–1264.
- (27) X. Cui; W. Li; P. Ryabchuk; K. Junge; M. Beller. Bridging Homogeneous and Heterogeneous Catalysis by Heterogeneous Single-Metal-Site Catalysts. *Nature Catalysis*. Nature Publishing Group June 1, 2018, pp 385–397.
- (28) J. Zhang; J. Liu; L. Xi; Y. Yu; N. Chen; S. Sun; W. Wang; et al. Single-Atom Au/NiFe Layered Double Hydroxide Electrocatalyst: Probing the Origin of Activity for Oxygen Evolution Reaction. *J. Am. Chem. Soc.* **2018**, 140 (11), 3876–3879.
- (29) H. Zhang; G. Liu; L. Shi; J. Ye. Single-Atom Catalysts: Emerging Multifunctional Materials in Heterogeneous Catalysis. *Adv. Energy Mater.* **2018**, 8 (1), 1701343.
- (30) L. Jiao; H. L. Jiang. Metal-Organic-Framework-Based Single-Atom Catalysts for Energy Applications. *Chem.* Elsevier Inc April 11, 2019, pp 786–804.
- (31) Y. Lu; J. Wang; L. Yu; L. Kovarik; X. Zhang; A. S. Hoffman; A. Gallo; et al. Identification of the Active Complex for CO Oxidation over Single-Atom Ir-on-MgAl<sub>2</sub>O<sub>4</sub> Catalysts. *Nat. Catal.* **2019**, 2 (2), 149–156.
- (32) S. Tian; Z. Wang; W. Gong; W. Chen; Q. Feng; Q. Xu; C. Chen; et al. Temperature-Controlled Selectivity of Hydrogenation and Hydrodeoxygenation in the Conversion of Biomass Molecule by the Ru1/Mpg-C<sub>3</sub>N<sub>4</sub> Catalyst. *J. Am. Chem. Soc.* **2018**, 140 (36), 11161–11164.
- (33) J. Zhou; W. An; Z. Wang; X. Jia. Hydrodeoxygenation of Phenol over Ni-Based Bimetallic Single-Atom Surface Alloys: Mechanism, Kinetics and Descriptor. *Catal. Sci. Technol.* **2019**, 9 (16), 4314–4326.
- (34) S. J. Park; M. K. Seo. *Interface Applications in Nanomaterials*; Elsevier, 2011; Vol. 18.
- (35) C. Antoniak; M. E. Gruner; M. Spasova; A. V. Trunova; F. M. Römer; A. Warland; B. Krumme; et al. A Guideline for Atomistic Design and Understanding of Ultrahard Nanomagnets. *Nat. Commun.* **2011**, 2 (1), 528.
- (36) N. Yan; C. Zhao; P. J. Dyson; C. Wang; L. T. Liu; Y. Kou. Selective Degradation of Wood Lignin over Noble-Metal Catalysts in a Two-Step Process.



- ChemSusChem* **2008**, *1* (7), 626–629.
- (37) E. M. Anderson; R. Katahira; M. Reed; M. G. Resch; E. M. Karp; G. T. Beckham; Y. Román-Leshkov. Reductive Catalytic Fractionation of Corn Stover Lignin. *ACS Sustain. Chem. Eng.* **2016**, *4* (12), 6940–6950.
- (38) A. G. Sergeev; J. F. Hartwig. Selective, Nickel-Catalyzed Hydrogenolysis of Aryl Ethers. *Science* (80-. ). **2011**, *332* (6028), 439–443.
- (39) J. Zakzeski; P. C. A. Bruijninx; A. L. Jongerius; B. M. Weckhuysen. The Catalytic Valorization of Lignin for the Production of Renewable Chemicals. *Chem. Rev.* **2010**, *110*, 3552–3599.
- (40) S. Van Den Bosch; T. Renders; S. Kennis; S. F. Koelewijn; G. Van Den Bossche; T. Vangeel; A. Deneyer; et al. Integrating Lignin Valorization and Bio-Ethanol Production: On the Role of Ni-Al<sub>2</sub>O<sub>3</sub> catalyst Pellets during Lignin-First Fractionation. *Green Chem.* **2017**, *19* (14), 3313–3326.
- (41) E. M. Anderson; M. L. Stone; R. Katahira; M. Reed; G. T. Beckham; Y. Román-Leshkov. Flowthrough Reductive Catalytic Fractionation of Biomass. *Joule* **2017**, *1* (3), 613–622.
- (42) B. Zhang; H. Asakura; J. Zhang; J. Zhang; S. De; N. Yan. Stabilizing a Platinum 1 Single-Atom Catalyst on Supported Phosphomolybdic Acid without Compromising Hydrogenation Activity. *Angew. Chemie* **2016**, *128* (29), 8459–8463.
- (43) D. T. Balogh; A. A. S. Curvelo; R. A. M. C. De Groote. Solvent Effects on Organosolv Lignin from *Pinus Caribaea Hondurensis*. *Holzforschung* **1992**, *46* (4), 343–348.
- (44) W. Schutyser; S. Van den Bosch; T. Renders; T. De Boe; S.-F. Koelewijn; A. Dewaele; T. Ennaert; et al. Influence of Bio-Based Solvents on the Catalytic Reductive Fractionation of Birch Wood. *Green Chem.* **2015**, *17* (11), 5035–5045.
- (45) Q. Song; F. Wang; J. Cai; Y. Wang; J. Zhang; W. Yu; J. Xu. Lignin Depolymerization (LDP) in Alcohol over Nickel-Based Catalysts via a Fragmentation–Hydrogenolysis Process. *Energy Environ. Sci.* **2013**, *6* (3), 994.
- (46) O. Yu; C. G. Yoo; C. S. Kim; K. H. Kim. Understanding the Effects of Ethylene Glycol-Assisted Biomass Fractionation Parameters on Lignin Characteristics Using a Full Factorial Design and Computational Modeling. *ACS Omega* **2019**, *4* (14), 16103–16110.
- (47) M. Fasching; P. Schröder; R. P. Wollboldt; H. K. Weber; H. Sixta. A New and Facile Method for Isolation of Lignin from Wood Based on Complete Wood Dissolution. *Holzforschung* **2008**, *62* (1).
- (48) G. S. Macala; T. D. Matson; C. L. Johnson; R. S. Lewis; A. V. Iretskii; P. C. Ford.

- Hydrogen Transfer from Supercritical Methanol over a Solid Base Catalyst: A Model for Lignin Depolymerization. *ChemSusChem* **2009**, 2 (3), 215–217.
- (49) X. Wang; R. Rinaldi. Solvent Effects on the Hydrogenolysis of Diphenyl Ether with Raney Nickel and Their Implications for the Conversion of Lignin. *ChemSusChem* **2012**, 5 (8), 1455–1466.

## Chapter 6 Conclusions and Outlooks

We have briefly introduced a hydrogen storage and delivery method using a Liquid Organic Hydrogen Carriers (LOHCs), and then utilized the obtained H<sub>2</sub> in biomass conversion.

In the first part, a “green” H<sub>2</sub> cycle is achieved by hydrogenation and dehydrogenation of N-heterocycles with Ru/*m*TPPTS under mild conditions. With the same catalyst for both hydrogenation and dehydrogenation, there is no need to separate the catalyst. In addition, H<sub>2</sub> can easily be separated as the only gas phase without any other gas by-product. It is an efficient and safe method for hydrogen storage/delivery which is adapted to the current facilities.

The second part focuses on using the obtained hydrogen in lignin reductive depolymerization with different kinds of catalysts, including an efficient Pt nanoparticle-ionic liquid pseudo-homogeneous catalytic system, a robust well-defined Rh nanoparticles dispersed in carbon hollow spheres heterogeneous catalyst and a highly active Pt single atoms in the surface of Ni nanoparticles on carbon catalyst. For the Pt nanoparticle-ionic liquid pseudo-homogeneous catalytic system, it is an excellent catalyst for the hydrodeoxygenation (HDO) of lignin monomer and dimer model compounds. However, it is vulnerable when is applied in real lignin conversion with harsh reaction conditions. To enhance the stability of the catalyst, heterogeneous catalyst with Rh nanoparticles dispersed inside of carbon hollow spheres was applied in hydrogenation of lignin monomers and dimers, and confirmed in reductive catalytic fractionation of birch sawdust as well. This special sphere structure of catalyst separates the catalytic sites from lignin in molecular level. With the nearly theoretical monomer yield, it is provided strong evidence that the solvent (i.e. MeOH) is almost entirely responsible for both fractionation and fragmentation of lignin.

To push the research further, the final part of the thesis concludes that with the unique advantages of atomically dispersed catalysts (ADCs), especially the possible synergistic effect in single atom alloys (SAAs). They are becoming new frontiers in

lignocellulosic conversion. With the minimal usage of noble metals, Pt<sub>1</sub>Ni/C, engineering Pt single atoms into Ni nanoparticles supported on carbon, produces lignin monomers with yield of 37% under 200 °C with 5 MPa H<sub>2</sub> in methanol, which is significantly higher than that using Ni nanoparticles or Pt single atoms as the catalyst. The high selectivity was attributed to the active single atoms unable to hydrogenate the aromatic ring.

Future efforts should be made in real lignin conversion with some ADCs that have high activity, good selectivity and good recyclability. For SAAs, the replacement of noble metals by nonprecious ones is also remain to be solved. To figure out the catalysis mechanism and to provide guidelines for catalysts design, *in situ* X-ray absorption spectroscopy (XAS) can indicate the evolution of the coordination environment and determine the coordination environments of active sites, both during the synthesis process and during the catalytic process. Combining the XAS results with density functional theory (DFT), it is significant in understanding and optimizing the coordination environments. Nevertheless, it is reasonable to expect that ADCs will put into practical use in chemical conversion of lignocellulosic biomass in the near future. With the aid of new advancing characterization technologies, ADCs also offer new opportunities for interpreting the structure-performance relationship from the atomistic perspective, and for bridging the gap between homogeneous and heterogeneous catalysis.

## Chapter 7 Acknowledgements

First and foremost, I would like to thank my PhD advisors Prof. Gabor Laurenczy and Prof. Paul Dyson. Thanks for giving me the opportunity to join their group. Both of them encouraged, supported and helped me since the first day I arrived. My first memories go back to the first discussion with them, I were touched not only by the inspiring and enjoyable discussions, but also goodness of Gabor and humor of Paul. I appreciated for their contribution to my life and career. All the times spent with them and all the things they taught me helped set a clear direction for me to follow. I am so lucky to have PhD with both. That was an invaluable experience. Both of them are professors from heaven.

I would like to thank my PhD exam jury, Prof. Kay Severin, Prof. Kevin Sivula, Prof. Qiang Xu, Prof. Huizhen Liu and my supervisors for reviewing my thesis and attending my defense.

I want to thank everyone in the lab as well as these technician who are patient in support of us. During my time in EPFL, I meet many awesome people. When the first day I arrived at the EPFL for my PhD, Fei, Martin and Cornel welcomed me into the group. Katerina, Martin, and Mick are ready to help all the time as well. I want to thank Mick for helping me progressing with my french study. Thank you for explaining each question clearly.

Cornel made me know that there is no kangaroos in Austria (where he comes from). Cornel brings me into the board of Swiss Young Chemists' Association. With his help, I finally became the vice president. Without him, I will never had such an amazing experience.

Antoine helped me a lot with chemistry. We know lignin is a tricky biomass, still we are together to solve the problems step by step. Thank you for so many encouraging discussions and generous support.

I owe special thanks to Lichen Bai and Weiyan Ni, that bring me so much fun. I thank my colleagues Xinjiang, Yun, Yameng, Fangmin, Zhangjun, Po-Jen, Wei-Tse, Serhii, Dimtry, Erfan, Martin, Lucy, Felix, Soumaila, Irina, Mouna and Kedar for your generous help.

Thanks also goes to people working behind the scenes. First of all, our secretary Ms. Jacqueline Morard. The groups won't work without you. NMR team helped me a lot especially Aurélien Bornet. Thank you for your kindness and patient.

Thank you for my best friends, Wen Zhu, Hailin Chen and Rong Xu. We have had our ups and downs, but in the end, you will always be my friends. Even if we don't talk for months, we still going to feel the same about each other in the end. Even though most of you are far away from me, we will meet again.

I also want to thank our families who support us thereby Linfeng and I could finish PhD here. Thank you, mom and dad for raising me so perfectly. Raising a child is difficult, I really understand it after I had one who used to cry just when I fall sleep, thank you for being so patient.

Linfeng, for the past 3 years, you have not only been my husband and father of our baby, you have been my best friend. Mucheng sets his sights higher because he has you as a role model. You have made me proud, and you will make him proud. Mucheng, thank you for making me a mother. Thank you for accompany with us since he born. I have always had you with me in all the good and bad times. Thank you for making me a stronger person, while giving me a softer heart. I will love you forever.

---

## CHEN Lu

Swiss Federal Institute of Technology, Lausanne, Switzerland  
Phone: +41 78 681 2259, Email: luchen\_090@outlook.com  
Address: Chemin du Bochet 18, 1024 Ecublens VD, Switzerland

### EDUCATION

---

#### Ph.D. Chemistry and Chemical Engineering

- ✧ **Swiss Federal Institute of Technology (EPFL)**, Switzerland  
Advisors: Prof. Gabor Laurenczy & Prof. Paul Dyson Nov. 2020

#### M.S. Chemical Engineering (Double-degrees program)

- ✧ **Institute of Process Engineering, Chinese Academy of Sciences**, China  
Advisors: Prof. Suojia Zhang June 2016
- ✧ **Technical University of Denmark (DTU)**, Denmark  
Advisors: Assi. Prof. Jakob Christensen July 2015

#### B.S.E. Chemical Engineering July 2013

- ✧ **Tianjin University**, Tianjin, China

### RESEARCH EXPERIENCE

---

#### Swiss Federal Institute of Technology, Lausanne, Switzerland Sep. 2016-present Propelling the hydrogen economy: from chemical storage and delivery to utilization in biomass conversion

- ✧ Developed advanced Pt nanoparticle - ionic liquids system for upgrading lignin model compounds at mild reaction conditions
- ✧ Designed heterogeneous catalyst, rhodium nanoparticles embedded into a hollow porous carbon sphere, for confirming the role of metal catalyst
- ✧ Established single atoms alloy catalyst for lignin conversion to maximize atom efficiency of noble metal

#### Institute of Process Engineering, Beijing, China Dec. 2014 - June 2016 Conversion of Lignin Model Compounds at Mild Conditions in Pseudo-Homogeneous Systems

- ✧ Synthesized pseudo-homogeneous system consists of noble metal nanoparticles uniform and stabilized in ionic liquids (Obtained 12/12 in DTU MSc defense)

### INTERNSHIP

---

#### BASF's China Headquarter, Shanghai July 2015

- ✧ Accomplished internship as one of the outstanding students to visited BASF Pudong Site & Innovation Campus Asia Pacific (**The only master in 23 persons in total of the whole Asia Area**)

#### Summer Activity, Technical University of Denmark, Denmark June - Aug. 2014

- ✧ Obtained **rank A** for unit operation experiments

#### Three Danish Chemical Companies, Denmark July 2014

- 
- ✧ Visited the production plant in Novozymes, Haldor Topsøe and Hempel

## Social Activity

---

### Swiss Young Chemists' Association

- ✧ Planed the SwissSnowSymposium (Annual conference) 2017 - 2020
- ✧ Vice President of the Swiss Young Chemists' Association 2019 - 2020
- ✧ Secretary of the Swiss Young Chemists' Association 2017 - 2019

### Teaching assistant, EPFL 2016 – 2020

- ✧ Fluid mechanics and transport phenomena 2016 - 2020
- ✧ Master project in Molecular & Biological Chemistry 2018 – 2019

### Summer School of IPE, Beijing July 2015

- ✧ Participated in preparing the schedule and guided junior students as a counselor

## PROFESSIONAL AND TECHNICAL SKILLS

---

- ✧ Language Skill: English (fluent), Chinese (native), French (A2-B1)
- ✧ Experienced in laboratory Instrument: GC-MS, TEM, SEM, XRD, NMR, TGA, etc.

## PUBLICATIONS

---

- ✧ **L. Chen**, A. van Muyden, G. Laurenczy, P. J. Dyson. Reductive catalytic fractionation of biomass: confirming the role of the catalyst. (in preparation)
- ✧ **L. Chen**, L. Pan, A. van Muyden, G. Laurenczy, P. J. Dyson. Embedding single platinum atoms into nickel nanoparticles to afford a highly selective catalyst for lignin conversion (in preparation)
- ✧ **L. Chen**, A. van Muyden, X. Cui, G. Laurenczy, P. J. Dyson. Selective hydrogenation of lignin-derived compounds under mild conditions. **Green Chemistry**, 2020, 22, 3069-3073. DOI: 10.1039/D0GC00121J (Front Cover)
- ✧ **L. Chen**, C. Fink, Z. Fei, P. J. Dyson, G. Laurenczy. An efficient Pt nanoparticle–ionic liquid system for the hydrodeoxygenation of bio-derived phenols under mild conditions. **Green Chemistry**, 2017, 19, 5435-5441. DOI: 10.1039/C7GC01870C (2017 Green Chemistry Hot Articles)
- ✧ **L. Chen**, J. Xin, L. Ni, H. Dong, D. Yan, X. Lu, S. Zhang. Conversion of lignin model compounds under mild conditions in pseudo-homogeneous systems. **Green Chemistry**, 2016, 18, 2341-2352. DOI: 10.1039/C5GC03121D (Front Cover)
- ✧ Y. Tong, Q. Sun, P. Chen, **L. Chen**, Z. Fei, P. J. Dyson. Nitrogen-Incorporated Cobalt Sulfide/Graphene Hybrid Catalysts for Overall Water Splitting. **ChemsusChem**, 2020, 13, 1 –8. DOI: 10.1002/cssc.202001413
- ✧ L. Ni, J. Xin, K. Jiang, **L. Chen**, D. Yan, X. Lu, S. Zhang. One-step conversion of biomass-derived furanics into aromatics by Brønsted acid ionic liquids at room temperature. **ACS Sustainable Chemical & Engineering**, 2018, 6, 2, 2541-2551. DOI: 10.1021/acssuschemeng.7b04017
- ✧ C. Fink, **L. Chen**, G. Laurenczy. Homogeneous catalytic formic acid



---

dehydrogenation in aqueous solution using ruthenium arene phosphine catalysts. ***Zeitschrift für Anorganische und Allgemeine Chemie***, 2018, 644, 14, 740-744. DOI: 10.1002/zaac.201800107

- ✧ F. Huang, T. Jiang, H. Dai, X. Xu, S. Jiang, **L. Chen**, Z. Fei, P. J. Dyson. Transformation of Glucose to 5-Hydroxymethylfurfural Over Regenerated Cellulose Supported Nb<sub>2</sub>O<sub>5</sub>·nH<sub>2</sub>O in Aqueous Solution. ***Catalysis Letters***, 2020. DOI: 10.1007/s10562-020-03160-9